Phosphorylated ubiquitin in the DNA damage response

By Abigail Farrell

A thesis submitted to the University of Birmingham

for the degree of Doctor of Philosophy

Institute of Cancer and Genomic Sciences

School of Cancer Sciences

College of Medical and Dental Sciences

University of Birmingham

September 2022

Abstract

Ubiquitylation and phosphorylation are key post-translational modifications in the response to, and repair of, DNA double strand breaks. Signalling through these modifications is detected rapidly upon induction of damage, and continues throughout DNA repair. Phospho-proteomic studies have found that ubiquitin itself can be phosphorylated at 11 different sites. Characterisation of several of these sites has revealed that phospho-ubiquitin can give rise to specific signalling, with roles in human health and disease.

In this thesis, I show detection of a previously uncharacterised phospho-ubiquitin as distinct nuclear foci after induction of DNA damage. I then demonstrate that this modification has a role in the DNA damage response, likely as part of the repair of double strand breaks by non-homologous end joining, non-phosphorylatable mutants of ubiquitin show reduced recruitment of 53BP1 to damage sites. This mutant causes no alteration to cell viability or cell cycle in unperturbed cells, but shows resistance to ionising radiation. Finally I show that foci formation by this modification is regulated through canonical DSB proteins, and is a novel factor in the double strand break response.

Acknowledgements

I have been incredibly lucky to be surrounded by amazing, talented, kind, and supportive individuals throughout my PhD. The thanks I feel is more than I can put into words, but I will try.

First to my supervisor, Aga, I can't thank you enough for the support you have given me over the course of the PhD. Your supervision and mentorship have been invaluable, and I am so glad to have had you as my supervisor.

To those in the Gambus lab, past and present: Shaun, Becky, Divya, Zeynep, Nev, Paolo, Cynthia, Georgia, Sarmi, Alijca, Angeliki, and Chongluan. It has been an absolute pleasure to work with you all. There is always a kind and supportive atmosphere, and your insightful comments have helped me overcome many obstacles along the way. Shaun and Becky, thank you for the pub trips, both the celebrations and commiserations, they have been welcome breaks throughout the PhD!

To Marco, Martina, Mao and Jianming, thank you for welcoming me so wholeheartedly. I am incredibly grateful for all your advice and support over the years, and look forward to our future work together.

To all those who are part of the Institute of Cancer and Genomic Sciences: It has been an incredible experience to be part of such an enthusiastic and collaborative work environment. In particular, to the members of the Morris lab, our tea point conversations have been incredibly helpful! And to Tracey, your boundless enthusiasm for science has rubbed off on me. I am very glad to have you as a mentor!

I would also like to thank my family and friends, for their patience and support over the years. To Dominika and Rich, we've had some amazing stories these past few years! Thank you for your support and encouragement, and putting a roof over my head whenever I miss the last train home. To my family, thank you for your love and support, and for the interest in my work. I promise I am finally done with school!

And finally, to my partner Adam. This would not have been possible without you backing me, celebrating my successes, and motivating me through difficulties. You are my keystone, and I am forever grateful.

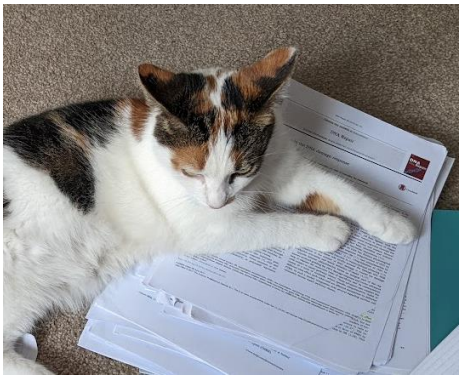

Contents

List of figures

List of Tables

Abbreviations used in this thesis

alt-EJ	alternative End Joining
A-T	Ataxia-Telangiectasia
CHR	CHRomatin fraction
CSR	Class Switch Recombination
CYT	CYToplasmic fraction
DDR	DNA Damage Response
DSB	Double Strand Break
DUB	De-UBiquitinating enzyme
EV	Empty Vector
FBS	Foetal Bovine Serum
HR	Homologous Recombination
IB	ImmunoBlotting
IF	ImmunoFluorescence
IR	Ionising Radiation
IRIF	Ionising Radiation Induced Foci
MFFR	Minimal Focus Forming Region
NHEJ	Non-Homologous End Joining
c-NHEJ	canonical NHEJ
alt-NHEJ	alternative NHEJ
NT	Non-Targeting
NUC	NUCleoplasm fraction
OMM	Outer Mitochondrial Membrane
PTM	Post-Translational Modification
RBR	RING-Between-RING
SDM	Site-Directed Mutagenesis
SDSA	Synthesis-Dependent Strand Annealling
ssDNA	single stranded DNA
UBL	Ubiquitin Like
UIM	Ubiquitin Interacting Motif
WCE	Whole Cell Extract
WT	Wild Type

Chapter 1: Introduction

1.1 Phosphorylation

Phosphorylation is a reversible post-translational modification (PTM), characterised by the covalent addition of a phosphate group to an amino acid side chain through the activity of kinase enzymes. In eukaryotic cellular signalling, phosphorylation of serine, threonine and tyrosine residues are well established, although phosphorylation at other residues has been reported (Adam and Hunter, 2017; Mann et al., 2002). The modification can be reversed through the catalytic activity of phosphatase enzymes. Kinase and phosphatase enzymatic activity can be incredibly rapid, with detectable changes in phosphorylation levels occurring within seconds of an input stimulus (Kanshin et al., 2015). This allows for rapid propagation and termination of signalling in response to a stimulus, enabling tight control of signalling pathways.

Phosphorylation is a powerful modification. Addition of the phosphate group to an amino acid alters the chemistry of the residue, creating a polar, hydrophilic site in place of the previously uncharged site. This change can alter intra-protein interactions responsible for a proteins tertiary structure, leading to conformational changes. These changes can cause loss or gain of functions in the phosphorylated protein, with the phosphorylation acting as a molecular “switch” regulating signalling pathways (Ardito et al., 2017; Zhang et al., 2021).

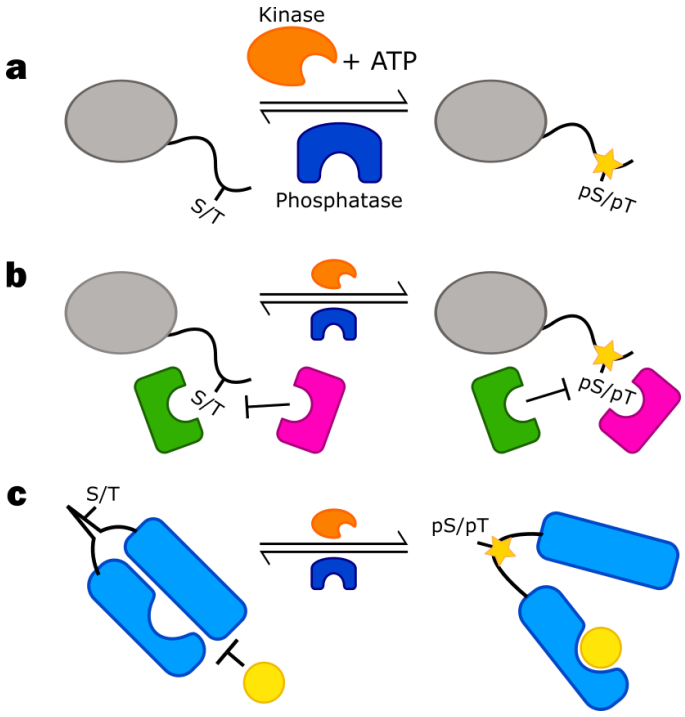

Figure 1.1: Phosphorylation is a reversible post-translational modification. Phosphorylation at a serine/threonine residue is shown as an example. **(a)** Phosphorylation requires the activity of a kinase and the presence of ATP, and is reversible through phosphatase activity. **(b)** Phosphorylation alters protein-protein interactions. **(c)** Conformational changes in proteins can be induced by phosphorylation, leading to changes in substrate activity.

Phosphorylated residues themselves can act as a binding site or recognition motif. Some proteins lose affinity for phosphorylated residues, reducing protein-protein interactions. Many proteins contain binding domains that specifically recognise phosphorylated residues. For example, FHA and BRCT domains are common in DNA damage response proteins, where kinase activity helps drive protein recruitment to damage sites (Reinhardt and Yaffe, 2013).

Selectivity of the kinases for their substrates has largely been ascribed to phosphorylation motifs present on the substrate protein. Directly linking a phosphorylation motif to a kinase has proved challenging, with kinases able to phosphorylate residues in a range of motifs. Work by Johnson et al. (2022) identified that rather than “positively” selecting for substrates with a specific phosphorylation motif, kinases were more dependent on “negative” selection, where certain motifs prevent binding. This distinction reinforces substrate driven specificity, and accounts for the redundancy seen in many kinase signalling pathways.

Protein phosphorylation is an abundant PTM, with over two-thirds of proteins identified as having phosphorylated residues, although this is likely an underestimate of the true total. Reflecting this abundance, over 500 kinases have been identified in the human genome, and over 150 phosphatases (Ardito et al., 2017; Zhang et al., 2021). Despite this abundance, the known importance of phosphorylation in health and disease, and the relevance of kinases as drug targets, there is still a lot unknown in the phospho-proteome. Approximately 1/3 of kinases have an unknown function, and less than 5% of phosphorylated sites have an assigned kinase. Even fewer have a known role. This large knowledge gap is often referred to as the "dark phospho-proteome" (Berginski et al., 2021; Needham et al., 2019). This represents an opportunity for greater understanding of mechanisms of health and disease, as well as opportunities for discovery of potential therapeutic targets.

1.1.1 Phosphorylation in the DNA damage response

Three kinases are master regulators of DNA damage signalling – ATM, ATR, and DNA-PK. All three proteins belong to the phosphoinositide 3-kinase (PI3K)-related kinase (PIKK) family, and share an affinity for S/TQ motifs. Despite the overlap in many substrates, their roles in the DDR are unique, and loss or mutation of one of the kinases cannot be completely compensated for by the others (Blackford and Jackson, 2017).

ATR is activated in response to a wide array of DNA lesions, which result in exposed single-stranded DNA. ATR forms a complex with ATRIP which enables recruitment to RPA, which in turn binds to ss-DNA. ATR also has an extended role outside DNA repair, contributing to checkpoint activation via CHK1 phosphorylation (Awasthi et al., 2015).

ATM kinase is the master kinase in the response to DNA double strand breaks (DSBs). DSBs are "sensed" by the MRN complex, which rapidly localises to altered DNA ends (Lamarche et al., 2010), where it promotes the dissociation of ATM from the inactive homodimer to the active monomer. Activated ATM has many target substrates in pathways including DNA repair, checkpoint signalling and apoptosis, making it a global regulator of DSB response (Paull, 2015).

DNA-PK is a holoenzyme formed from the Ku complex, which is recruited to free ds-DNA ends, and DNA-PKcs. DNA-PK is essential for DSB repair by Non-Homologous End-Joining (NHEJ), although which substrates are important for NHEJ remains unclear. Better characterised are the PTMs on DNA-PK itself, which help drive its activity and localisation (Yue et al., 2020).

ATM, ATR, and DNA-PK are apical kinases, forming the first phosphorylation signals in response to DNA damage. Many other kinases have been described in DNA repair, though their role is often not well defined, or difficult to unpick from other kinases. Cyclin dependent kinases, for example, impact the transcription of DDR proteins and help drive repair pathway choice (Kciuk et al., 2022). The checkpoint kinases CHK1 and CHK2, which are activated by ATR and ATM, are reported to have their own direct roles in DNA repair (Smits and Gillespie, 2015; Zannini et al., 2014). The role of kinases involved in the DDR outside of the PIKK triad are still under studied, yet may hold the key to some of the mechanistic questions surrounding DNA repair.

1.2 Ubiquitylation

Another key PTM in DNA repair signalling is ubiquitylation, a reversible PTM in which a ubiquitin protein is covalently attached to a substrate, usually at a lysine residue. Originally noted for its role in targeting proteins for degradation by the proteasome, ubiquitin signalling has since been identified in all major signalling pathways, with roles distinct from protein degradation, truly earning its name as a ubiquitous protein.

Ubiquitin is a small protein, at just 76 amino acids. It is found in all eukaryotic organisms and is highly conserved, highlighting its importance in cellular homeostasis (Zuin et al., 2014). With no enzymatic activity of its own, conjugation of ubiquitin to target proteins relies on a series of conjugation reactions, termed the ubiquitin cascade (Figure 1.2). In this cascade, ubiquitin is first conjugated to an E1 "activating" enzyme in an ATP-dependent manner, then transferred to an E2 "conjugating" enzyme via a transthiolation reaction. Attachment of ubiquitin to its final substrate is facilitated by an E3 "ligating" enzyme. Ubiquitylation is reversible through the activity of de-ubiquitylating enzymes (DUBs), and the ubiquitin released is available for use in the ubiquitin cascade again.

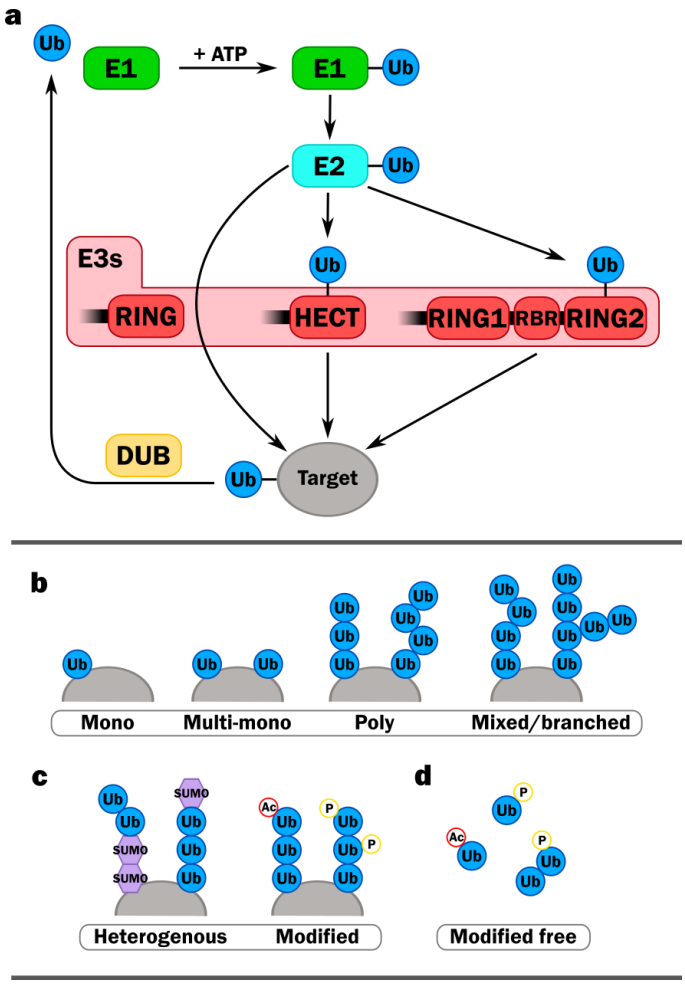

Figure 1.2: Ubiquitin signalling is orchestrated via the ubiquitin cascade. (a) Ubiquitylation of a target protein is a reversible, multistep process. **(b)** Ubiquitin signalling is often regarded as a "code", with poly-ubiquitin chains lending increasing complexity. **(c)** Further expansion of the ubiquitin code is found through post-translational modifications of ubiquitin. **(d)** Free ubiquitin itself has signalling and regulatory roles, and modification of free ubiquitin expands these roles further.

Ubiquitin itself is a target for ubiquitylation, enabling the formation of poly-ubiquitin chains. Ubiquitin can be conjugated at each of its 7 lysine residues as well as at the N-terminal methionine. Each of these 8 linkages has a distinct conformation, which allows the chain types to be specifically "read" by ubiquitin binding domains within ubiquitin binding proteins. This forms the basis of specific signalling pathways activated by different ubiquitin modifications, and has come to be termed the "ubiquitin code" (Figure 1.2).

Understanding the roles of these ubiquitin chains remains incomplete, in part due to the complexity and overlap of many of the roles of ubiquitylated proteins. Ubiquitin was first described as a key driver of proteasome mediated degradation, and this signalling is largely attributed to K48-linked chains (Chau et al., 1989; Finley et al., 1994). However, K11- and K63-linked chains, branched ubiquitin chains and simple mono-ubiquitylation have all been linked to proteasome degradation of ubiquitylated proteins (Braten et al., 2016; Grice and Nathan, 2016). It is likely that the complexity of the ubiquitin code is not simply due to the conformation of the ubiquitin chains itself, but is contextual, relying on the "readers" of the ubiquitin code present around the ubiquitylation mark.

1.2.1 Writing the ubiquitin code

In humans, 2 ubiquitin-specific E1s have been identified, 41 E2 enzymes and over 600 E3 enzymes (George et al., 2018; van Wijk and Timmers, 2010). The E3 ligases are broadly categorised into 3 families, HECT, RING (and RING-like), and RING-between-RING (RBR), based on their catalytic domains and mechanism of ubiquitylation. Despite the common catalytic domains, the other features of the proteins are incredibly varied within groups, with little homology outside of the catalytic domain (Yang et al., 2021). This diversity allows for recognition and ubiquitylation of specific substrates, as well as building of specific ubiquitin chains, providing mechanisms for regulating ubiquitin signalling that would not be possible with a smaller subset of proteins (Figure 1.2).

RING (Really Interesting New Gene) E3 ligases are the largest family of E3s, with over 600 proteins identified. This family also contains the RING-like E3 ligases, such as the U-box ligases, as they share a common ability to transfer ubiquitin directly from the E2 to a target protein without forming an intermediate. As this transfer is direct, the ubiquitin modification is largely driven by the E2 enzyme, rather than the ligase (Stewart et al., 2016). Whilst many of the RING ligases act as monomers, there is a tendency for RING-ligases to form protein complexes. Many are found as homo- or hetero-dimers, with the DNA damage complex BRCA1-BARD1 representing a well characterised RING-heterodimer (Irminger-Finger et al., 2016). Larger multi-subunit complexes are also seen, with the Cullin family E3 ligases using multiple adaptor proteins to target and regulate substrate ubiquitylation (Fouad et al., 2019). At the extreme end, the APC/C complex has 14 subunits, with a mass in excess of 1.2 MDa (Yamano, 2019). Complex formation adds another element of regulation to these ligases, altering E2 choice or substrate specificity, as well as enzymatic activity.

The HECT (Homologous to E6AP Carboxyl Terminus) E3 ligases ubiquitylate substrates in two steps, first conjugating ubiquitin to a cysteine residue in the catalytic domain via a transthiolation reaction, then transferring ubiquitin to a lysine residue on the target protein. Regulation of HECT activity is achieved in multiple ways, with interactions with additional proteins and post-translational modifications reported (Chen et al., 2017; Ronchi et al., 2014). Several members of the HECT family are regulated by non-covalent binding of ubiquitin at a site away from the catalytic domain, termed a ”ubiquitin exosite” (Maspero et al., 2011). Unlike with the RING E3 ligases, regulation of ubiquitin signalling does not appear to be tied to the E2 enzyme present, with HECT enzymes able to build specific ubiquitin chains regardless of the associated E2 (Weber et al., 2019).

The final group, the RBR ligases, consist of two ring domains separated by an in-between-RING (IBR) domain. Nomenclature of these domains has been challenged (although alternatives have not been adopted), as the RING2 domain contains a catalytically active site, not present in “canonical” RING domains. This leads to a RING-HECT hybrid mechanism of ubiquitylation, where RING1 interacts with

the E2 enzyme, and RING2 forms an intermediate with ubiquitin via a catalytic cysteine, before finally transferring the ubiquitin to its target.

RBRs are typically auto-inhibited, and release of this inhibition is achieved in different ways, with post-translational modifications and inter-protein interactions playing key roles in modulating RBR ligase activity (Dove and Klevit, 2017). Similarly to the HECT E3 ligases, RBRs appear to determine their own ubiquitin chain specificity, rather than this being directed by the E2. The mechanism of specific ubiquitin chain formation by these ligases is still an area of ongoing research.

1.2.2 Deubiquitylating enzymes

In addition to the E3 ligase "writers" of the ubiquitin code, the activity of the DUBs, or "erasers" is essential for ubiquitin homeostasis. Over 100 DUBs have been identified, spanning six families. Whilst some DUBs show a broad range of activity against mono- or poly-ubiquitin chains, others show selective activity against specific ubiquitin signals. This specificity changes the role of DUBs from simply "eraser" to "editor", facilitating the formation of some chain types whilst supressing others.

DUBS also play a regulatory role in the ubiquitin cascade, increasing global ubiquitylation as well as reducing it. Ubiquitylation of E3s is common, and can alter ligase activity, or target the ligase for proteasomal degradation. DUB activity can stabilise the E3, promoting ubiquitin signalling (Zheng and Shabek, 2017). The DUB OTUB1 has been shown to regulate K63-linked polyubiquitylation in the DNA damage response, though not through its catalytic activity. OTUB1 binds to the E2 complex UBC13~Ub, preventing ubiquitin transfer and blocking E3 binding sites. This interaction is another example of allosteric ubiquitin regulation, with free ubiquitin increasing the affinity of OTUB1 for UBC13~Ub (Nakada et al., 2010; Wiener et al., 2012).

1.3 Post-translational modifications of ubiquitin

Proteomic studies have revealed that ubiquitin is the target of several other post-translational modifications besides ubiquitylation, and the role of these modifications is starting to come into focus. Lysine acetylation has been detected on 6 out of 7 lysines on ubiquitin, although acetylation of K6 and K48 have been the focus of many studies (Lacoursiere et al., 2022). As expected, acetylation of these sites prevents ubiquitin chain formation at these sites. Less evidently, acetylation also limits ubiquitin chain formation at other ubiquitin lysines, with E2 enzymes unable to mediate the formation of ubiquitin chains with the modified ubiquitin. This modification can be regulated by the histone de-acetylases, suggesting a role for acetylated ubiquitin in maintaining mono- vs poly-ubiquitin signalling on histones (Ohtake et al., 2015; Seto and Yoshida, 2014).

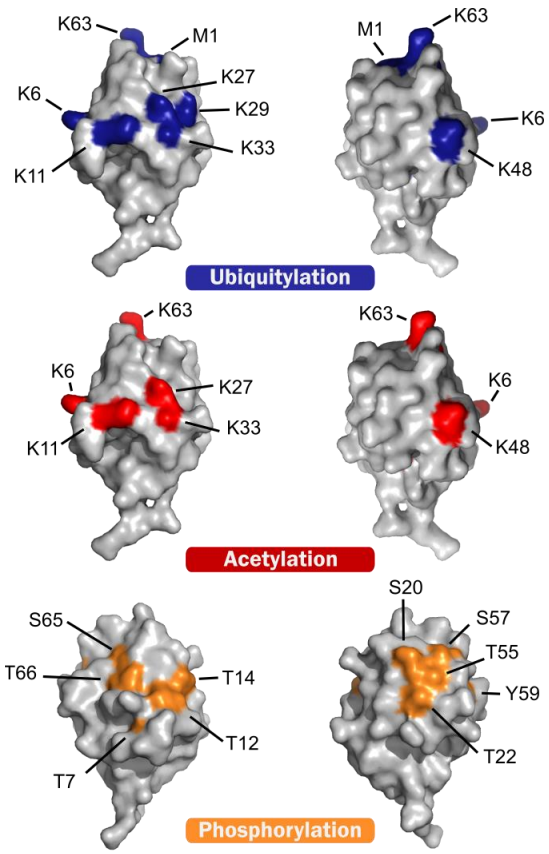

Figure 1.3: Ubiquitin is the target of several post-translational modifications. Modified sites on ubiquitin are highlighted and labelled. Images of ubiquitin 1UBQ from the Protein Data Bank (H.M. Berman et al., 2000; Vijay-Kumar et al., 1987) created with Pymol (Schrödinger and DeLano, 2020).

Ubiquitin-Like proteins (UBLs) share many structural features with ubiquitin, including the characteristic beta-grasp fold. Several members of this family, including NEDD4, and SUMO have been found to modify ubiquitin. The Small Ubiquitin-like MOdifiers (SUMO) family has several members (SUMO1, 2 and 3) that have been shown to form hybrid chains with ubiquitin, both as ubiquitylated SUMO, and SUMOylated ubiquitin (Pérez Berrocal et al., 2020). Ubiquitylation of SUMO is better characterised than the reverse, and the role of SUMOylated ubiquitin remains unclear.

1.3.1 Phosphorylation of Ubiquitin

An expanding area of research, and the focus of this thesis, is modification of ubiquitin by phosphorylation. Phospho-proteomics has revealed 10 unambiguous phospho-sites on ubiquitin (Figure 1.3) with an additional phospho-site at T9 proposed, indicating every serine and threonine on ubiquitin are targets for phosphorylation (Swatek and Komander, 2016). Of these 11 sites, only phosphorylation at S65 is well established, although more recent work has described roles for ubiquitin phosphorylated at S57 and T12, indicating the expanding roles of phosphorylated ubiquitin (Hepowit et al., 2020; Lee et al., 2017b; Walser et al., 2020). The body of work available gives insight not only into the expanding ubiquitin code, but regulation of ubiquitin signalling, as well as new insights into ubiquitin itself.

Phosphorylation at S65 was the first phosphorylated ubiquitin site to be described in a signalling pathway. Ubiquitin phosphorylated at S65 (pS65 ubiquitin) is an important modification in mitophagy, where damaged mitochondria are targeted for lysosomal degradation. Mutations in Parkin, an RBR ubiquitin ligase, and PINK1, a serine/threonine kinase, have been demonstrated to cause a heritable form of early onset juvenile Parkinson's Disease (Kitada et al., 1998; Valente et al., 2004). PINK1 is stabilised on the Outer Mitochondrial Membrane (OMM) of damaged mitochondria, where it phosphorylates Parkin in its UBiquitin-Like (UBL) domain at serine 65. This PTM was thought to be responsible for activating Parkin's E3 ligase activity, leading to increased ubiquitylation of proteins on the OMM, driving mitophagy. Work by Lazarou et al. (2013) identified that this model of mitophagy was incomplete. PINK1 activity was necessary but not sufficient to recruit Parkin to damaged mitochondria, and mutation of Parkin's UBL domain to prevent phosphorylation allowed for recruitment, but not ligase activity. Recruitment and activation of Parkin were separate events, and another step is required for full Parkin activity.

The “missing link” of this puzzle was identified as ubiquitin itself, with PINK1 not only phosphorylating the UBL domain of Parkin, but also ubiquitin at S65 (Kane et al., 2014). Studies using phospho-mimetic mutants of ubiquitin in the absence of PARK1 activity showed that this modification was sufficient for the recruitment of Parkin to mitochondria (Okatsu et al., 2015). An allosteric interaction between pS65 ubiquitin and Parkin, followed by phosphorylation of Parkin’s UBL domain by PINK1, releases the auto-inhibition of Parkin’s E3 ligase activity, enabling ubiquitylation of proteins on the OMM (Aguirre et al., 2017; Kazlauskaite et al., 2015; Kumar et al., 2017). Interestingly, there appears to be a requirement for modulating the ratio of ubiquitin to pS65 ubiquitin, with excessive pS65 ubiquitin inhibiting Parkin activity, as well as recruitment of the mitophagy machinery (Ordureau et al., 2018; Ordureau et al., 2014; Wauer et al., 2015a).

1.3.2 pS65-ubiquitin in the ubiquitin cascade

The discovery of a role for pS65 ubiquitin opened a path for research into pS65 ubiquitin itself. What impact does this phosphorylation have on ubiquitin’s structure, and is it used differently by other proteins in the ubiquitin cascade?

Ubiquitin is understood to be a well organised, stable, globular protein (Vijay-Kumar et al., 1987), so it was unexpected when phosphorylation at S65 was found to stabilise a second conformation of ubiquitin, in which the C-terminal tail is retracted, and the loop preceding the final β-pleated sheet, containing pS65, is flipped out and solvent exposed (Figure 1.4) (Dong et al., 2017; Wauer et al., 2015b). Even more of a surprise, non-phosphorylated ubiquitin was also found to adopt this conformation, and this “minor” form of ubiquitin is required for its phosphorylation by PINK1 (Gladkova et al., 2017; Schubert et al., 2017). In pS65 ubiquitin, the minor conformation has been detected in both free ubiquitin and K63 linked dimers, indicating the potential for this conformation in poly-ubiquitin conjugates (Wauer et al., 2015b).

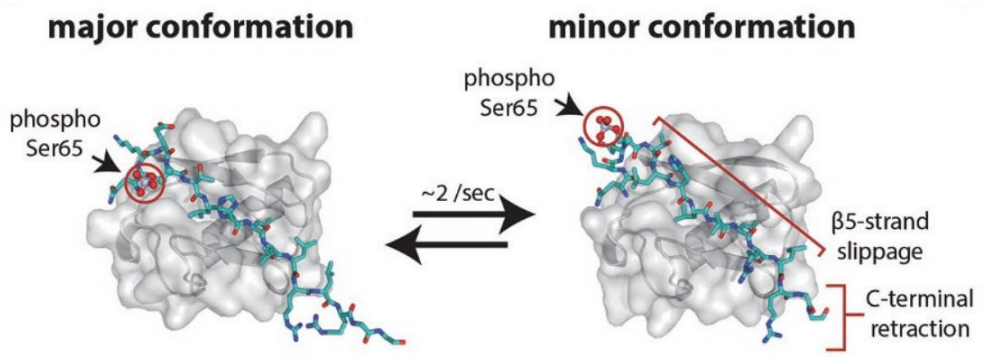

Figure 1.4: Phosphorylation of ubiquitin at S65 stabilises a minor conformation of ubiquitin. In this minor conformation, the C-terminal tail is retracted, and the preceding loop is flipped out and solvent exposed. Image adapted from Swatek and Komander (2016)

In addition to retraction of the C-terminal tail, adoption of the minor conformation disrupts the main ubiquitin recognition domains used by components of the ubiquitin cascade and readers of the ubiquitin code, including the Ile36 and Ile44 patches (Gladkova et al., 2017). Even without adopting the minor conformation, addition of a phosphate group introduces a large electronegative charge onto ubiquitin's surface, which was also predicted to alter protein interactions with ubiquitin (Wauer et al., 2015b).

Ubiquitin was found to be phosphorylated in both free and conjugated forms, presenting several ways phosphorylation could impact the ubiquitin cascade. The E1 enzyme UBA1 was found to use pS65 ubiquitin and charge the E2s tested, although mutation of the serine residue (to phospho-mimic or phospho-dead residues) were reported to be charged onto E2s less efficiently than WT ubiquitin (Swaney et al., 2015; Wauer et al., 2015b). Conjugation of pS65 ubiquitin by E2s and E3 enzymes to proteins was found to be affected, although there was variability in how different enzymes were affected. Some E2-E3 pairs showed increased activity with pS65 ubiquitin, while others were unable to use the modified ubiquitin at all in chain building. Importantly, many of these differences could be recapitulated using a phospho-mimetic mutant of ubiquitin (S65E) which does not stabilise the minor conformation of ubiquitin, allowing these changes to be attributed primarily to phosphorylation on the major conformation (Swaney et al., 2015; Wauer et al., 2015b).

The most striking impact of pS65 ubiquitin is on DUB activity. Wauer et al (2015b) tested 12 DUBs ability to dismantle poly-ubiquitin chains, of which 10 DUBs showed reduced activity against phospho-ubiquitin chains. Work with S65E ubiquitin revealed that this is not an "all or nothing" response. Ubiquitin dimers consisting of WT-WT, WT-S65E, or S65E-S65E ubiquitin revealed that DUB activity was partially reduced against the heterodimer, and was reduced further against the S65E homodimer (Swaney et al., 2015). The order of the di-ubiquitin species was not tested in this study (WT-S65E vs S65E-WT ubiquitin, e.g.), yet directionality may be important for DUB activity, with DUBs recognising different binding sites on distal and proximal ubiquitin (Komander et al., 2009). Nevertheless, the results together indicate a role for pS65 in regulating ubiquitin chain formation and turnover, as well as indicating ways this modification can be further fine-tuned.

1.3.3 Ubiquitin's other phosphosites

Phosphorylation of ubiquitin's surface tyrosine, Y59, has been detected in multiple phospho-proteomic datasets (Gu et al., 2011; Moritz et al., 2010; Rikova et al., 2007). Tyrosine phosphorylation is associated with many critical pathways in cell homeostasis, particularly in pathways responding to extracellular signalling, such as cell proliferation, cell cycle and transcription pathways (Aschner and Downey, 2018; Hunter, 2009). The Y59 residue of ubiquitin is important in the formation of K48 linked ubiquitin chains, a key chain type in signalling for proteasomal degradation (Chong et al., 2014). As such, it is interesting to speculate that phosphorylation of Y59 may be a deliberate modification in these signalling pathways, perhaps in preventing formation of K48 linked chains and promoting stability of the target protein. As of yet, an exact role for this modification remains unknown.

More recently, work investigating the roles of phosphorylation at ubiquitin's phosphoserine sites has begun. Using genetic code expansion techniques, phospho-serine can be directly incorporated into recombinant proteins in *E. coli* (Park et al., 2011). Non-hydrolysable analogues of phospho-serine are also possible, ensuring that this modification is not removed by endogenous phosphatases

(Rogerson et al., 2015). Using this approach, Huguenin-Dezot et al. (2016) explored the impact of phosphorylation of ubiquitin's other serine residues, S20, S57 and S65, on the ubiquitin cascade.

Phosphorylation at these residues was not found to impact E1 activity, or the loading of ubiquitin on E2 enzymes, consistent with the previous studies of pS65 ubiquitin. The impact on E2 and E3 enzymes was evaluated through ubiquitin chain building, by using specific E2/E3 combinations known to build specific chain types with WT ubiquitin. This work revealed that phosphorylation of different ubiquitin sites leads to different impacts on ubiquitin chain formation. The linear ubiquitin chain builders UBE2L and HOIP built many fewer chains with pS65 ubiquitin, and rather than purely M1-linked linear chains, 10% were instead K33 linked. Ubiquitin phosphorylated at S20 did not show a reduction in chain formation, but the chain types were again altered, this time from purely M1 to 9% K11 linked chains. Phosphorylation at S20 also altered chain formation by UBE3C, altering the chains built from roughly equal K29 and K48 linked chains, to primarily K48 linked chains.

DUB activity was tested using homodimers of ubiquitin, with the activity of the DUBs against phosphorylated homodimers compared against WT ubiquitin dimers. In agreement with the previous report by Wauer et al. (2015b), phosphorylation at the three sites tested was generally inhibitory towards DUB activity. Interestingly there are exceptions, with some DUBs showing increased activity against phosphorylated dimers. This increased activity was generally limited to just one phospho-ubiquitin species per DUB, and could be linkage specific, highlighting the role for specific chain recognition by DUBs, and showing how this could be regulated by phospho-ubiquitin. Crucially, the differences between the phospho-ubiquitin species makes it clear that there is specific phospho-ubiquitin signalling, and not just a generic "phospho-ubiquitin" signal. This allows for different phospho-ubiquitin species to be used in different specific pathways, such as the recently discovered role for pS57 in regulating the oxidative stress response in yeast, and endocytic trafficking, and makes it likely that the other ubiquitin phospho-sites also have specific roles in varying pathways (Hepowit et al., 2020; Lee et al., 2017b).

1.3.4 A role for pT12 ubiquitin

Phosphorylation of ubiquitin at T12 has been reported in a number of phospho-proteomic studies since 2009 (Bennetzen et al., 2010; Kettenbach et al., 2011; Lee et al., 2009; Zhou et al., 2013), but it is only recently that pT12 ubiquitin's role in the DNA damage response has been described (Walser et al., 2020). In response to DNA damage, histone H2A is ubiquitylated at K15, and this modification is required for the recruitment of 53BP1, a damage response protein involved in DNA repair by NHEJ, to chromatin around break sites. Phosphorylation of T12 of this ubiquitin modification prevents recruitment of 53BP1 whilst still being permissive to recruitment of proteins such as BRCA1 and RAD51, which are involved in DNA repair by HR. This indicates a potential role for pT12 ubiquitin in regulating DNA repair pathway choice.

Other roles for pT12 ubiquitin are possible. A phospho-dead ubiquitin mutant was also found to increase 53BP1 foci numbers in undamaged cells, and although pT12 was found to be increased upon treatment with DNA damaging agents, a considerable number of pT12 foci were identified in undamaged cells. Consistent with this, the authors report a basal level of pT12 present in cells, which is not decreased by inhibiting the DDR kinases, or by knocking down RNF168, the E3 ligase responsible for histone H2A-K15 ubiquitylation in the DNA damage response. Taken together, this could indicate that phosphorylated ubiquitin regulates histone modifications more generally, not just in the DNA damage response.

Many questions remain with pT12 ubiquitin. The kinase responsible has not been identified, and the authors of the paper recognise that there are likely to be other target proteins for pT12 ubiquitylation. However, the discovery of an additional modification in the DDR highlights how much is still unknown about this pathway, and expands the possibilities for phosphorylation-ubiquitylation crosstalk more generally in cellular homeostasis.

1.4 Double-Strand Break repair pathways

The DNA within cells is continually damaged from both endogenous and exogenous sources. The different sources of damage give rise to different lesions on the DNA, for which cells have evolved specialised pathways to detect and repair. Of all these lesions, breaks across both strands of the DNA (Double-Strand Breaks, DSBs) are widely recognised to be the most deleterious to the cell, with serious consequences for incomplete or inappropriate repair.

If DSBs are unrepaired, genetic information can be lost, particularly during mitosis or meiosis where acentromeric fragments fail to segregate and may not be incorporated into daughter nuclei (Tang et al., 2018). Fragments of unincorporated DNA may form micronuclei, which are not only an indicator of genomic instability, but are also a driver for further DSBs and instability, driving oncogenesis (Krupina et al., 2021). Unrepaired DNA damage also triggers the global DNA damage response, with cells exiting the cell cycle, leading to senescence, or triggering apoptosis (d'Adda di Fagagna, 2008; De Zio et al., 2013). Cells have evolved several, non-redundant pathways to repair DSBs, with the main repair pathways discussed below.

1.4.1 Homologous Recombination

Double strand break repair by Homologous Recombination (HR) is a multi-step process, requiring extensive resection of the break site, followed by homology search for template DNA, DNA synthesis to repair the break and terminating with resolution of secondary DNA structures formed during the process (Figure 1.5). The use of a DNA template, generally in the form of a sister chromatid, enables error free repair of the break. However this also limits HR repair to S/G2 of the cell cycle, when this sister chromatid is present, with active repression of HR observed in G1 (Fugger and West, 2016; Her and Bunting, 2018; Orthwein et al., 2015).

The DSB sensing complex MRN is found at the start of the HR pathway. The MRN complex is comprised of three proteins: MRE11, RAD50 and NBS1, which give rise to the complex's various functions. MRN has roles in both sensing DSBs, activating the DSB response pathway and as an

effector complex in DNA repair (Qiu and Huang, 2021; Stracker and Petrini, 2011). The MRN complex recruits CtIP, a protein with endonuclease activity, to the DSB. CtIP acts as a cofactor with MRN, and together with MRE11, which is also a nuclease, nicks the 5' strand of DNA and begins its 3' to 5' exonuclease activity to resect DNA towards the break site (Cejka, 2015; Zhao et al., 2020). This generates short sections of ssDNA overhangs, which recruits exonucleases for long-range resection of DNA. The long-range resection is effected by EXO1 or BLM-DNA2, and generates long 3' ssDNA overhangs which serve as a recruitment platform for Replication Protein A (RPA) (Daley et al., 2020).

RPA protects the ssDNA from nucleases, and prevents the formation of secondary structures which would inhibit DNA repair. The recombinase RAD51 then competes with RPA for binding, replacing the RPA with RAD51 filaments (Ma et al., 2017; Sun et al., 2020). RAD51 catalyses the homology search and strand invasion, with transient interactions with other proteins regulating and directing the recombination event (Ranjha et al., 2018). Strand invasion enables DNA synthesis of the damaged and resected DNA, using the homologous strand as a template.

From here, HR can proceed via one of two pathways. The predominant path is believed to be synthesis-dependent strand annealing (SDSA), in which a shorter tract of synthesised DNA can displace from the homologous template and re-anneal to the original DNA, repairing the break. The other mechanism leads to formation of secondary DNA structures called Holliday junctions, which must be resolved to repair the break site (Shah Punatar et al., 2017; Wright et al., 2018).

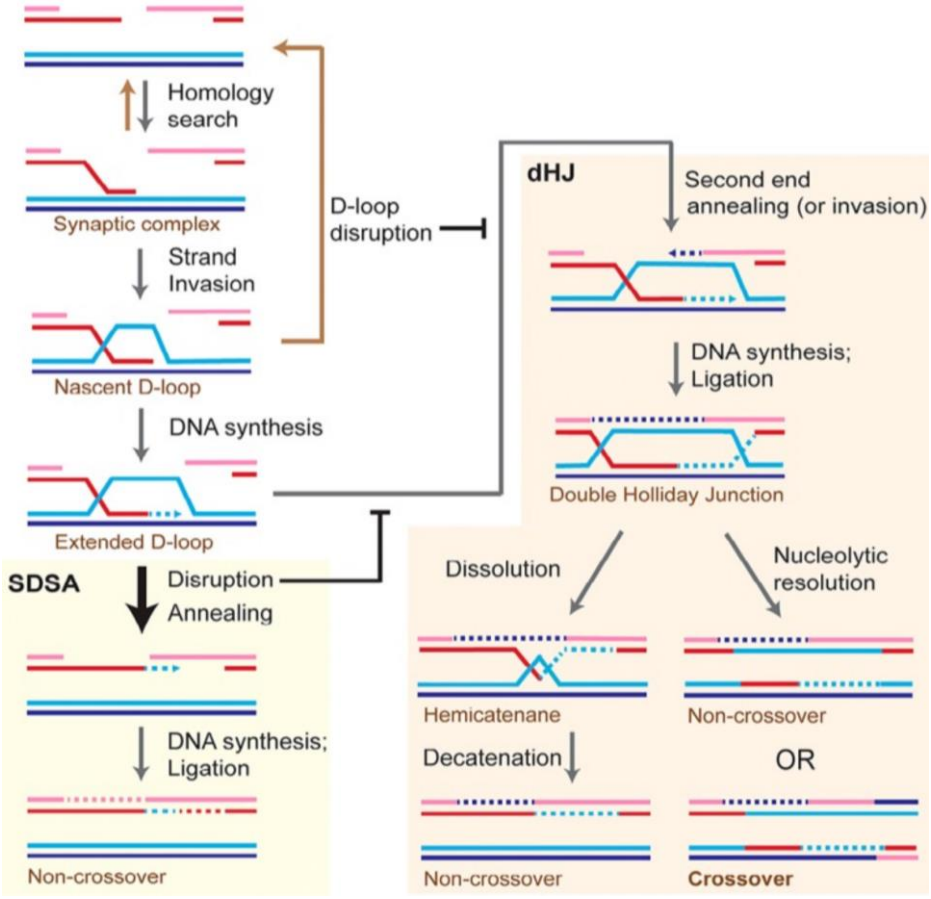

Figure 1.5: Model of Homologous recombination demonstrating the formation of crossover and non-crossover products. Image adapted from Wright et al. (2018)

In the process of resolving these structures, genetic material may be swapped between the original DNA, containing the break, and the template DNA, leading to “crossover products”. If the sister chromatid is used as a template, the crossover products are functionally neutral. However, HR can use homologous chromosomes as templates, with crossover products here potentially exchanging alleles between chromosomes. This mechanism is deliberately exploited in meiosis, where DSBs are deliberately introduced and repaired by HR, with crossover products enhancing the genetic diversity of the gametes produced (Baudat et al., 2013; Keeney et al., 2014). Exactly how the sub-pathway is determined in general DSB repair is still unclear, though it is likely highly regulated (Elbakry and Löbrich, 2021).

1.4.2 Repair by Non-Homologous End Joining

In contrast to the complexity of repair by HR, Non-homologous end joining (NHEJ) repair is a blunter instrument, directly ligating DNA ends to repair breaks. As there is no requirement for template DNA, NHEJ can occur throughout interphase. NHEJ is repressed during mitosis, as inappropriate activation leads to fusion of telomeres (Her and Bunting, 2018; Orthwein et al., 2014).

Like HR, NHEJ repair has sub-pathways, dictated by the complexity of the break site. With a simple blunt-end break, NHEJ requires very few proteins to effect repair. Ku70 and Ku80 form a ring-shaped heterodimer around the DNA ends. This recruits XRCC4-DNA ligase IV, which can bridge the gap between DNA ends and facilitate direct re-ligation of the break (Gu et al., 2007; Nick McElhinny et al., 2000). DSBs are not always so clean however, with ssDNA overhangs, damaged bases, and secondary structures all impeding direct ligation (Chang et al., 2017). This is observed in the biphasic kinetics of NHEJ repair, where 80% of breaks are repaired quickly, and the remaining 20% are slower and require additional proteins for repair (Riballo et al., 2004).

The Ku heterodimer is able to bind to a variety of DSB end structures, so it is quickly recruited to more complex breaks (Neal and Meek, 2011). DNA-PKcs is a large serine/threonine kinase that forms a holoenzyme, DNA-PK, with Ku at DNA ends. This kinase’s activity is required for ligating more

complex breaks, with a wide number of substrates phosphorylated by this enzyme. Oddly, the only phosphorylation by DNA-PK required for NHEJ is phosphorylation of DNA-PK itself (Neal and Meek, 2011). DNA-PK recruits the key NHEJ nuclease, Artemis, and the autophosphorylation of DNA-PK activates Artemis's enzymatic activity (Löbrich and Jeggo, 2017). Artemis can process several types of incompatible ends, including both 3' and 5' ssDNA overhangs, as well as hairpin ends, generating ligatable ends (Chang et al., 2016; Pannunzio et al., 2018).

Additional core proteins are XLF and PAXX, which play important roles in stabilising DNA ends that are distant from one another, facilitate bringing the DNA ends into proximity for ligation. It is unclear what role each of these proteins play – loss of either protein confers NHEJ defects for spontaneous breaks, and double knockout mice are embryonic lethal. However in lymphocytes, where DSBs are deliberately introduced and repaired by NHEJ, a repair defect is only seen in a double knockout (Balmus et al., 2016; Hung et al., 2017; Kumar et al., 2016).

1.4.3 Fidelity of NHEJ repair

NHEJ has traditionally been referred to as an error-prone pathway, particularly when compared to HR repair, but this characterisation does not fit with how DSBs are repaired during the cell cycle. Even in G2, when a template is available for error-free DNA repair, most breaks are still repaired quickly by NHEJ, with repair by HR occurring more slowly. Due to this, the repair of DSBs would be very mutagenic most of the time if NHEJ was a strongly error-prone pathway (Beucher et al., 2009). The slow, resection dependent NHEJ pathway is associated with small DNA insertions and deletions (indels), but it is not yet known whether the fast NHEJ pathway also contributes to these indels (Shibata and Jeggo, 2020). Analysis of I-Sce1 sites, which generate compatible ends when cut, indicates that NHEJ is largely error free, at least when repaired without resection (Bétermier et al., 2014).

At a chromosomal level, rearrangements caused by ligation of incorrect ends has been reported (Lieber, 2010). With no or very limited homology, re-ligation of broken ends is not specific, and

rearrangements of distal breaks is possible. However, safeguards such as break synapse formation by XLF and PAXX help guard against inappropriate re-ligation by stabilising neighbouring breaks and preventing “wandering” DNA. There is also evidence suggesting that end processing is limited until breaks form a short-range synapse, limiting translocations caused by free, easily ligatable ends (Stinson et al., 2020).

1.4.4 Alt-NHEJ

In the absence of canonical NHEJ (c-NHEJ) proteins, repair by DNA ligation still occurs (Daley and Wilson, 2005). This repair is slow, resection dependent, and also uses microhomologies to direct repair. Termed alt-NHEJ, this pathway is distinct from c-NHEJ, using different sensors, nucleases and ligases to effect repair. This is best exemplified by Ku, a necessary c-NHEJ protein, supressing repair by alt-NHEJ (Bennardo et al., 2008; Chang et al., 2017).

Questions remain as to whether alt-NHEJ is simply a backup pathway, or whether it has its own distinct roles in repair. Arguments have also been made that alt-NHEJ may not be one pathway, but a collection of minor repair pathways (Boboila et al., 2010; Chiruvella et al., 2013; Saha et al., 2021; Sfeir and Symington, 2015). The finding that HR deficient tumours, which are common in breast and ovarian cancers, rely on alt-NHEJ is suggestive of alt-NHEJ having its own roles in DSB repair, and highlights the therapeutic potential of manipulating DNA damage pathways (Ceccaldi et al., 2015).

1.4.5 Programmed DSBs and repair by NHEJ in lymphocytes

Because of c-NHEJ’s potential for translocations, programmed DSBs repaired by NHEJ are critical in the development of the immune system. V(D)J recombination, the process by which the antigen recognition sites of antibodies and T-cell receptors are generated, relies on translocations and small mutations introduced by resection-dependent NHEJ to generate the extreme diversity of antigen-recognition sites required (Slatter and Gennery, 2020). In addition to antigen recognition, the antibody isotype also needs to be varied in order to activate the full immune complement. In immature B cells, IgM heavy chain antibodies are predominant, but during maturation genomic

rearrangements enable the production of other isotypes in a process known as Class Switch Recombination (CSR). These rearrangements are again achieved through translocations during DSB repair at specific loci (Kotnis et al., 2009).

As c-NHEJ is critical for immune system development, deficiencies in c-NHEJ proteins manifest as immunodeficiencies, collectively referred to as RS-SCID (RadioSensitive, Severe Combined ImmunoDeficiency). Specific phenotypes are observed within this broad category, depending on the protein affected (Woodbine et al., 2014). This has made lymphocytes an interesting model for studying NHEJ repair, and has led to insights into the interplay between c-NHEJ and alt-NHEJ pathways, and highlighted the more direct roles in repair of proteins normally associated with DSB response (Saha et al., 2021; Slatter and Gennery, 2020; Sundaravinayagam et al., 2019).

1.5 The DNA Damage Response drives repair pathway choice

Upon detection of a double strand break, a wider signalling network known as the DSB response is activated. The DSB response can prevent cell cycle progression through use of DNA damage checkpoints, which can delay progression, but also lead to permanent exit from the cell cycle, or trigger apoptotic pathways under specific conditions (Matthews et al., 2022). The DSB response also alters transcription, increasing transcription of regulatory and pro-apoptotic factors within the cell. Local to the break site transcription of genes is repressed. Transcription of small non-coding RNAs is induced however, and these transcription products are coming into focus as a key signalling mechanism in DSB repair (Long et al., 2021).

As well as this outward signalling, from the DSB to global cell signalling, the DSB response also signals inward towards the break site, collating information about the cell to direct repair pathway choice. Commitment to a repair pathway is regulated by controlling the extent and timing of DNA end resection (Symington and Gautier, 2011). Extensive resection of the break site is necessary for repair by HR, but the long ssDNA overhangs are inhibitory towards repair by NHEJ. The DDR steers the recruitment of proteins that protect or resect DSB ends to ensure that repair takes place,

factoring in information such as the cell cycle stage, to ensure that repair takes place in the most appropriate manner (Chapman et al., 2012b). Phosphorylation and ubiquitylation take centre stage in these signalling pathways, directing repair pathway choice (Blackford and Jackson, 2017; Kciuk et al., 2022; Schwertman et al., 2016).

1.5.1 Early responders of the DDR

The start of the DSB Response is common to both repair pathways – the detection of the DSB. Whilst there are other proteins involved in sensing DSBs, two come into focus when discussing repair pathway choice – the MRN complex and the Ku heterodimer. The MRN complex is generally associated with repair by HR due to its partnership with CtIP and its own endonuclease activity, required for generating the ssDNA required for HR progression (Limbo et al., 2007). The Ku heterodimer is a core part of the NHEJ repair machinery, forming the holoenzyme DNAPK when in complex with the catalytic subunit (Yue et al., 2020). Both proteins are rapidly loaded onto dsDNA ends, helping to sense the break. Retention, removal and activation of these proteins are governed by PTMs placed by downstream signalling in the DSB response, directing repair pathway choice.

Ubiquitylation of the Ku heterodimer is important in regulating pathway choice. Before repair, retention of Ku on DNA can act as a barrier to resection, protecting against the endonuclease activity that promotes HR. In S/G2 phases of the cell cycle RNF138, a ubiquitin E3 ligase, ubiquitylates Ku to promote its removal from DSB, promoting HR (Ismail et al., 2015). This activity may be downstream of initial resection by the MRN-CtIP complex, as RNF138 acts to retain CtIP at DSB sites, and shows a strong preference for ssDNA, which would be generated following initial resection. Another E3 ligase, RNF8 also ubiquitylates Ku, but in G1 of the cell cycle. This removal of Ku is likely to be pro-NHEJ, as removal of Ku is required for successful completion of DSB repair by NHEJ (Feng and Chen, 2012). These two signals are dependent upon cell cycle stage, and illustrate one aspect of the DSB response in repair pathway selection.

The MRN complex has so far been viewed with respect to its endonuclease activity in DSB repair. This complex also has a fundamental role in the DSB response, activating the apical DSB response kinase, ATM. In this way, the MRN complex acts as a transducer between the physical DNA break and the chemical signalling pathway that follows (Paull, 2015). As the apical kinase, ATM activation impacts a wide range of cellular processes, including cell cycle progression and recruitment of DDR proteins, through phosphorylation directly of DSB proteins and through chromatin-based DDR signalling (Menolfi and Zha, 2020). Deficiencies in ATM are responsible for the disorder Ataxia Telangiectasia (A-T), which is characterised by radiosensitivity, immunodeficiency and cancer predisposition as a result of compromised DSB repair (Rothblum-Oviatt et al., 2016).

One of the targets of ATM is the histone variant H2AX, which is phosphorylated at S129. This phosphorylated form of H2AX is known as γH2AX. This mark appears rapidly after DSB induction and spreads to the surrounding chromatin, where it serves as a recruitment platform for downstream DDR proteins through their phospho-recognition domains (Rogakou et al., 1999). MDC1 is one of these proteins, recruited via its tandem BRCT domains (Stucki et al., 2005). MDC1 itself also acts as a recruitment platform, with phosphorylation of this protein by ATM creating additional recognition motifs for DDR proteins (Ruff et al., 2020). The E3 ligase RNF8 is one of these proteins, recruited to phosphorylated TQXF motifs on MDC1 via its FHA domains (Kolas et al., 2007). RNF8 is the first of two “classical” E3 ubiquitin ligases in the DSB response, the activity of which recruits the second ligase, RNF168. Initially RNF8 and RNF168 were thought to act in partnership to drive the DDR, with RNF8 placing an initial priming ubiquitylation, and RNF168 extending this modification as ubiquitin chains (Doil et al., 2009; Stewart et al., 2009). This has since been challenged, with RNF168 shown to monoubiquitylate histone H2A at lysine 13/15, and RNF8 promoting polyubiquitylation of other proteins (Mattiroli et al., 2012).

Despite the importance of these ubiquitin ligases, the exact targets of RNF8 and the mechanism of recruitment for RNF168 remain unclear. Work by Thorslund et al. (2015) proposed K63-linked

polyubiquitylation of histone H1 by RNF8 as the driver of RNF168 recruitment to damage sites. Doubt has been cast on this being the mechanism of recruitment for RNF168, as other studies report only monoubiquitylation, or ubiquitylation catalysed by other E2-E3 complexes at this site (Liu et al., 2013; Nowsheen et al., 2018). RNF8 interacts with other E3 ligases, including HERC2 and HUWE1, the latter of which is proposed to also ubiquitylate histone H1 (Mandemaker et al., 2017). Ubiquitylation of histone H1 has been linked to the recruitment of BRCA1 to DSB sites, with downstream effects of chromatin remodelling, relaxing chromatin to allow repair proteins access to the break site (Clouaire et al., 2018; Sherker et al., 2021). This remodelling appears to promote repair by HR over NHEJ, but recruitment of RNF168 by RNF8 helps drive NHEJ, giving RNF8 roles in both pathways (Tsai et al., 2020).

More recently, ubiquitylation of L3MBTL2 has been identified as a recruitment site for RNF168, with L3MBTL2 knockdown causing normal MDC1 and RNF8 recruitment, but impaired RNF168 localisation and reduced ubiquitylation (Nowsheen et al., 2018). It remains to be seen whether RNF168 is solely dependent upon this PTM, or if other substrates also facilitate recruitment.

Two proteins downstream of RNF8/168 are often seen as reflections of commitment to a repair pathway. The first, BRCA1, has been mentioned above, and is seen as a commitment to repair by HR. The second, 53BP1, is a marker of repair by NHEJ. Both proteins can be visualised as foci using immunofluorescence microscopy following induction of DSBs, colocalising with sites of damage. These proteins and their roles in DSB repair are explored below.

1.5.2 BRCA1 drives DSB repair by HR

BRCA1 is a clinically important protein, with mutations causing a highly penetrant pro-oncogenic phenotype. Before the age of 70, 65% of mutation carriers develop breast cancer, and 48% develop ovarian cancer (Chen et al., 2020). Other cancer types are also seen, including pancreatic and prostate cancers. Critically, BRCA1 mutations lead to a deficiency in HR repair which drives genomic instability and the oncogenic phenotype, but also presents opportunities for chemotherapeutic

drugs in patients with these mutations (Aly and Ganesan, 2011; Pilarski, 2019). BRCA1 has a number of roles, including replication fork protection during DNA synthesis (Daza-Martin et al., 2019) and repair of inter-strand DNA cross-links (Bunting et al., 2012), however it is its role in double strand break repair and response that will be the focus of this section.

BRCA1 is a RING-type E3 ubiquitin ligase, and forms an obligate heterodimer with another RING E3 ligase, BARD1 (Brzovic et al., 2001). This partnership promotes the stability of both proteins, as well as their E3 ligase activity (Hashizume et al., 2001). BRCA1-BARD1 can also form larger complexes (BRCA1-A, B, and C) which contribute to its varying functions, as well as its recruitment to DSBs. Alone, the BRCA1-BARD1 complex has a bipartite recognition mechanism, reading both histone ubiquitylation and methylation status. Ubiquitylation at histone H2A at K13/15 is one requirement, and this modification is placed by RNF168 throughout the cell cycle in response to DSBs (Hu et al., 2017). Additionally, the complex requires an absence of methylation at histone H4 lysine 20 (H4K20Me0), with this modification present on newly synthesised chromatin through the incorporation of novel histones to replicated DNA (Becker et al., 2021; Nakamura et al., 2019). This bipartite recruitment mechanism limits recruitment of BRCA1 to S/G2 phases of the cell cycle, where this modification is present. BRCA1 has another ubiquitin dependent pathway for recruitment to DSBs through formation of a larger complex, BRCA1-A. This complex includes RAP80, which contains UIM motifs that recognise K63 linked chains placed by RNF8 in response to DSBs, promoting recruitment of BRCA1 to damage sites (Yan and Jetten, 2008).

At DSB sites, BRCA1 both promotes repair pathway choice towards HR, and has a direct role in repair by HR, by recruiting BRCA2 to damage sites. BRCA2 mediates the recruitment of the recombinase RAD51 to the ssDNA overhangs formed by DNA end-resection, which is an essential step in repair by HR (Moynahan et al., 2001). BRCA1 does not recruit BRCA2 directly – instead both proteins interact with PALB2, which bridges the interaction (Zhang et al., 2009). This interaction is mediated by the DSB response through the cell cycle. Throughout the cell cycle, PALB2 is ubiquitylated by CUL3-RBX1

in complex with KEAP1, a PALB2 interacting protein, and this supresses the BRCA1-PALB2 interaction. The DUB USP11 counteracts this modification, balancing PALB2-BRCA1 interaction. In G1 of the cell cycle, USP11 is targeted for degradation by the proteasome in response to DSBs by the activity of CUL4. In S/G2 however, USP11 is not degraded and is free to deubiquitylate PALB2, enabling the BRCA1-PALB2 interaction and promoting repair by HR (Orthwein et al., 2015).

Outside its direct role in HR, BRCA1 also promotes pathway choice towards HR by promoting DNA end resection. One mode is through its interaction with phosphorylated CtIP. BRCA1 interacts with the phospho-motif via its tandem BRCT domains, and subsequently poly-ubiquitylates CtIP, which promotes the interaction between CtIP and chromatin, facilitating its endonuclease activity (Yu et al., 2006). Whilst the BRCA1-CtIP interaction is not required for CtIP activity, as shown by separation of function mutations (Polato et al., 2014; Reczek et al., 2013), this interaction facilitates end resection and promotes repair by HR (Cruz-Garcia et al., 2014).

A major role for BRCA1 in promoting HR is in overcoming barriers to end resection. The HR deficiency seen with BRCA1 mutations can be overcome by concomitant loss of 53BP1, a protein that forms part of an end protection complex and promotes repair by NHEJ (Aly and Ganesan, 2011; Bouwman et al., 2010). This indicates that whilst BRCA1 is not directly responsible for the resection of DNA, it is critical in overcoming the barriers to resection posed by 53BP1. BRCA1 orchestrates this activity by relocating 53BP1 to the periphery of the damage site, rather than the epicentre of the DSB (Chapman et al., 2012a). Ubiquitin signalling is important for the relocation of 53BP1, with BRCA1's own E3 ligase activity serving to recruit the chromatin remodeller SMARCAD1, which promotes the repositioning (Densham et al., 2016). Additionally the DUB activity of POH1 helps move 53BP1 to the periphery of the break site (Kakarougkas et al., 2013). Removing 53BP1 and its associated end-protection complex from the break site allows the extensive end resection required for progression of HR.

1.5.3 53BP1 guards against resection to drive repair by NHEJ

53BP1 is a large scaffolding protein with a wide array of roles, but is particularly known for its role in the DDR, where it promotes repair by NHEJ. 53BP1 contains many domains which contribute to its recruitment to DSBs, and also the recruitment of downstream effector proteins (Figure 1.6). Recruitment to DSB sites can be visualised by immunofluorescent microscopy as discrete foci, and a subset of domains has been identified as essential for this localisation and termed the minimal focus forming region (MFFR). Of these domains, the role of the UDR and Tudor domains are best characterised.

Ubiquitylation of histone H2A at K13/15 is strictly required for recruitment of 53BP1 to DSBs, and is recognised by the UDR domain. Monoubiquitylation of H2AK15 by RNF168 is described as the canonical mark required for recruitment, although RNF168 is also known to ubiquitylate K13, with evidence that polyubiquitylation at this site is also capable of recruiting 53BP1 (Fradet-Turcotte et al., 2013; Liang et al., 2019; Wilson et al., 2016). Histone-fusion proteins with ubiquitin fused at the N-terminal end of histone H2A were also sufficient to give a partial rescue of 53BP1 foci formation in absence of RNF168, further suggesting plasticity in 53BP1 recruitment (Kocyłowski et al., 2015). The activity of RNF168 appears to be essential for 53BP1 recruitment, with knockdown of RNF168

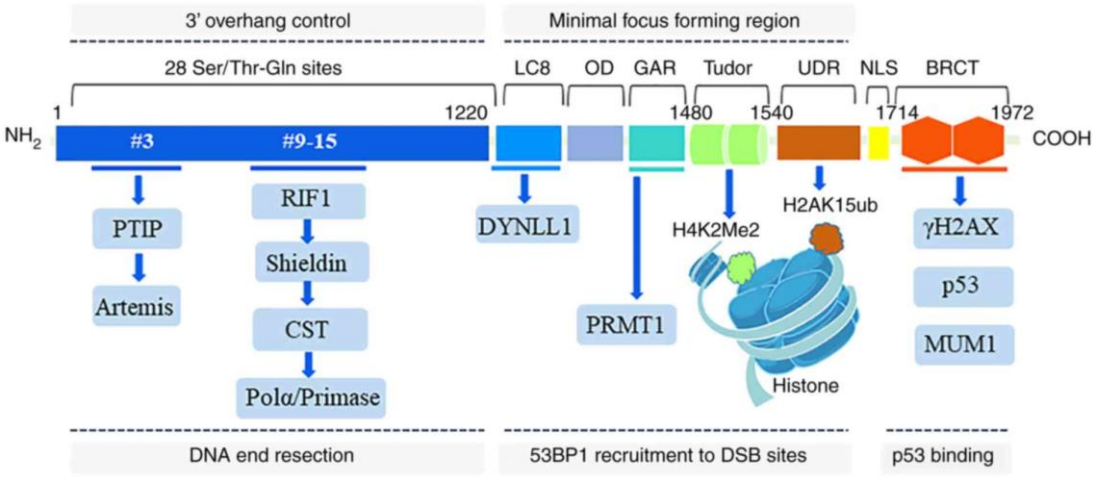

Figure 1.6: 53BP1's domains contribute to its recruitment, and recruitment of downstream effector proteins. Image from Lei et al. (2022)

leading to loss of 53BP1 foci, and cells from patients with a defect in RNF168 (called RIDDLE syndrome) also showing this loss of 53BP1 foci (Kelliher et al., 2022; Stewart et al., 2007).

53BP1 is a bivalent reader of histones, simultaneously recruited to ubiquitylated histone H2A and di-methylated histone H4 at lysine 20 ($H4K20Me_2$), which it recognises via its Tudor domain. $H4K20Me_2$ is a very common histone modification, and is not directly induced by DNA damage, hence 53BP1's interaction with this site must be regulated to prevent inappropriate recruitment. This regulation happens at the nucleosome, as well as on 53BP1 itself. The $H4K20Me_2$ mark is diluted in newly synthesised chromatin, due to the incorporation of newly synthesised nucleosomes. This may make binding of BRCA1, and repair by HR preferable in this condition (Simonetta et al., 2018). The di-methylation PTM is quickly restored on the new nucleosomes, so 53BP1 binding can occur throughout the cell cycle and is not limited to pre-replicative chromatin.

53BP1's interaction with the $H4K20Me_2$ mark is often sterically hindered. In undamaged conditions, 53BP1's Tudor domain is masked by a secondary protein, TIRR (Tudor-Interacting repair regulator). This protein dissociates from 53BP1 after DNA damage, freeing the Tudor domain for interaction (Drané et al., 2017). The $H4K20Me_2$ site itself is also masked by various proteins, including L3MBTL1/2 and JMJD2A. Ubiquitylation of these proteins promotes their removal from chromatin, unmasking the $H4K20Me_2$ site and allowing 53BP1 interaction (Acs et al., 2011; Mallette et al., 2012).

Although the activities of the UDR and Tudor domains are best understood, other domains in the MFFR also contribute to 53BP1's recruitment and retention at DSBs. 53BP1's MFFR contains an oligomerisation domain, with dimerization and higher order oligomers found to contribute to both 53BP1's recruitment to DSBs and its role in NHEJ, possibly in synapsing long distance synapses between DNA ends (Lottersberger et al., 2013; Zgheib et al., 2009). Recent work suggests that recruitment of 53BP1 can be independent of oligomerisation through interactions between the LC8 domain in the MFFR and the hub protein DYNLL1 (also known as LC8), though it appears that under

normal conditions both domains contribute to recruitment and oligomerisation of 53BP1 (Becker et al., 2018).

Perhaps surprisingly, given their roles in other DDR proteins, 53BP1's tandem BRCT domains do not form part of the MFFR. A direct interaction between 53BP1 and γH2AX is known, but is not required for 53BP1 recruitment to DSBs (Kleiner et al., 2015; Kocyłowski et al., 2015). These domains are largely dispensable for 53BP1's role in NHEJ repair (Bothmer et al., 2011; Ward et al., 2006), but do contribute to 53BP1's wider roles in cellular homeostasis and the DSB response through regulation of p53, a master regulatory protein with vital roles in the DNA damage response (Cuella-Martin et al., 2016; Joo et al., 2002).

The GAR domain, which does form part of the MFFR, has a poorly defined role in 53BP1's activity. GAR domains in other proteins are associated with nuclear localisation, and guide interactions with other proteins, particularly when methylated (Shubina et al., 2020). PRMT1 methylates 53BP1's GAR domain, and SIRT7, known to interact with GAR domains in other proteins, also interacts with 53BP1 with knockdown of SIRT7 reducing 53BP1 foci formation. Despite these links, and exact role and mechanism for the GAR domain and interacting proteins is still unclear (Boisvert et al., 2005; Vazquez et al., 2016).

Recruitment of 53BP1 to DSBs promotes NHEJ repair by blocking end resection of DNA. Whilst there is some suggestion that 53BP1 can prevent resection by steric occlusion of DSB ends, recruitment of downstream effector proteins such as PTIP, RIF1 and the Shieldin complex likely provide the main mechanism of DNA end protection (Callen et al., 2020; Marini et al., 2019; Setiaputra and Durocher, 2019). These proteins are recruited through phosphorylation by ATM or ATR of the S/TQ repeats in 53BP1's N-terminal region.

RIF1 links 53BP1 and the shieldin complex (comprised of REV7, SHLD1/2/3), a major effector of 53BP1's end protection role (Callen et al., 2020). This complex protects DNA ends from the extensive resection required for HR, in part by physically blocking access and activity of endonucleases

(Mirman et al., 2018; Paiano et al., 2021). SHLD2, a core component of the shieldin complex, has ssDNA binding OB domains, analogous to those found in RPA. These OB domains are critical to the function of the shieldin complex (Dev et al., 2018; Noordermeer et al., 2018). Interaction of these domains with the ssDNA may act to prevent or displace RPA binding, antagonising repair by HR (Dev et al., 2018).

The shieldin complex also recruits the CST complex (CTC1, STN1, TEN1), which in turn brings Pol α-primase. The action of Pol α-primase directly counteracts the activity of endonucleases by synthesising DNA at DSB ends, restoring dsDNA (Mirman et al., 2018). Inhibition of this DNA synthesis did increase the length of DNA resection though not to the same extent as observed with loss of 53BP1, indicating that this synthesis is unlikely to be the primary means by which 53BP1 limits end resection and promotes repair by NHEJ (Mirman et al., 2018; Paiano et al., 2021).

RIF1 and PTIP are recruited to overlapping phosphorylated motifs on 53BP1, leading to competition for their recruitment to 53BP1. The overlap is incomplete however, allowing their functions to be ascertained by differential mutations of 53BP1. Through this, two distinct pathways of end protection were established, with PTIP preventing the endonuclease activity of DNA2, and RIF1 acting to prevent EXO1's endonuclease activity. Additional roles for these effector proteins have also been established - RIF1 recruits the Shieldin complex to sites of damage, further preventing end resection and preventing RAD51 loading (Callen et al., 2020). PTIP also interacts with Artemis, a core NHEJ nuclease, creating a link between 53BP1 and NHEJ repair (Wang et al., 2014).

1.6 Project aims and objectives

Appropriate repair of DSBs is a vital part of cellular homeostasis. Post-translational modifications, particularly ubiquitylation and phosphorylation, are key drivers of this repair, with considerable impacts on human health and disease. Despite their importance, understanding of their roles and regulation remains incomplete. Further complexity has also been introduced, with the discovery of ubiquitin phosphorylated at T12 as an additional PTM in the DSB response.

An incidental finding from the Gambus lab suggests that T12 is not the only phospho-site on ubiquitin with a role in the DSB response. Ubiquitin phosphorylated at T66 was identified in mass spectrometry data from samples of chromatin from *Xenopus laevis* egg extract after induction of DSBs. This discovery led to the start of my PhD project, and the following aims have been identified:

1) **Is phosphorylation of ubiquitin at T66 in response to DNA damage conserved in mammalian cells?**

   Although identified in our lab in *Xenopus laevis* egg extract, phospho-proteomic screens of mammalian cells have also identified pT66 ubiquitin. Despite identification, no work has been undertaken to characterise this modification. My first aim is to determine whether pT66-ubiquitin is a conserved modification in mammals, and whether this modification is part of a response to DNA damage.

2) **What is the role of this modification in the DSB response?**

   Ubiquitin modifications are emerging as significant signalling modifications. Phosphorylation of ubiquitin at serine 65 was found to be clinically relevant, with dysregulation linked to Juvenile Parkinson's Disease. Identification of the signalling pathway that pT66-ubiquitin is part of, and its role within this pathway, not only expands our understanding of ubiquitin signalling, but may also highlight clinically relevant targets.

3) **How is this modification regulated in the DSB response?**

   What proteins are involved in the formation and recruitment of pT66 ubiquitin in the DDR? Using the phenotypes identified from using the ubiquitin mutants to narrow down potential pathways, the proteins involved in regulating this PTM will be explored.

Chapter 2: Materials and Methods

2.1 Tables

Table 2.1: Plasmids used. Shown is a summary of the plasmids used in this thesis.

Plasmid	Backbone	Source
HIS-tagged ubiquitin		
WT ubiquitin	pcDNA 5.1 FRT/TO	Morris lab (not published)
T66A ubiquitin		This Study
FLAG-tagged ubiquitin – extended tail		
WT ubiquitin	pcDNA 3.1	Penengo lab (Walser et al., 2020)
S65A ubiquitin		This Study
T66A ubiquitin		This Study
K63R ubiquitin		This Study
FLAG-tagged ubiquitin – introduced stop codon		
WT ubiquitin	pcDNA 3.1	This Study
S65A ubiquitin		This Study
T66A ubiquitin		This Study
T66D ubiquitin		This Study
K63R ubiquitin		This Study
T12A ubiquitin		This Study
T12D ubiquitin		This Study
Other Plasmids		
pOG44 recombinase	pOG44	Morris lab (Daza-Martin et al., 2019)
Empty vector	pcDNA5.1 FRT/TO	Morris lab (Daza-Martin et al., 2019)

Table 2.2: Primers used for site-directed mutagenesis. Shown are the primers and their sequences used to create the plasmids used during this PhD.

Primer name	Sequence	
S65A forward	CCA GAA AGA GGC CAC CCT GCA CC	Mutation of serine 65 to alanine in ubiquitin
S65A reverse	ATG TTG TAG TCA GAC AGG GTG CG	
T66A forward	GAA AGA GTC CGC CTT GCA CCT G	Mutation of threonine 66 to alanine in ubiquitin
T66A reverse	TGG ATG TTG TAG TCA GAC AG	
T66D forward	GAA AGA GTC CGA CCT GCA CCT GG	Mutation of threonine 66 to aspartic acid in ubiquitin
T66D reverse	TGG ATG TTG TAG TCA GAC	
K63R forward	AAC ATC CAG AGA GAG TCC ACC C	Mutation of lysine 63 to arginine in ubiquitin
K63R reverse	GTA GTC AGA CAG GGT GCG	
Stop codon forward	TCT CAG AGG TGG GTA ATT CTG CAG ATA TC	Introduction of stop codon after G76
Stop codon reverse	CGG AGG ACC AGG TGC AGG	
T12A forward	GAC TGG TAA GGC CAT CAC TCT CG	Mutation of threonine 12 to alanine in ubiquitin
T12A reverse	AGG GTC TTC ACG AAG ATC TG	
T12D forward	GAC TGG TAA GGA CAT CAC TCT CG	Mutation of threonine 12 to aspartic acid in ubiquitin
T12D reverse	AGG GTC TTC ACG AAG ATC	

Table 2.3: siRNA oligos used. Shown are the siRNA oligos and their sequence, used for knockdown of the indicated proteins. Referenced is the source for the original sequence.

siRNA	Sequence	Source
UBA52 (ubiquitin)	ACA CCA TTG AGA ATG TCA A	Dharmacon (Gatti et al., 2015)
RPS27A (ubiquitin)	AGG CCA AGA TCC AGG ATA A	Dharmacon (Gatti et al., 2015)
RNF168	CGT GGA ACT GTG GAC GAT AAT TCA A	Dharmacon (Gatti et al., 2015)
BRCA1	Commercial siRNA pool	Dharmacon SiGenome (M-003461-02)
Non-Targeting	Commercial siRNA pool	Dharmacon On-TARGET (D001810-10)

Table 2.4: Antibodies used. Shown are the antibodies used during this project, including their application, dilution, and diluent.

Antibody	Species	Company	Use	diluent
Primary antibodies				
53BP1	Mouse	Sigma Aldrich (MAB3802)	IF, 1:1000	3% BSA in TBS or PBS
53BP1	Rabbit	Novus Biologicals (NB100-904)	IF, 1:1000	3% BSA in TBS or PBS
α-tubulin	Mouse	Sigma Aldrich (T9026)	IB, 1:5000	3% milk in TBST
β-actin (HRP conjugated)	Mouse	Santa Cruz (sc-47778)	IB, 1:20,000	3% milk in TBST
BRCA1 (D9)	Mouse	Santa Cruz (sc-6954)	IF, 1:200	3% BSA in TBS or PBS
BrdU	Rat	Bio-Rad (MCA2060)	IF, 1:250	3% BSA in TBS or PBS
CENPF (mitosin)	Mouse	BD Biosciences (610768)	IF, 1:1000	3% BSA in TBS or PBS
FLAG (L5)	Rat	Biolegend (637301)	IF, 1:1000	3% BSA in TBS or PBS
FLAG (M2)	Mouse	Sigma Aldrich (F1804)	IB, 1:1000 IF, 1:1000	3% milk in TBST 3% BSA in TBS or PBS
γH2AX	Mouse	Sigma Aldrich (JBW301)	IF, 1:1000	3% BSA in TBS or PBS
γH2AX	Rabbit	Trevigen (4418-APC-100)	IF, 1:1000	3% BSA in TBS or PBS
Histone H3	Rabbit	Cell Signalling (9715S)	IB, 1:2000	3% milk in TBST
Poly-HIS	Mouse	Sigma (H1029)	IB, 1:1000	3% milk in TBST
MDC1	Rabbit	Stewart lab (Stewart et al., 2003)	IF, 1:500	3% BSA in PBS
pT66 ubiquitin	Rabbit	Dundee Cell Products	IB, 1:1000 IF, 1:1000	3% BSA in TBST 3% BSA in TBS
U1 snRNP	Mouse	Santa Cruz (sc-390899)	IB, 1:1000	3% BSA in TBST
Ubiquitin (P4D1)	Mouse	Cell Signalling (3936S)	IB, 1:1000 IF, 1:1000	3% milk in TBST 3% BSA in TBS or PBS
Secondary Antibodies				
AF488 anti-mouse		Invitrogen (A32723)	IF, 1:1000	3% BSA in TBS or PBS
AF555 anti-rabbit		Invitrogen (A32732)	IF, 1:1000	3% BSA in TBS or PBS
AF647 anti-mouse		Invitrogen (A32728)	IF, 1:1000	3% BSA in TBS or PBS
AF647 anti-rat		Invitrogen (A48272)	IF, 1:1000	3% BSA in TBS or PBS
HRP-IgG anti-mouse		Sigma (5278)	IB, 1:10,000	3% milk in TBST
HRP-IgG anti-rabbit		Sigma (A05451)	IB, 1:25,000	3% milk in TBST

Table 2.5: Buffers used. All buffers diluted in dH_2O unless otherwise indicated. When inhibitors are to be added to a buffer, these should be added immediately prior to use.

Buffer	Composition
Hypotonic buffer	20 mM Tris-HCl (pH 7.4) 10 mM NaCl 3 mM $MgCl_2$
Inhibitors To be added to buffers immediately prior to use, where indicated, then kept on ice or at 4°C. Do not store.	1 µg/ml Aprotinin 1 µg/ml Pepstatin 1 µg/ml Leupeptin 0.1 mM PMSF 2 mM Sodium Orthovanadate 1 mM β-glycerophosphate 10 mM Chloroacetamide 10 mM N-ethylmaleimide
Methylene blue	2% w/v Methylene blue 50% Ethanol in dH_2O
Nuclei lysis buffer	1% v/v IPEGAL 20 mM HEPES (pH 7.5) 300 mM NaCl 0.2 mM EDTA 1 M Urea 3 mM $MgCl_2$
TBST	20 mM Tris-HCl (pH 7.4) 150 mM NaCl 0.1% w/v SDS
Transfer buffer	25 mM Tris-HCl (pH 7.4) 190 mM Glycine 20% v/v Methanol
Tris-glycine running buffer	25 mM Tris-HCl (pH 7.4) 250 mM Glycine 0.1% w/v SDS
UT buffer	8 M Urea 50 mM Tris-HCl (pH 8) 150 mM β-mercaptoethanol

Table 2.6: Drugs used in tissue culture. Shown are the drug names and working concentrations.

Drug	Company	Working concentration	Diluent
ATM inhibitor (KU55933)	Selleckchem (S1092)	20 µM	DMSO
ATR inhibitor (AZD6738)	Selleckchem (S7693)	8 µM	DMSO
CldU	Sigma-Aldrich (C6891)	10 mM	Distilled water
DNA-PK inhibitor (AZD7648)	Selleckchem (S8843)	20 µM	DMSO
Doxycycline	Sigma-Aldrich (D9891)	2 µg/ml	Distilled water
Hygromycin B	Gibco (10687010)	200 µg/ml	PBS
MG132	Sigma-Aldrich (M7449)	10 mM	DMSO
Olaparib	Selleckchem (AZD2281)	10 mM	DMSO
Zeocin	Gibco (R25001)	400 µg/ml	Distilled water

2.2 Working with Bacteria

2.2.1 Bacterial Transformation

Plasmids were transformed into XL-10 Gold Ultracompetent bacteria (Agilent, 200314) following manufacturer's protocol. Briefly, 0.4 µl of the supplied β-mercaptoethanol was added to 10 µl of thawed bacteria. The bacteria were incubated on ice for 10 minutes, then 1 µl of plasmid was added. The mixture was kept on ice for 30 minutes, heated in a 42°C water bath for 45 seconds, then returned to ice for 2 minutes. After 2 minutes 250 µl of SOC media at room temperature was added to the bacteria, which were then incubated at 37°C for 1 hour. The bacteria were then plated onto agar plates with the appropriate antibiotic, and incubated overnight at 37°C.

2.2.2 Plasmid preparation

To prepare small quantities of plasmids for sequencing, a Monarch Plasmid Miniprep Kit (New England Biosciences, T1010L) was used, following the manufacturer's protocol. For each miniprep, 10 ml of an overnight culture of transformed bacteria was used. The final plasmid was eluted into the supplied TE buffer.

For large quantities of plasmids, or plasmids for use in tissue culture, a NucleoBond Xtra Maxiprep Kit (Machery-Nagel, 740414) was used following the manufacturer's protocol. For each maxiprep, 500 ml of bacterial culture grown overnight at 37°C was used. The final plasmid was eluted into RNase free water.

Plasmids were sequenced externally by Source BioScience Limited using their Sanger Sequencing service.

2.3 Working with Cell culture

2.3.1 Cell line maintenance

All cells were tested for mycoplasma contamination upon entry to the laboratory. U2OS cells (ATCC) were cultured in Dulbecco's Modified Eagle's Medium (DMEM, Gibco, 41996) supplemented with

10% Foetal Bovine Serum (FBS, Sigma-Aldrich) and 2 mM l-glutamine (Sigma-Aldrich, G7513). For U2OS cells used in clonogenic assays, the FBS was substituted for 10% Gibco FBS (Gibco) and 1% penicillin/streptomycin (Gibco, 15070-063) was added. U2OS Flp-In cell lines (gifted from the Morris laboratory) were cultured as standard U2OS with the FBS substituted for 10% tetracycline free FBS (Pan Biotech, P30-3602). Cells were maintained in a humidified incubator at 37°C with 5% CO_2.

2.3.2 Counting cells

Cells were counted by first harvesting them from the plate using trypsin. Of the harvested cells, 20 µl were mixed with an equal volume of Trypan blue stain (Trypan blue 0.4% solution, Gibco 1525006), then 20 µl of this mixture was loaded onto a Countess automated cell counter to determine total and live cell counts.

2.3.3 Transfection of plasmid DNA

Only plasmids obtained from maxiprep DNA preparations were used to transfect cells. U2OS were seeded onto plates in their standard medium 24 hours prior to transfection, such that the cells would be 70-80% confluent at the time of transfection. FuGENE HD (Promega, E2311) was used to transfect plasmid DNA at a 3 µl FuGENE HD to 1 ng DNA ratio, according to the manufacturer's protocol. Culture medium was replaced the following day to increase cell viability.

2.3.4 Transfection of siRNA

siRNA was transfected using Oligofectamine (Invitrogen, 12252011) according to the manufacturers protocol. Briefly, cells were plated onto a 6 well plate such that they would be 70-80% confluent at the time of transfection the following day. Per well, 9 µl of siRNA at 20 µM concentration was used to 3 µl of Oligofectamine.

2.3.5 Generation of stable cell lines

U2OS Flp-In cell lines (Gift from Morris lab) were co-transfected with ubiquitin mutants in the pcDNA5 FRT/TO backbone and pOG44 Flp-recombinase (Thermo Fisher, V600520) using FuGENE 6 (Promega, E2691) following the manufacturer's protocol for FuGENE 6 transfections. The ratio of DNA used was 1 ng of pcDNA5 vector plus 0.5 ng pOG44, to 4 µl of FuGENE 6. After 48 hours, cells were gently washed with PBS, and cells were maintained in tetracycline free medium containing hygromycin B (100 µg ml^{-1}, Invivogen, ant-hg-1) for 4 weeks. At this point, individual colonies could be identified. These colonies were isolated and expanded. Further selection with hygromycin B in parallel with Zeocin (100 µg ml^{-1}, Thermo Fisher, R25001) was used to determine correct insertion. Clonal populations that were resistant to hygromycin B and sensitive to Zeocin were selected for further expansion and expression testing.

Expression of ubiquitin mutants from generated Flp-In cell lines was determined by the addition of doxycycline (2 µg ml^{-1}, Sigma Aldrich, D9891) to the medium for 72 hours. After 72 hours, whole cell lysates were obtained following the method outlined in section 2.3.7, and immunoblotting using an anti-His antibody was performed, as outlined in section 2.4.2.

2.3.6 Irradiation of cells

Due to equipment access issues during the COVID19 pandemic, two sources of irradiation have been used. Where "caesium source" is indicated, this refers to a caesium 137 source contained in an IBL437C Blood Irradiator (Schering). Where "X-ray source" is indicated, this refers to a CellRad Benchtop X-ray Irradiator (Precision X-Ray). In-house validation by the Beggs group found no significant differences in the number of DNA damage foci, or changes to repair kinetics between these two sources.

2.3.7 Preparation of whole cell lysates for immunoblotting

Whole cell extracts for immunoblotting were obtained by harvesting cells with trypsin, and counted to obtain an equal number of cells per condition. Cells were centrifuged, and the pellet washed with PBS. Samples were again centrifuged, and all supernatant removed. The pellet was resuspended in UT buffer and incubated on ice for 10 minutes, then sonicated using a BioRuptor (Diagenode) set to "high" for 5 minutes, alternating on/off every 30 seconds. Samples were then centrifuged at 16,000 x g for 10 minutes. The supernatant was removed and retained, and the pellet discarded. Loading buffer (NuPAGE SDS Sample Buffer 4X, Novex by Life Technologies) was added to the sample to reach a 1x final concentration and the sample was boiled at 95°C for 5 minutes. Samples could then be loaded onto a gel, or stored at -20°C until used.

2.3.8 Preparation of subcellular fractions for immunoblotting

2.3.8a Harvesting cells

Subcellular fractions were obtained using a modified version of the REAP protocol (Suzuki et al., 2010). U2OS cells were grown in 10 cm dishes until 70-80% confluent. These cells were then optionally treated with 4 Gy of ionising radiation from an X-ray source. At the indicated time post-treatment, cells were harvested using trypsin, and the total cell count determined as outlined in section 2.3.2. An equal number of cells were carried forward in each condition used.

2.3.8b Fractionation

From this point, cells were kept on ice, and all buffers were pre-chilled and kept ice-cold. Protease, phosphatase, and DUBs inhibitors were added to all buffers. The counted cells were centrifuged at 400 x g, the supernatant removed, and the pellet resuspended in PBS complete buffer. Cells were again centrifuged, and the pellet was resuspended in 900 µl of 0.05% IPEGAL in PBS using a cut P1000 tip. Of this, 300 µl was removed as the "whole cell" fraction. The remaining sample was centrifuged for 10 seconds using a benchtop microfuge. The supernatant was removed, with 300 µl retained as the cytoplasmic fraction and the rest discarded. The pellet was washed with PBS and

centrifuged as before, with all supernatant discarded. The pellet was resuspended with 180 µl of 0.5% Triton X-100 in PBS buffer. The sample was incubated on ice for 2 minutes, then centrifuged at 16,000 x g for 2 minutes at 4°C. All the supernatant was removed and retained as the nucleoplasm fraction. The pellet was washed with 200 µl of Triton X-100 lysis buffer and pelleted as before. All supernatant was removed, and the pellet retained as the chromatin fraction.

2.3.8c Preparation of samples for immunoblotting

Immediately following fractionation, samples were prepared for immunoblotting. To the "whole cell" and cytoplasmic fractions, 100 µl of 4x Loading buffer was added. To the nucleoplasm and chromatin fractions, 220 µl and 380 µl of 2x Loading buffer was added, respectively. These samples were then sonicated using a Bioruptor set to "high" for 5 minutes, alternating on/off every 30 seconds. Samples were then incubated at 95°C for 5 minutes. At this point, samples were stored at -20°C until used for immunoblotting. To achieve equal loading of protein samples on SDS -PAGE gels, half the volume of nucleoplasm and chromatin fractions compared to whole cell and cytoplasmic fractions were loaded.

2.3.9 Preparation of nuclear lysates for HIS-pulldown and mass spectrometry

U20S cells were seeded onto 10 cm dishes (5 dishes per condition) such that they were 70-80% confluent the following day. The next day, cells were transfected with either HIS-tagged wild-type ubiquitin(or an empty vector control (pcDNA5 FRT/TO vectors)using FuGENE HD. The day after transfection the medium was replaced, cells were harvested by trypsin and a total cell count obtained using a Countess II automated cell counter. An equal number of cells were carried forward to fractionation in each condition.

All subsequent steps for fractionation took place with ice-cold buffers, pre-cooled centrifuges and samples kept on ice, unless otherwise stated. Protease, phosphatase, and DUB inhibitors are present in all buffers. Cells were pelleted at 400 x g and all supernatant removed. The pellet was washed with PBS, then pelleted as before. To the pellet, 500 µl of hypotonic buffer per 5 x 10^6 cells was

added, and the pellet was resuspended gently using a cut P1000 tip, then incubated on ice for 15 minutes. After this, 10% IPEGAL in PBS was added to achieve a final concentration of 0.05%, and the sample mixed using short pulses on a vortex mixer. Samples were then centrifuged at 16,000 x g for 10 minutes.

The supernatant was retained as the cytoplasm fraction. The remaining pellet, comprising the nuclear fraction, was washed twice with nuclei wash buffer at a volume of 800 µl per 5 x 10^6 cells. Washed nuclei were collected by centrifugation at 400 x g for 1 minute. On the second wash, nuclei were transferred to a clean microtube. Nuclei were resuspended in 200 µl nuclei lysis buffer. To this, 2 U/µl of Benzonase (Millipore, E1014) was added, and the solution was incubated at room temperature for 15 minutes, kept mixing by rotation. The sample was then sonicated using a Bioruptor (Diagenode) set to "high" for 5 minutes, alternating on/off every 30 seconds.

2.3.10 Preparation of samples for Immunofluorescence microscopy

For experiments looking at DNA damage foci in cells without additional transfections, 2.2 x 10^5 cells per well were seeded onto glass coverslips (Scientific Lab Supplies, MIC2168) in a 6 well plate, such that the cells would be 70-80% confluent at the time of irradiation. Flp-In cell lines were optionally induced with doxycycline such that they had been induced for 48-72 hours at the time of irradiation. Cells were treated with ionising radiation at the indicated dose, and fixed at the stated time post-treatment with 4% Paraformaldehyde (PFA) in PBS (Alfa Aesar, J61899) for 10 minutes at room temperature. Coverslips were kept covered in PBS and stored at 4°C for up to two weeks prior to staining.

When transient protein expression or siRNA knockdown was required, cells were seeded onto glass coverslips in a 6-well plate at a density of 2.2 x 10^5 cells per well, such that they would be 70-80% confluent for transfection the following day. Treatment with ionising radiation took place 48 hours after transfection, and cells were fixed as before.

Pre-extraction of cells was only used when indicated. At the indicated time post IR, cells were washed quickly with PBS, then 1 ml of ice-cold CSK buffer was added to the well. After 5 minutes the CSK buffer was removed, and the cells washed gently with PBS then fixed, as before.

For MG132 (Sigma-Aldrich, M7449) treatment, cells were treated with a final concentration of 10 mM in medium, 1 hour prior to IR. Where CldU was also used, this was added to the medium to a final concentration of 10 mM, 20 minutes prior to IR. Drugs were washed out with fresh medium immediately prior to IR treatment.

2.3.11 Kinase Inhibitor screen

U2OS cells were grown on coverslips to be 70-80% confluent at the time of irradiation. Kinase inhibitors, shown in Table 2.6, were diluted in DMSO to ensure equal volumes of inhibitors were added to cell medium. DMSO and DNAPK inhibitor were added to medium 2 hours prior to irradiation, and ATM and ATR inhibitors were added 1 hour prior to irradiation. Inhibitors remained in the medium throughout the experiment. Samples were treated with 4 Gy IR from an X-ray source, and fixed after 1 hour. Coverslips were stained for pT66 and γH2AX, and images were acquired and analysed as in section 2.4.2.

2.3.12 Clonogenic assay

U2OS cells for this assay were maintained in a modified medium, described in section 2.3.1. U2OS cells were seeded onto 6-well plates such that they were 70-80% confluent the following day. The next day, cells were transfected with FLAG-tagged ubiquitin mutants.

To test colony formation in undamaged conditions, 800 live cells per well were seeded into a 6-well plate, then allowed to grow undisturbed for 7 days. To test colony formation after damage, 2000 live cells per well were seeded onto a 6-well plate. The following day, cells were treated with 2 Gy from an X-ray source, then allowed to grow undisturbed for 7 days. If treated with MG132, this was added to medium to a final concentration of 10 mM an hour before irradiation, and the drug washed out with fresh medium immediately prior to irradiation. At the end point of each experiment, medium

was carefully removed from the wells, and methylene blue solution was added to cover the bottom of the wells. Cells were incubated in this solution at room temperature for 10 minutes to both fix and stain the samples. Wells were subsequently washed thoroughly with tap water and allowed to dry at room temperature overnight. Dried samples were scanned using an Epson scanner, and visualised in FIJI for ease of analysis.

2.3.13 PARP inhibitor assay

U2OS cells were grown in 6 well plates, and transfected with WT, T66A or K63R FLAG-tagged ubiquitin. The following day, cells were transfected with either NT or BRCA1 siRNA. Cells were harvested and counted the next day to be seeded for further experiments. For clonogenic assays, cells were seeded onto a 24 well plate at 200 cells per well. For proliferation assays, cells were seeded onto a 96 well plate in triplicate, at 1000 cells per well. PARP inhibitor (olaparib) was immediately added to the samples to the final concentration indicated. Volume of drug added to samples was kept equal through dilution in DMSO.

Proliferation assays were halted and analysed 5 days after plating, following the manufacturers protocol (Vybrant™ MTT cell proliferation assay kit, Invitrogen, V13154). Clonogenic assays were halted at 7 days, then stained and analysed as outlined in section 2.3.12.

2.3.14 Acquiring cell cycle profile by FACS

U2OS cells were seeded into 6 well plates such that they would be 60-70% confluent the following day, to ensure log phase. The next day, cells were transfected with FLAG-tagged mutants of ubiquitin, as described previously. Cells were harvested using trypsin 48 hours after transfection, washed once with PBS, then resuspended in 2% PFA in PBS. Samples were stored at 4°C for up to 7 days before staining and analysis.

2.4 General Molecular Biology

2.4.1 Site directed mutagenesis

Site directed mutagenesis was carried out using the Q5 Site Directed Mutagenesis Kit from NEB (NEB E05545) following the manufacturer's protocol. Briefly, reagents were mixed in a thin-walled PCR tube with a final template DNA amount of between 10-25 ng. Primers and conditions used are listed in Table 2.2. For primers with a GC content above 40%, the GC enhancer provided was used. Annealing time was set to 30 seconds, and 30 seconds per kilobase of template DNA was allowed for extension. After the final extension, reactions were kept at 4°C for up to 3 days before use in the KLD reaction.

The KLD reaction was set up according to the manufacturers protocol, with additional optimisation to reduce the amount of un-modified template in the final transformation mix. The KLD reaction was modified by incubating the reaction mixture at room temperature for 5 minutes, then at 37°C for 1 hour. The resultant mixture was transformed into XL10 gold bacteria (Agilent 200314) as described in section 2.2.1.

2.4.2 Immunoblotting

Protein samples were resolved using SDS-PAGE gel electrophoresis. Single percentage SDS-PAGE gels were made inhouse immediately prior to use. These gels were run with tris-glycine running buffer at 160 volts until the dye front reached the bottom of the gel. Gradient gels were obtained from Invitrogen (NuPage 4-12% Bis-Tris gels) and run with NuPage MOPS SDS buffer (Novex by Life Technologies, NP000102) at 160 volts until the dye front reached the bottom of the gel. PageRuler Plus Prestained Protein Ladder (Thermo Fisher Scientific, 26619) was run in the first and last well of each gel.

Following gel electrophoresis, proteins were transferred from gels to PVDF membranes (Merck Millipore, IPVH00010) using the wet transfer system from BioRad at 120 volts for 60 minutes. Following transfer, the membrane was incubated in a blocking solution for 1 hour at room

temperature. This solution was either 5% milk blocking buffer or 3% BSA blocking buffer, as indicated in the antibody table. The membrane was subsequently incubated with a primary antibody against the indicated protein, diluted in its respective blocking buffer, at 4°C overnight. Membranes were then washed three times with TBST, then incubated with horseradish peroxidase (HRP) conjugated secondary antibodies diluted in milk blocking buffer for 1 hour at room temperature. Where the primary antibody was HRP conjugated, this step was omitted. Membranes were again washed three times with TBST, then treated with ECL spray (Advansta, K-12049) to induce chemiluminescence.

2.4.3 Staining coverslips and acquiring images by immunofluorescence microscopy

Staining of coverslips began by permeabilising cells with 0.3% Triton X-100 in PBS for 5 minutes. For cells stained with the pT66 ubiquitin antibody, all subsequent steps were undertaken replacing PBS with TBS in the buffer. Coverslips were then incubated in blocking buffer for 1 hour. For cells treated with CldU, after permeabilisation coverslips were incubated with 2M HCl at 37°C for 30 minutes, then incubated in blocking solution for 1 hour. After blocking, coverslips were incubated with primary antibody overnight at 4°C at the concentrations listed in

Table **2.4**.

After primary antibody incubation, coverslips were washed once with TBST, then twice more with TBS. Secondary antibodies were then added to the coverslips and incubated at room temperature for 2 hours, protected from light. Coverslips were again washed with TBST, twice in TBS and finally dipped in dH_2O immediately prior to mounting. Coverslips were mounted onto glass microscope slides (Thermo Fisher Scientific, 12372098) using Fluoroshield with DAPI (Sigma-Aldrich F6057) and allowed to dry at room temperature, protected from light. Once dry, slides were stored protected from light at 4°C until imaged.

Immunofluorescence images were acquired using a Leica DM600B widefield microscope with LasX software (Leica). Images were visualised and quantified in FIJI (v1.53n) and assembled into figures using Inkscape (v1.0).

2.4.4 Pulldown of HIS-tagged ubiquitin from nuclear lysates

Samples from 2.3.9 were processed to pulldown of HIS-tagged proteins. Following sonication of the nuclear fraction, 1800 µl of UT buffer was added then incubated at room temperature for 30 minutes, kept mixing by rotation. Of this mix, 100 µl was retained and added to 100 µl of 2x Loading buffer. This is the "input" sample for analysis by immunoblotting.

Meanwhile, 300 µl of HIS-Pur Ni-NTA beads (Thermo Fisher, 25215) were added to a 1.5 ml microtube. Double the volume of PBS was added, and the beads then centrifuged for 5 seconds using a benchtop microfuge. The microtubes were placed in a magnetic rack, and once the beads had settled, the supernatant was removed and discarded. This process was repeated twice more with UT buffer.

The beads were transferred to a fresh tube and mixed with the nuclear fraction. Samples were incubated at room temperature for 2 hours, kept mixing by rotation. Tubes were then placed in a magnetic rack and the beads allowed to settle. The supernatant was removed, with 100 µl retained and mixed with 100 µl of 2x Loading buffer as the "depleted" sample, for analysis by immunoblotting.

Table 2.7: Buffers used to wash nickel beads after HIS- pulldown

Wash	**Buffer**		
		Plus	**Plus**
1	UT buffer		
2	UT buffer	5 mM imidazole	
3	UT buffer	20 mM imidazole	
4	UT buffer	20 mM imidazole	0.05% Tween 20
5	UT buffer	20 mM imidazole	0.2% Triton X-100
6	UT buffer adjusted to pH6.5 with HCl		
7	UT buffer adjusted to pH6.5 with HCl	300 mM NaCl	
8	UT buffer		

The remaining beads were washed using 1 ml of the buffers outlined in Table 2.7. Between each washing step, beads were retained using a magnetic rack and the supernatant was removed and discarded.

After the final washing step, 75 µl of 2x Loading buffer was added to the beads, and the sample was incubated at 95°C using a heat block for 5 minutes. The beads were allowed to settle using a magnetic rack, and the supernatant was removed and retained as the "pulldown" sample. The beads were retained for analysis by immunoblotting.

Input, depleted and pulldown samples were run on a gel and analysed by immunoblotting with an anti-HIS antibody, as described in section 2.4.2. Once enrichment of HIS-tagged proteins was confirmed in the "pulldown" compared to the "depleted" sample, the remaining pulldown sample was prepared for mass spectrometry.

2.4.5 Preparation of HIS-pulldown samples for analysis by mass spectrometry

40 µl of the pulldown samples from section 2.4.4 were resolved by SDS-PAGE using a 10-well NuPAGE 4-12% Bis-Tris gel with NuPAGE MOPS SDS buffer, run at 160 volts for about 1.5 cm. Gels were subsequently stained with SimplyBlue SafeStain (Invitrogen, LC6060), and each stained protein lane was cut into 10 equally sized bands using a scalpel. Protein bands were transferred to individual wells in a 96 well reaction plate. Plates were sealed thoroughly and sent for analysis at MS Bioworks.

MS Bioworks further processed the samples for analysis. Peptides for analysis were acquired by tryptic digestion of the protein bands. The digests were analysed by nano LC/MS/MS, using a Waters NanoAcquity HPLC system interfaced to a Thermo Fisher Q Exactive. Data was searched using a local copy of Mascot (Matrix Science) with SwissProt Human as the database. The resulting Mascot files were parsed into Scaffold software (Proteome Software) to allow for viewing. Files were reviewed using Scaffold 5 (v5.0.1) in viewer mode.

2.4.6 Staining and analysis of FACS samples

Staining of FACS samples was carried out immediately prior to analysis. Cells were first pelleted, then resuspended in 500 µl 0.3% Triton X-100 for 3 minutes at room temperature to permeabilise the samples. Cells were resuspended in PBS with Hoechst 33582 (5 µM, Merck, 861405) and taken for analysis. Samples were run on a CytoFLEX system with CytExpert acquisition software (Beckman Coulter). Analysis was undertaken using FlowJo (v10.8.0, BD Biosciences).

Chapter 3: Detection of ubiquitin phosphorylated at T66 in mammalian cells

3.1 Introduction

Prior to my joining the Gambus lab, work was underway to use the *Xenopus laevis* egg extract system to identify substrates ubiquitylated by BRCA1 on chromatin after DNA damage. To identify such substrates, recombinant HIS-tagged K6-only ubiquitin (ubiquitin with all lysines except K6 mutated to arginine) was added to extract, and double strand breaks were induced using the endonuclease EcoR1. Chromatin was isolated from the extract after 60 minutes of reaction (middle of S-phase with continuous induction of DSB), and a HIS-pulldown was used to obtain a sample of proteins modified with the HIS-tagged ubiquitin. This sample was sent for analysis by mass spectrometry at MS Bioworks. Intriguingly, ubiquitin phosphorylated at threonine 66 was identified in the pulldown from EcoR1 treated extracts, with subsequent repeats of this experiment also finding this modification. The ubiquitin modifications identified in the first experiment are displayed in Table 3.1.

Table 3.1: Post-translational modifications of ubiquitin identified from the chromatin fraction of *Xenopus laevis* egg extract after damage. Ubiquitin chains are identified as a di-glycine residue (+GG) remaining on the a peptide following tryptic digestion

Total ubiquitin spectra		**1066**
Amino Acid	**Modification**	**Total spectra**
M1	+acetylation	37
K6	+GG	41
K11	+GG	13
K27	+GG	0
K29	+GG	13
K33	+GG	18
K48	+GG	44
K63	+GG	36
S65	+phospho-	0
T66	+phospho-	1

At the time of starting my PhD, the only phospho-site of ubiquitin that had been characterised was phosphorylation of S65, with its role in mitophagy. This gave a clear indication that phosphorylated ubiquitin could have its own distinct role, separate from either phosphorylation or ubiquitylation alone. It was also an indication that such modifications were possible in human cells, with clinically significant roles. Both phosphorylation and ubiquitylation are key in the DNA damage response, both in repair

and the wider cellular response – could phosphorylated ubiquitin, specifically pT66 ubiquitin also play a role in the mammalian DDR?

3.2 Results

3.2.1 Mass spectrometry from human tissue culture

I first tried to identify pT66 ubiquitin in tissue culture using mass spectrometry, modifying the original experiment in *Xenopus* egg extract for use in tissue culture. HIS-tagged wild-type ubiquitin was transfected into U20S cells, rather than a K6-only mutant, to enable capture of a wider array of ubiquitin chain types. Transfection of an empty vector plasmid was used as a control to ensure enrichment of ubiquitin in the final HIS-pulldown. The double strand breaks were induced in culture using 4 Gy of ionising radiation (IR) from a caesium source, with cells harvested 1 hour after treatment. The chromatin fraction was isolated from this sample, and used for a HIS-pulldown to isolate ubiquitin and ubiquitylated proteins. The pulldown sample was sent for analysis by MS Bioworks.

Table 3.2: Di-glycine residues identified on ubiquitin by mass spectrometry from HIS-ubiquitin pulldown. Only di-glycine modifications are shown. No spectra corresponding to phosphorylated ubiquitin were identified in the screen

		Empty Vector	***His-Ubiquitin***
Total Spectra		**115**	**518**
Modifications	M1	0	0
	K6	0	0
	K11	0	6
	K27	0	1
	K29	0	37
	K33	0	4
	K48	2	23
	K63	0	23

Analysis of the results of mass spectrometry data, revealed a 4-fold increase in ubiquitin peptides identified in the HIS-ubiquitin sample compared to the empty vector sample, indicating that the transfection and subsequent pulldown has been successful in enriching for HIS-tagged proteins (Table 3.2). Despite this enrichment, no peptides of phosphorylated ubiquitin were identified. Proteins identified in the pulldown with at least 5 peptides and at least 4-fold increase in abundance in the HIS-pulldown are displayed in Table 3.3. These proteins have been displayed as they are candidates for ubiquitylated proteins on chromatin after IR, and may be interesting to pursue in later work.

Table 3.3: Proteins identified by mass spectrometry enriched by HIS-pulldown. Proteins with a minimum of 5 peptides in the HIS-ubiquitin sample, with at least 4-fold enrichment are displayed in the table.

			Number of peptides	
Identified Proteins	Accession Number	Gene name	empty vector	His-ubiquitin
Ubiquitin-40S ribosomal protein S27a	P62979	RS27A	115	518
Cytoplasmic dynein 1 heavy chain 1	Q14204	DYHC1	2	80
Eukaryotic translation initiation factor 4 gamma 2	P78344	IF4G2	9	72
E3 ubiquitin-protein ligase HUWE1	Q7Z6Z7	HUWE1	0	41
Eukaryotic translation initiation factor 4 gamma 1	Q04637	IF4G1	6	25
eIF-2-alpha kinase activator GCN1	Q92616	GCN1	0	21
Cyclin-dependent kinase 1	P06493	CDK1	0	18
26S proteasome non-ATPase regulatory subunit 12	O00232	PSD12	3	16
Coatomer subunit alpha	P53621	COPA	3	15
ATP-dependent DNA helicase Q1	P46063	RECQ1	2	13
CD63 antigen	P08962	CD63	2	12
Heat shock protein HSP 90-beta	P08238	HS90B	2	12
Activating signal cointegrator 1 complex subunit 3	Q8N3C0	ASCC3	0	11
snRNA-activating protein complex subunit 1	Q16533	SNPC1	0	11
Solute carrier family 43 member 3	Q8NBI5	S43A3	2	11
Cyclic GMP-AMP synthase	Q8N884	CGAS	2	11
Protein argonaute-2	Q9UKV8	AGO2	0	9
Signal recognition particle receptor subunit beta	Q9Y5M8	SRPRB	0	8
Fatty acid synthase	P49327	FAS	0	8
Threonine--tRNA ligase 1, cytoplasmic	P26639	SYTC	0	8
Eukaryotic translation initiation factor 3 subunit B	P55884	EIF3B	2	8
ATP-dependent RNA helicase DHX33	Q9H6R0	DHX33	2	8
Protein arginine N-methyltransferase 5	O14744	ANM5	0	7
AP-1 complex subunit gamma-1	O43747	AP1G1	0	7
Nucleophosmin	P06748	NPM	0	6
Pre-rRNA-processing protein TSR1 homolog	Q2NL82	TSR1	0	6
Cullin-3	Q13618	CUL3	0	6
DNA replication licensing factor MCM7	P33993	MCM7	0	6
Translation initiation factor eIF-2B subunit alpha	Q14232	EI2BA	0	6
Protein furry homolog-like	O94915	FRYL	0	6

There are several reasons why phosphorylated ubiquitin may not have been detected in this sample – failure to detect this modification does not indicate that pT66 ubiquitylation does not occur in mammalian cells. The potential reasons for the lack of detection in this sample, and approaches that may enable detection by mass spectrometry will be discussed at the end of this chapter.

3.2.2 Immunofluorescence detection of pT66

Without optimisation, mass spectrometry can miss low abundance proteins and modifications from complex samples (Peck Justice et al., 2021). It was hoped that immuno-detection methods such as immunofluorescence (IF) and Western Blotting (WB) would enable detection of pT66, if present, as these methods do not have the same intrinsic bias against low abundance proteins as mass spectrometry. To this end, an antibody was raised against pT66 ubiquitin by Dundee Cell Products and purified against a phosphorylated peptide, corresponding to amino acids 62-72 of ubiquitin, with the threonine corresponding to T66 phosphorylated.

To test whether the raised antibody can detect a signal in cells upon DNA damage, U2OS cells seeded onto coverslips were exposed to 4 Gray of ionising radiation from an X-ray source or left untreated, then fixed at 1 hour post treatment. Cells were then stained with the pT66-ubiquitin antibody, and a 53BP1 antibody, used as a marker of DSBs. Representative images are shown in Figure 3.1.

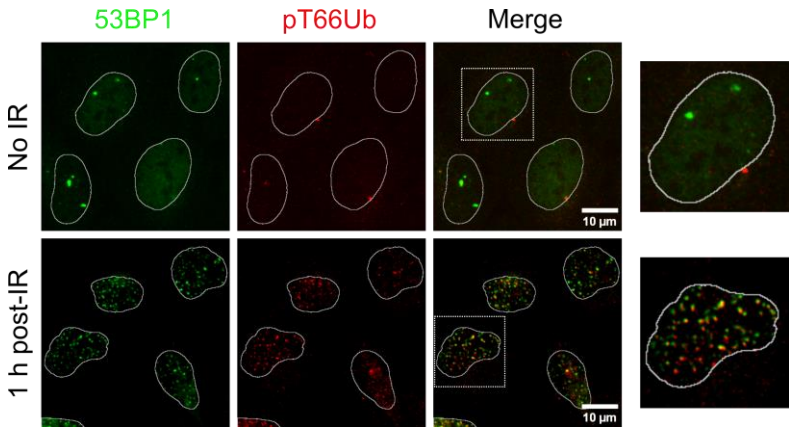

Figure 3.1: pT66 ubiquitin forms foci which co-localise with 53BP1 in response to DNA damage. U2OS cells were treated with 4 Gy IR and fixed after 1 hour. Samples were then stained with pT66 and 53BP1 antibodies. Representative images are shown.

In untreated cells, 53BP1 shows localisation at several large foci in the nucleus of many cells. These foci are usually ascribed as being 53BP1 bodies, which are nuclear compartments found in G1 cells that mark DNA lesions inherited from mother cells during mitosis (Fernandez-Vidal et al., 2017). Signal from the pT66-ubiquitin antibody shows localisation to discrete foci, although they appear to be outside of the nucleus. This signal will be discussed at the end of this chapter.

After irradiation, 53BP1 localises to many small foci and a reduction in nuclear background staining is seen. Excitingly, the pT66-ubiquitin antibody also shows foci formation after damage, with many of these foci co-localising with 53BP1, suggesting localisation at DSB sites. Not all cells show pT66 staining however, with between 40 and 60 percent of cells making clear pT66 IRIF (irradiation induced foci, to distinguish from the damage independent foci observed). Variability between samples is high, and there are no obvious differences between cells (such as condensed chromatin or signs of apoptosis) to suggest what is contributing to pT66-ubiquitin IRIF formation. This observation is explored further in chapter 6 of this thesis.

3.2.3 Validating the specificity of the pT66 antibody

The detection of pT66-ubiquitin IRIF is an encouraging sign that this modification is present in mammalian cells, and has a role in the DDR. However it is important to validate the specificity of the antibody before further use, to ensure that the observed signal is from phosphorylated ubiquitin and not non-phosphorylated ubiquitin or other proteins.

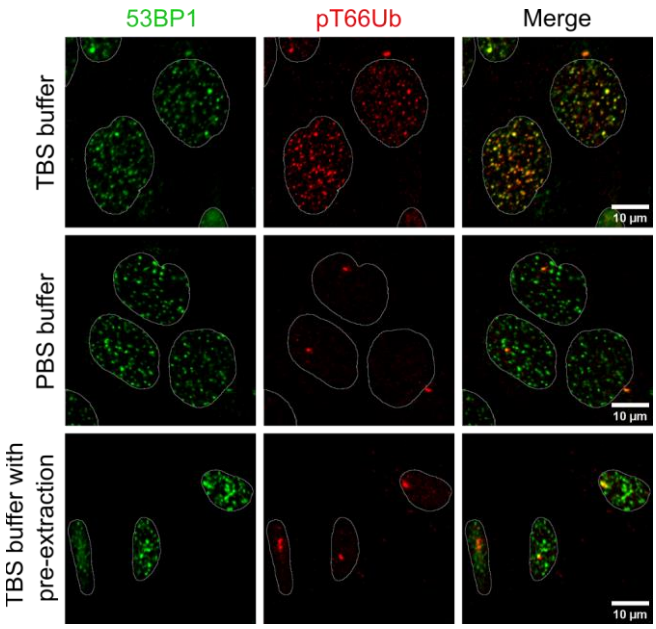

Figure 3.2: pT66-ubiquitin foci require specific staining conditions to be detected. U2OS cells treated with IR were fixed one hour after treatment, then stained using pT66-ubiquitin and 53BP1 antibodies diluted in either PBS or TBS-based buffers. Pre-extraction took place immediately prior to fixation.

3.2.3.a. Evidence of phospho-specificity from staining conditions

Some evidence for the phospho-specificity of this antibody is found in the staining conditions required to detect pT66-ubiquitin IRIF. The foci were only detected when the antibody was diluted in a TBS-based buffer, with PBS-based buffers leading to loss of this signal (Figure 3.2). This loss of signal in the presence of a phosphate buffer is a known phenomenon of many phospho-specific antibodies, and is an early indicator of the pT66-ubiquitin antibody showing phospho-specificity. The use of TBS vs PBS buffers did not appear to affect the detection of 53BP1 foci.

When optimising staining conditions for pT66 ubiquitin, pre-extraction was attempted to reduce background staining present in the nucleus by removing soluble and weakly chromatin-bound proteins from the cell prior to fixation. Pre-extraction led to a loss of pT66 IRIF, which may indicate that pT66-ubiquitin is not strongly bound to chromatin. It is interesting to note that in both the PBS-based buffer and pre-extracted conditions, signal from the extra-nuclear foci remained. It is unclear whether this extra-nuclear signal is specific or caused by non-specific binding of the antibody.

3.2.3.b Competition assay using phosphorylated peptide provides further evidence of phospho-specificity

A more robust method of determining whether the pT66 antibody recognises phosphorylated ubiquitin is using a peptide competition assay. It was reasoned that if the antibody recognised phosphorylated ubiquitin, then incubating the antibody with phosphorylated peptide spanning the epitope should compete with endogenous binding sites in the sample. This could be detected as a decrease in fluorescence intensity across the nucleus. If the antibody is specific to the phosphorylated peptide, then addition of a non-phosphorylated form of the peptide should not compete with endogenous sites, and so not decrease the signal intensity.

The pT66 antibody was incubated in a 1:1, 1:50 or 1:100 molar ratio of antibody to peptide, either phosphorylated or non-phosphorylated (referred to as "standard"). This mix was then used directly to stain U2OS cells, with samples generated as in section 3.2.2, and the fluorescence intensity across the nucleus was measured using ImageJ. Representative images and the quantification from this experiment are shown in Figure 3.3.

When the pT66 antibody was incubated with the standard non-phosphorylated peptide, damage induced foci were still visible, even at a 1:100 antibody to peptide ratio. In contrast, incubation of the antibody with the phosphorylated peptide at this ratio led to a complete loss of these IRIF, and the extra-nuclear foci are also no longer visible. Quantification of the fluorescence intensity revealed that there was a decrease in fluorescence signal when the antibody was incubated with the standard peptide at higher ratios. This reduction, when put in context of the pT66 IRIF remaining visible indicates that the signal reduction is likely due to non-specific binding of the antibody, causing background fluorescence. In contrast, the addition of the phosphorylated peptide leads to an almost complete loss of fluorescence signal at higher molar ratios, demonstrating that the antibody does have a strong affinity for the phosphorylated peptide.

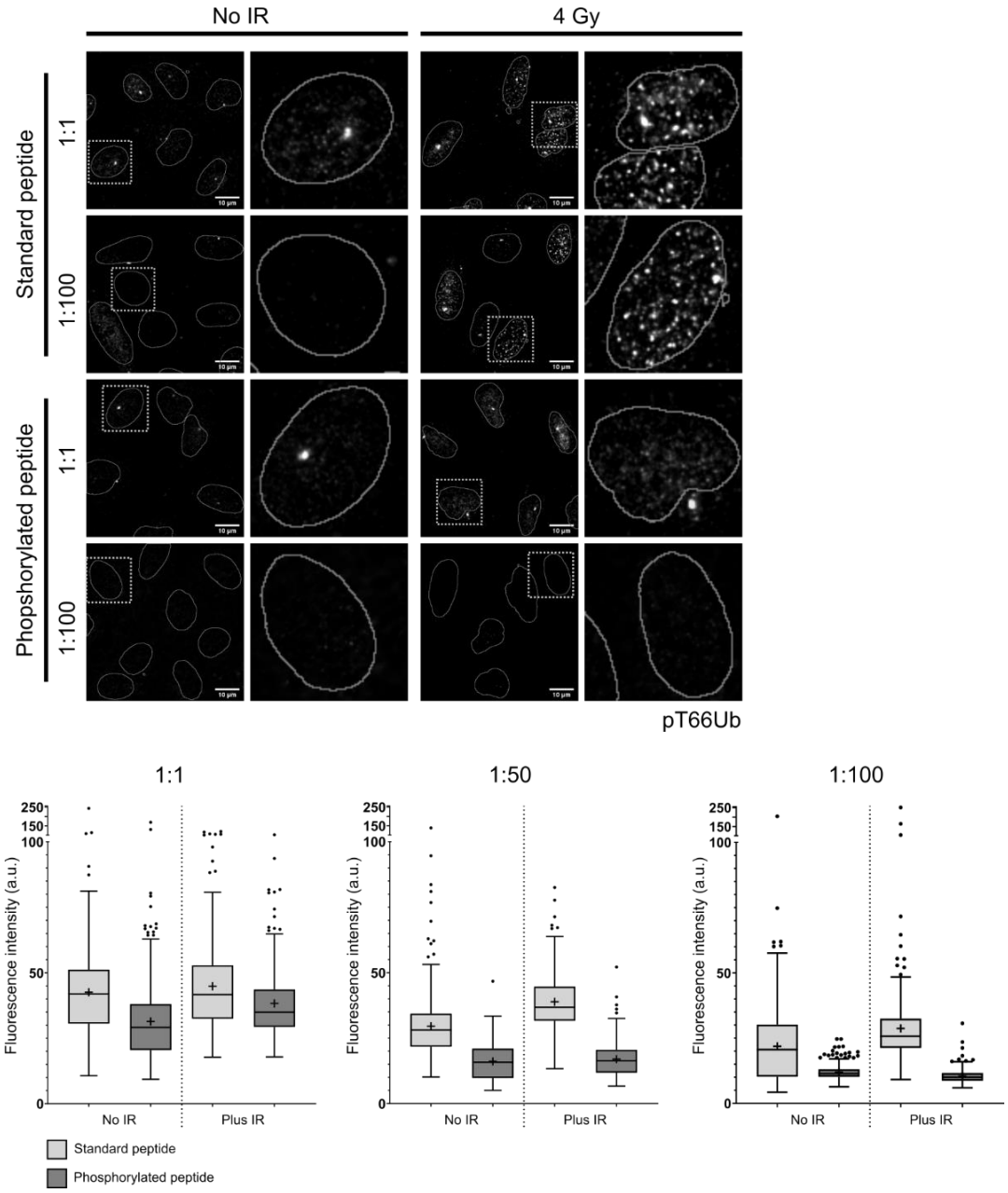

Figure 3.3: Phosphorylated peptide, but not standard peptide, competes with endogenous proteins for antibody binding. U2OS were grown on coverslips, then optionally irradiated with 4 Gy of IR. Cells were fixed 1-hour post-treatment, then stained for pT66-ubiquitin using an antibody pre-incubated with peptides. The peptides used correspond to the peptide used to generate the antibody, optionally phosphorylated at the equivalent to T66.Representative images from the experiment are shown, with quantification beneath. Quantification is of fluorescence intensity across the nucleus from the pT66-ubiquitin antibody, displayed as a Tukey boxplot. Data is from 3 experiments, with at least 145 cells counted in each treatment.

Table 3.4: Ubiquitin mutants used in determining antibody specificity

Name	Details
WT	Wild-type ubiquitin
T66A	Cannot be phosphorylated at T66
S65A	Cannot be phosphorylated at S65
T66D	Mimics phosphorylation at T66
K63R	Cannot form K63 linked ubiquitin chains

3.2.3.c Mutations of T66A and surrounding amino acids on ubiquitin lead to a loss of antibody binding

To determine whether the pT66 foci observed after damage were specific to ubiquitin, we decided to express a mutant of ubiquitin that could not be phosphorylated at this site (T66A). If there is a reduction in the number of pT66 IRIF seen, then this is an indicator that the antibody is specifically recognising phosphorylated ubiquitin. This mutation and others were introduced using Site-Directed Mutagenesis (SDM) into a plasmid encoding a FLAG-tagged, siRNA resistant ubiquitin. The mutations introduced are listed in Table 3.4. Substitution of threonine for aspartic acid is used to mimic some of the properties of phosphorylation at this residue, so a T66D ubiquitin mutant was used to determine whether the pT66 antibody would recognise this mimic. Mutation of the adjacent serine to alanine (S65A) was used to show that any signal or phenotype seen was due to phosphorylation specifically at T66, and not recognition of pS65. Finally, mutation of lysine 63 to arginine (K63R) was also introduced, preventing formation of K63 linked ubiquitin chains. These ubiquitin chains are known to be important in DDR signalling, and the proximity of this residue to T66 makes it potentially interesting to study.

Transient transfection was used to express the FLAG-tagged ubiquitin mutants in U2OS, with IR treatment (4 Gy from an X-ray source) taking place 48 hours after transfection. Cells were fixed an hour after irradiation, and stained for pT66, 53BP1 and FLAG, to identify cells expressing the mutants of ubiquitin. The representative images and quantification from this experiment are displayed in Figure 3.4.

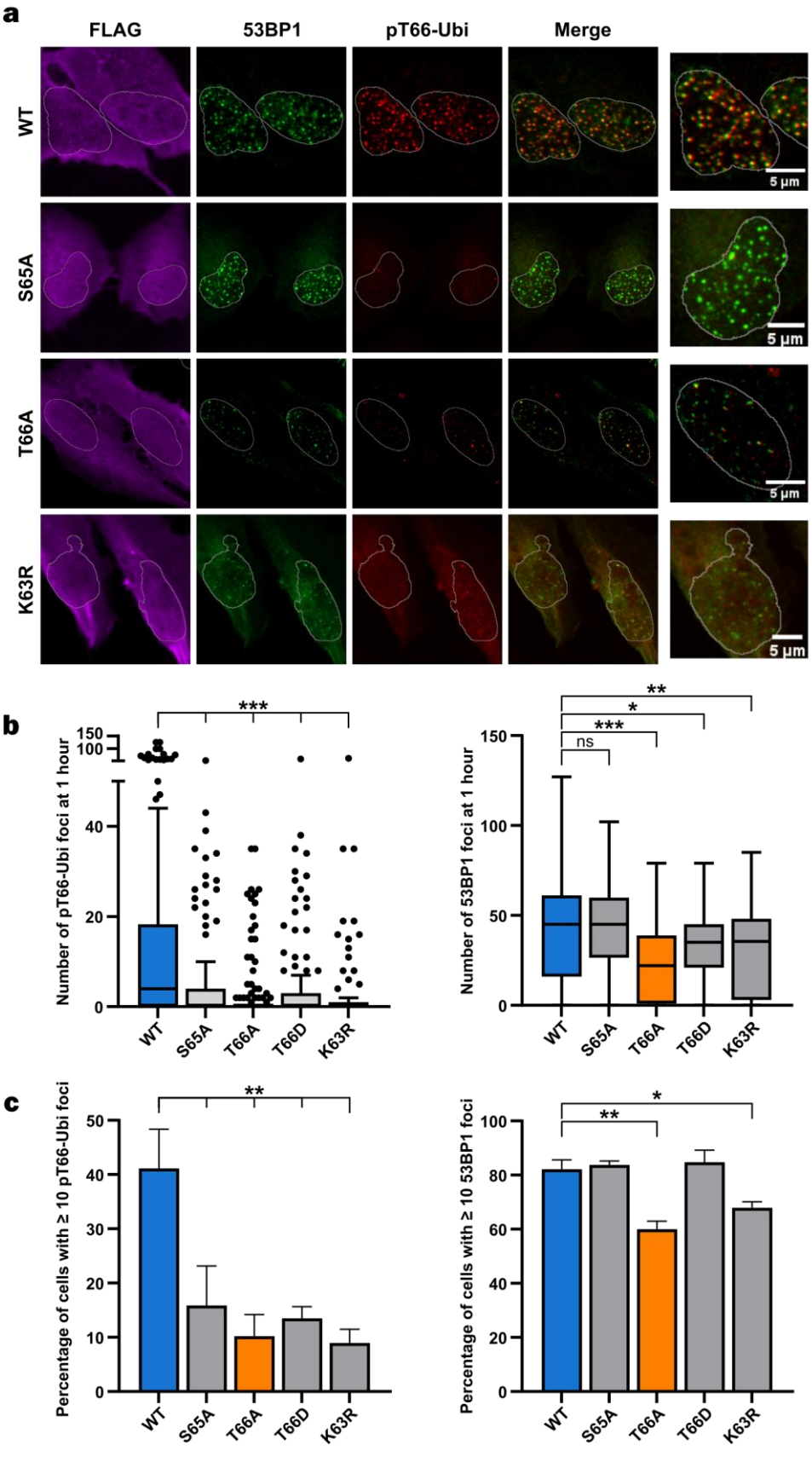
a
FLAG
53BP1
pT66-Ubi
Merge
WT
S65A
T66A
K63R
5 µm
b
Number of pT66-Ubi foci at 1 hour
Number of 53BP1 foci at 1 hour
WT
S65A
T66A
T66D
K63R
ns
c
Percentage of cells with ≥ 10 pT66-Ubi foci
Percentage of cells with ≥ 10 53BP1 foci

Figure 3.4: Mutation of ubiquitin at T66 or the surrounding amino acids leads to a loss of detectable pT66 IRIF. U2OS cells transfected with FLAG-tagged mutants of ubiquitin were treated with 4 Gy of IR from an X-ray source, fixed 1-hour post-treatment, and stained for FLAG, pT66-ubiquitin, and 53BP1. Representative images from the experiment are shown in **(a)**. (b) The number of pT66-ubiquitin and 53BP1 foci were counted from cells with FLAG staining. Data is displayed as Tukey boxplots. (c) The average (mean) percentage of cells with 10 or more pT66-ubiquitin or 53BP1 foci is displayed, with error bars showing the SEM. Data from 3 repeats. Statistical analysis is Kruskal-Wallis ANOVA, comparing ubiquitin mutants to WT-ubiquitin sample. Reported p values are as follows: ns, $p>0.05$; *, $p<0.05$; **, $p<0.01$; ***, $p<0.001$.

Approximately 40% of cells expressing WT ubiquitin formed 10 or more pT66 foci after treatment with IR, consistent with what had been seen previously in non-transfected cells. In contrast, only 10% of cells expressing T66A ubiquitin showed pT66 foci, with 82% of cells showing no foci at all. This reduction in pT66 foci was not specific to mutations of T66, with all the ubiquitin mutants tested displaying a reduction in the number of pT66 IRIF compared to WT ubiquitin. These mutations are close to T66, and are part of the peptide that was used to purify the pT66 antibody. The loss of pT66 IRIF in these mutants is most likely due to mutation of the epitope recognised by the antibody, rather than a true loss of T66 phosphorylation signal. These results indicate that the observed foci reflect pT66-ubiquitin signal, rather than from non-specific binding.

Moreover, looking at the 53BP1 IRIF in these cells, originally intended as a control, reveals an unexpected finding. Cells expressing WT ubiquitin were able to form 53BP1 IRIF, with 82% of cells making more than 10 53BP1 foci, and a median value of 45 foci per cell. Unexpectedly, expression of T66A ubiquitin impaired 53BP1 IRIF formation, with only 60% of cells making 53BP1 foci, and a median value of 22 53BP1 foci per cell, under half the number found in cells expressing WT ubiquitin. Expression of S65A was not found to impact 53BP1 foci formation. This indicates that there may be a defect in recruitment of 53BP1 when ubiquitin cannot be phosphorylated at T66. Interestingly the K63R mutant, which was expected to have an impairment in the number of 53BP1 foci observed, did show a reduction in the number of 53BP1 foci, but not to the same extent as observed in the T66A mutant, with 68% of cells making 10 or more foci, and a median of 35.5 foci per cell. This finding is explored further in chapter 2 of this thesis.

Loss of pT66 IRIF when expressing the K63R ubiquitin mutant could also be attributed to changes in the ubiquitin cascade. If ubiquitin is phosphorylated as part of K63 linked chains, or by a kinase recruited to this modification, expression of K63R would cause a genuine reduction in pT66 ubiquitin. To determine whether the pT66 antibody can recognise K63R ubiquitin an additional phosphorylated peptide, with the lysine mutated to arginine, was used in a competition assay (Figure 3.5).

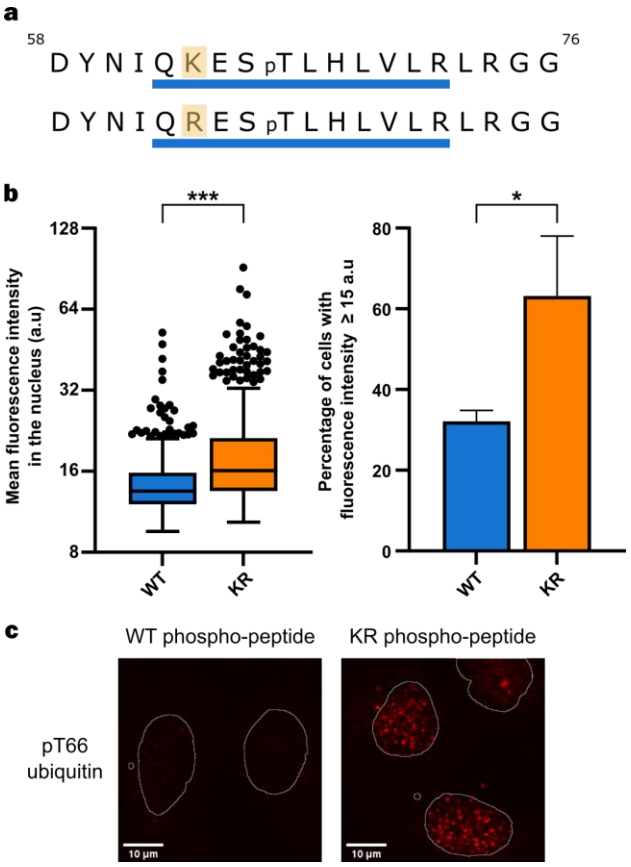

Figure 3.5: Mutating K63 prevents pT66 antibody recognition. U2OS cells were prepared as for Figure 3.3, with the pT66-ubiquitin antibody pre-incubated with optionally phosphorylated K to R peptide. **(a)** comparison of the WT (top) and K to R peptide sequence (bottom) within ubiquitin's sequence. The peptide sequence used is underlined in blue. **(b)** Quantification of fluorescence intensity across the nucleus from pT66-ubiquitin staining after incubation of the antibody with the peptides indicated. Data is displayed as a Tukey boxplot (left) and mean percentage with SEM error bars (right) N=3, Statistical analysis uses the Mann-Whitney T-test (left), and Ratio paired T-test (right). Reported p values are: *, $p<0.05$; ***, $p<0.001$. **(c)** Representative images from the experiment showing the loss of pT66 IRIF with the WT but not K to R peptide.

Incubating the pT66 antibody with the WT phospho-peptide led to a loss of pT66 IRIF, as shown previously, but incubation with the K to R phospho-peptide did not lead to the same loss, with IRIF readily visible after damage. Fluorescence intensity was also reduced with the WT peptide, compared to the K to R peptide. Together, this indicates that the pT66 antibody does not recognise ubiquitin with alterations around T66, and again reflects the specificity of the pT66 antibody for phosphorylated ubiquitin.

3.2.3.d Detection of pT66 by immunoblotting

The antibody we have raised appears to specifically detect pT66 ubiquitin by immunofluorescence, so we asked whether the antibody could also be used for immunoblotting. U2OS cells were irradiated with 4 Gy using an X-ray source or left untreated, then split into subcellular fractions an hour after treatment. The resulting samples were run on an SDS PAGE gel and processed for immunoblotting. The full length of the membrane was probed for either ubiquitin, using the P4D1 antibody, or pT66 ubiquitin. Actin was used as a general loading control, with U1 snRNP marking the nucleoplasm fraction and histone H3 marking the chromatin fraction. The immunoblots are presented in Figure 3.6.

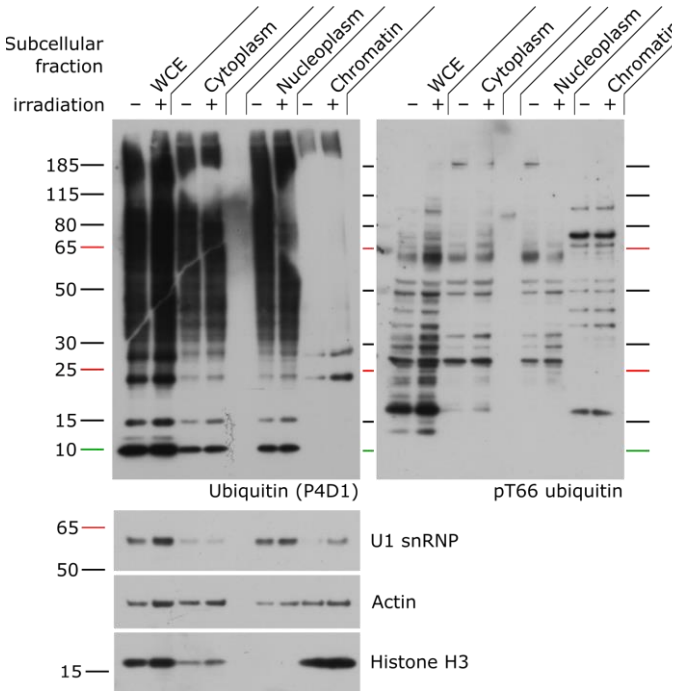

Figure 3.6: Immunoblotting with the pT66 antibody reveals a pattern of bands that is distinct from ubiquitin. Example blot of U2OS cells, optionally exposed to 4 Gy IR then harvested and fractionated 1 h post-treatment. Actin is used as a general loading control, with U1 snRNP used as a nucleoplasm fraction marker, and Histone H3 used as a marker of chromatin. Ubiquitin can be detected in its unconjugated form just below 10 kDa, with a characteristic "smear" of conjugated proteins at higher molecular weights. In contrast, the pT66 ubiquitin antibody seems to mark specific proteins, with less "smearing" evident.

The anti-ubiquitin P4D1 antibody detects both unconjugated and conjugated ubiquitin. Unconjugated ubiquitin is detected as a single band just below

10 kDa, and di-ubiquitin chains are seen at around 15 kDa. Above these bands, a characteristic "smear" is seen, as the antibody detects all ubiquitylated proteins and free ubiquitin chains present in these fractions.

The blot obtained using the pT66 antibody is strikingly different from the ubiquitin blot. The band of unconjugated ubiquitin detected with the P4D1 antibody is not seen, with the lowest detected band seen between 10 and 15 kDa. Although this is higher than the expected molecular weight for ubiquitin, this band could still be unconjugated ubiquitin. Phosphorylation is known to slow protein migration through SDS-PAGE gels due to the electronegativity of the phosphate group and can lead to bands that run above the expected weight. Use of a higher percentage gel to increase the resolution of the bands may help determine whether this band is unconjugated phospho-ubiquitin. At higher molecular weights, there is limited ubiquitin "smears", with single bands seen the length of the blot. If found to be specific, this indicates that pT66 ubiquitin is used to modify specific proteins, and suggests a specific role for this modification.

Surprisingly, there doesn't appear to be a difference between the irradiated and untreated samples in either the ubiquitin or phospho-ubiquitin blots. The darker signal in the irradiated samples correspond with an increase in signal in the actin loading control, suggesting that this apparent increase in signal is likely due to an increase in protein level in these samples, rather than a true increase in either ubiquitin or pT66 ubiquitin.

Antibodies that are specific and reliable in immunofluorescence are not always specific and reliable when used for immunoblotting, and vice versa. The lack of observable difference between irradiated and untreated samples by immunoblotting when striking differences are observed by IF suggested that at least some of the bands observed with the pT66 ubiquitin antibody may not be specific.

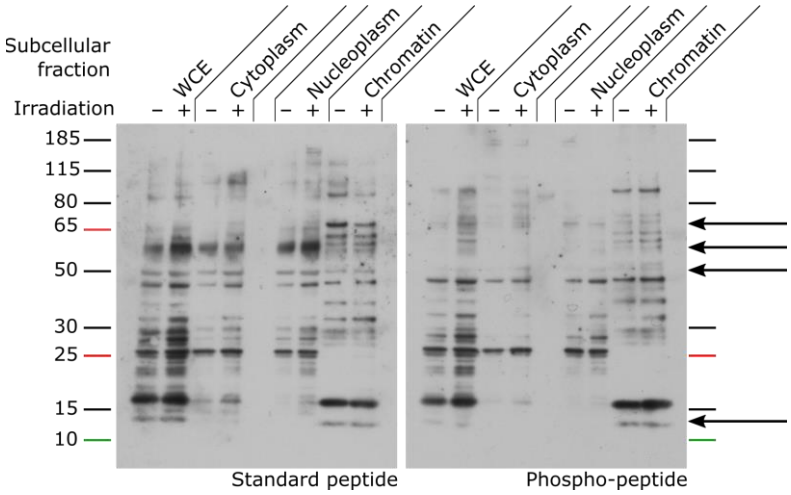

Figure 3.7: Signal from multiple bands is outcompeted by the T66 phospho-peptide. Representative blot of fractionated sample probed with pT66-ubiquitin antibody pre-incubated with peptide. There is a loss or reduction of signal from several bands after the antibody has been incubated with the phospho-peptide compared with the standard peptide, particularly seen between 50 and 80 kDa, and at the lowest band between 10 and 15 kDa. Overall signal is weaker in the membrane stained with the phospho-peptide antibody mix compared to the non-phosphorylated peptide.

The competition assay used previously was adapted for use in immunoblotting, anticipating that bands remaining when the antibody is incubated with the phospho-peptide may correspond to non-specific binding. The samples used in Figure 3.5 were again run on an SDS PAGE gel and processed for immunoblotting. To probe the membrane, the pT66 antibody was incubated with either the phosphorylated or standard peptide at a 1:100 molar ratio of antibody to peptide, and the whole mix was used for immunoblotting. The resulting blots are shown in Figure 3.7.

The antibody incubated with the standard peptide showed a similar blot to Figure 3.6, indicating that the antibody did not show affinity for the standard peptide over the proteins on the membrane. When the antibody was incubated with the phosphorylated peptide some of the bands reduced in intensity or disappeared entirely, indicating that these bands may be specifically recognised by the pT66-ubiquitin antibody. Some of these bands are not found on chromatin – the lowest molecular weight band in whole cell extract was shown to be reduced in intensity in the presence of the phospho-peptide, but a band at the same molecular weight in the chromatin fraction appears unaffected. A large band seen in all fractions except chromatin, at a molecular weight just below 65 kDa was also observed to be out-competed by the phospho-peptide.

The competition assay relies on the pT66 antibody having a greater affinity for the phospho-peptide than for endogenous proteins. Whilst this might be the case in IF, it is not necessarily so in immunoblotting. To test whether the pT66 antibody was recognising phosphorylated proteins, lambda phosphatase, a phosphatase with activity against phospho-serine, threonine and tyrosine, was used to de-phosphorylated proteins directly on the immunoblot membrane, to see whether the pT66 antibody was binding to non-phosphorylated proteins. Samples for immunoblots were prepared as before, with the addition of a sample collected 4 hours after irradiation. These samples were run on a gel in duplicate, then transferred to membranes, as before. Membranes were then incubated in enzyme buffer, with or without lambda phosphatase, then probed using the pT66 antibody. The resulting blots are shown in Figure 3.8.

Many of the bands present in the control membrane are reduced or absent after treatment with lambda phosphatase, indicative of the pT66 ubiquitin antibody being phospho-specific.

The band at around 65 kDa that was lost in the competition assay is also lost upon phosphatase treatment. Additional bands are also seen to be lost or reduced compared to the competition assay. Previously a reduction in intensity was observed only in the WCE fraction of the bands at 10-15 kDa, but upon phosphatase treatment a reduction is also seen in the chromatin fraction. Also of note is the increased signal in the irradiated samples compared to the untreated samples, which is sensitive to treatment with the phosphatase. Unlike previous blots, this increase in signal does not appear to be linked to uneven protein loading, as evidenced by the loading controls, and may indicate induction of pT66 following DNA damage.

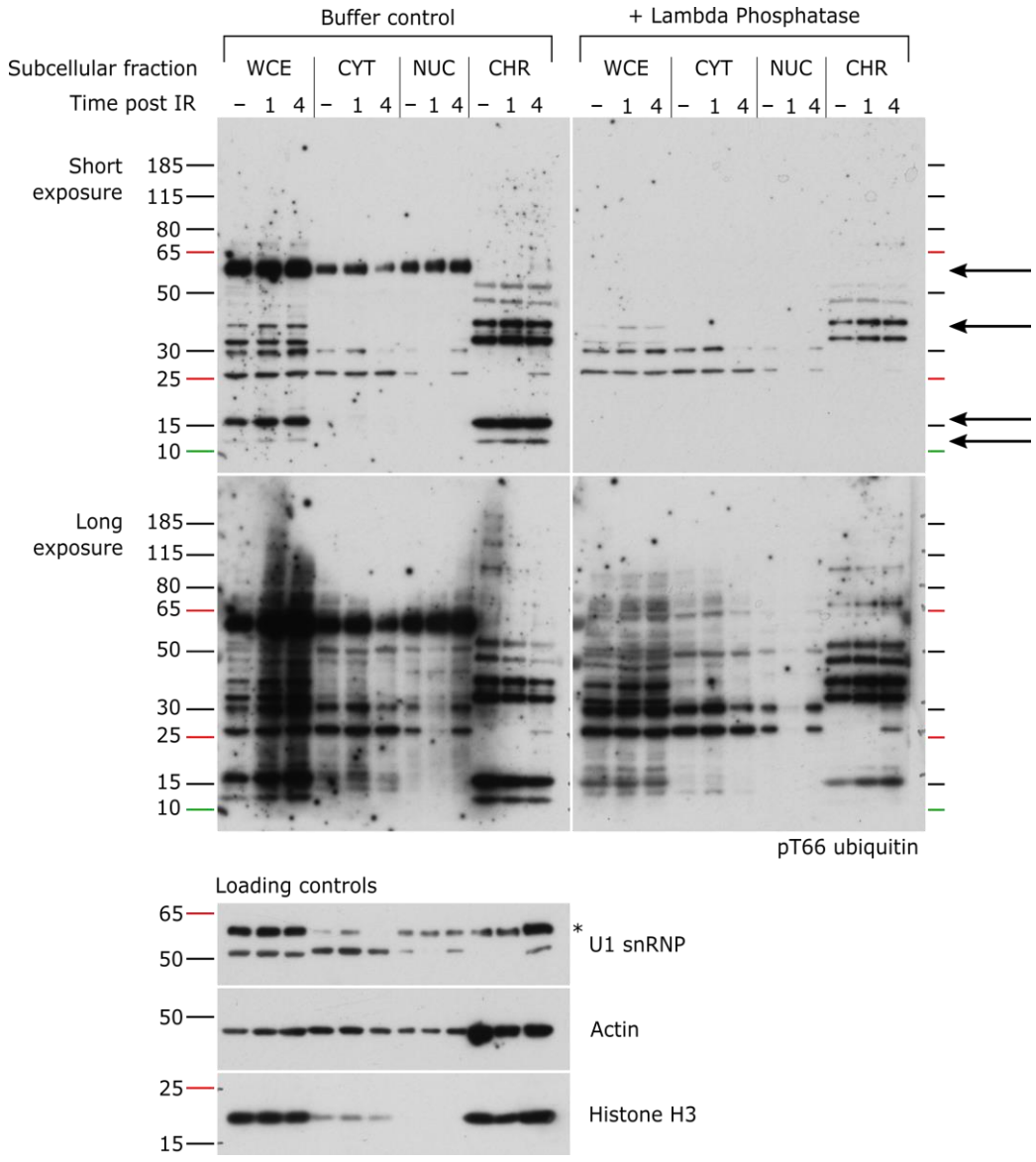

Figure 3.8: Signal from pT66 ubiquitin is reduced following phosphatase treatment of membrane bound proteins. Example blot showing pT66-ubiquitin staining when membrane has been optionally treated with lambda phosphatase. Bands observed to disappear or reduce in intensity in the peptide competition assay were also reduced following treatment with lambda-phosphatase. Additional bands were reduced following phosphatase treatment. Notably, the bands between 10 and 15 kDa were lost in both WCE and chromatin fractions following phosphatase treatment, whereas the peptide competition assay only saw reduction in the WCE fraction. Two bands of U1 snRNP were observed in this assay. The top band (labelled *) is specific for U1 snRNP.

3.3 Discussion

Through validation of an antibody raised against pT66 ubiquitin, I have demonstrated that this modification is detected in mammalian cells, and localises to IRIF after inducing DNA damage. These IRIF colocalise with a known marker of DSBs, 53BP1, suggesting a role for pT66 ubiquitin in the DSB response. As an incidental finding during validation of the antibody, a mutant of ubiquitin that could not be phosphorylated at T66 (T66A) showed a reduction in the number of 53BP1 foci after damage, providing a useful insight for further work into identifying the role of this modification within the DSB response.

3.3.1 A raised antibody detects pT66-ubiquitin in mammalian cells

pT66 ubiquitin in mammalian cells is seen by both immunofluorescence microscopy and immunoblotting, with both techniques revealing a signal that is distinct from bulk unmodified ubiquitin. The evidence for specificity of the pT66 antibody by IF is strong, with confirmation from the competition assays and the introduction of ubiquitin mutants both indicating the phospho-specificity and specificity for ubiquitin itself (Figure 3.3, Figure 3.4). The difference in staining with the pT66 antibody, which shows discrete foci, compared to the anti-FLAG antibody, which showed whole cell staining of FLAG-tagged ubiquitin, also indicates the specificity of this antibody for the phosphorylated epitope (Figure 3.4).

The foci formed by pT66 ubiquitin co-localise with 53BP1, suggesting a role for pT66 at break sites. Unlike 53BP1 which is detected in most cells after DNA damage, pT66 IRIF are identified in 40-60% of cells. One explanation for this difference is that pT66 IRIF could be formed in specific conditions, with cell cycle stage a likely candidate for further study. A limit of detection issue cannot be ruled out, however. Many cells do show high background staining with the pT66 ubiquitin antibody, without detectable foci. This raises possibility that foci formation may be missed in these cells. Further work is needed to optimise staining conditions, with scope for using different microscopes that may overcome issues from background staining.

Unlike the signal detected by IF, detection of pT66 by immunoblotting gives a less clear result. Competing for binding sites using the phosphorylated peptide revealed a few candidate bands that were likely to be specific – the bottom most band between 10 and 15 kDa, which may represent unconjugated phosphorylated ubiquitin, and a strong band between 50 and 65 kDa, which is an unknown protein (Figure 3.7). Treatment with lambda phosphatase led to a greater overall reduction in signal than was seen with the peptide competition assay, with several additional bands disappearing. This could indicate that the antibody is non-specifically recognising other phospho-proteins (Figure 3.8). The bottom band in the chromatin fraction could indeed be non-specific. The molecular weight would correspond to free phosphorylated ubiquitin, but this would not be expected to be present in the chromatin fraction – free ubiquitin marked using the P4D1 antibody is seen in all fractions excluding chromatin in a previous figure (Figure 3.7).

Of note is the lack of difference between irradiated and untreated samples when pT66 ubiquitin is visualised by IB. An increase in pT66 ubiquitin signal intensity in damaged samples would be expected if this PTM is induced by IR. There is an increase in signal in Figure 3.8 in the whole cell extract sample, but this increase is not mirrored in the cell fractions, so may be an artifact rather than true signal.

IB can be less sensitive to changes than IF. IB relies on changes in a population – if only a small amount of ubiquitin is phosphorylated upon DNA damage, and this only occurs in a proportion of cells (up to 60% of cells observed forming foci by IF), then the increase across the population may not be detected by IB. Identifying what causes some cells to make pT66 foci would enable manipulation of conditions to boost the pT66 signal. For example, if pT66 is cell cycle dependent, then using a synchronised culture would ensure that more of the population were in the appropriate cell cycle phase, boosting the signal compared to asynchronous culture. Similarly, increasing the dose of IR cells are exposed to could increase detection of pT66. Increasing the dose of IR will

increase the amount of DNA damage, which may in turn increase the amount of pT66 in the cells, aiding detection.

3.3.2 Cells expressing T66A ubiquitin show a decrease in 53BP1 IRIF

Expression of T66A ubiquitin, which cannot be phosphorylated at this residue, led to a significant decrease in the number of 53BP1 foci per cell, as well as the number of cells overall with a robust response to DNA damage (measured as 10 or more 53BP1 foci in the cell). This decrease was not seen with modification of the adjacent phospho-site, S65. 53BP1 is dependent on ubiquitin signalling for its recruitment, so pT66 ubiquitin may play a direct role in this pathway. During my PhD, work from the Penengo lab identified a different ubiquitin phospho-site, T12, as also regulating 53BP1 recruitment (Walser et al., 2020). Phosphorylation at T12 prevents recruitment of 53BP1, which seems to directly oppose my finding of phosphorylation at T66 promoting this recruitment – this is an exciting prospect for a phosphorylation "switch" in pathway choice.

Other DDR proteins also require ubiquitin for recruitment, and the impact of T66A in these other pathways has yet to be explored. If pT66 impacts proteins earlier in the pathway, then 53BP1 will also be disrupted. The role of pT66 ubiquitin in the DNA damage response is an exciting area for study, and will be followed up in this thesis.

3.3.3 The pT66-ubiquitin antibody shows centrosomal staining in undamaged cells

By IF, a clear signal that is independent of DNA damage is seen outside of the nucleus, which may represent centrosomes (Figure 3.9). The focus is seen to divide, relocate to opposite sides of the nucleus when chromatin is seen to condense, and appears at the spindle poles during mitotic segregation, following a pattern consistent with centrosomes (Bergmann et al., 2020). This signal was seen to reduce in intensity at only high molar ratios of phosphorylated peptide to antibody (Figure 3), and was not lost in staining conditions that disrupted detection of pT66 IRIF.

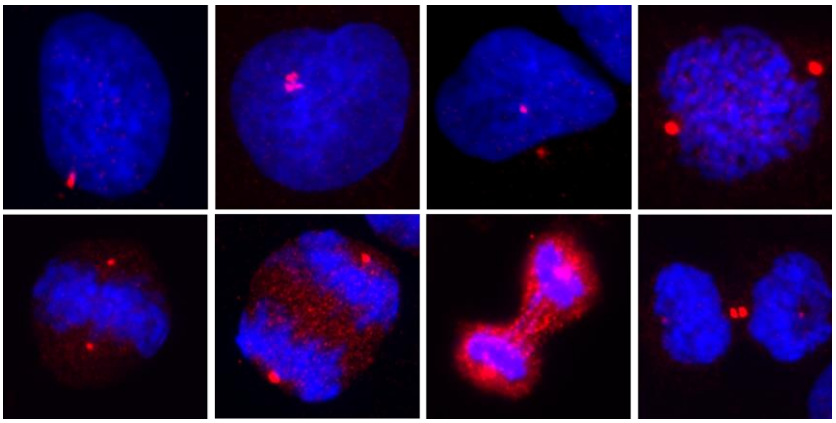

Figure 3.9: The pT66 antibody recognises an extra-nuclear signal that follows centrosomal patterns during the cell cycle. Representative images from multiple experiments showing the single focus duplicating, then moving to opposite sides of the nucleus when chromosomes condense. The foci are then found at the spindle poles during mitosis, with signal becoming bright between the segregating chromosomes. Signal is subsequently seen at the midbody after mitosis.

Centrosomes are important in the DDR, acting as a hub for signals relating to cell cycle progression and arrest after damage (Mullee and Morrison, 2016). Centrosomes also directly interact with chromatin re-modellers, and impact chromatin mobility through formation of γ-tubulin, allowing repair proteins access to damaged chromatin (Ma et al., 2021). It could be that the signal seen by IB in undamaged cells is from this centrosomal staining, although further confirmation that the signal is located at centrosomes and is specific is required. If this signal is found to be linked to centrosomes, then there is a possibility that the signal detected in damaged cells is not new formation of pT66 ubiquitin, but relocation of pT66 ubiquitin to damaged sites, which could explain why there are no strong differences detected between irradiated and untreated samples when viewed by IB.

3.3.4 Mass spectrometry did not identify pT66-ubiquitin peptides from mammalian tissue culture

Despite pT66 ubiquitin being identified by mass spectrometry originally, this modification was not found in the sample from mammalian cells. There are many reasons why this may have been the case, and it is hoped that through optimisation of both sample preparation and mass spectrometry method detection of pT66 ubiquitin by mass spectrometry may be possible. This would enable

additional experiments, such as quantification of pT66 peptides, which could enable identification of proteins involved in creating and placing this modification.

The number of ubiquitin peptides identified in the original sample from *Xenopus* egg extract was more than double the number identified from tissue culture. This discrepancy alone could contribute to the lack of detection of pT66, as only 1 peptide from 1066 was identified with the pT66 modification originally. Other identified modifications of ubiquitin have been found to make up a small proportion of total ubiquitin, and the signal tends to be highly localised to the area of signalling (Swatek and Komander, 2016). Mass spectrometry has a known bias against "rare" peptides in complex samples, so in non-optimised conditions these less common modifications can be missed (Peck Justice et al., 2021).

Increasing the amount of starting material to increase the number of ubiquitin peptides only addresses half the problem – although there is more ubiquitin, the complexity of the sample remains unchanged. Altering the mass spectrometry technique itself can help overcome this limitation. Using selected ion monitoring limits the spectrum generated by mass spectrometry by limiting the detected mass to charge ratios to the expected values for the target protein. By using a targeted approach rather than a whole spectrum approach, this can greatly increase the sensitivity of mass spectrometry for these low abundance peptides, and may enable robust detection of pT66 ubiquitin (Li et al., 2012).

Altering the sample preparation itself is also key to detecting pT66 ubiquitin. Between the *Xenopus* and tissue culture samples, several variables were altered that may have impacted the formation of pT66 ubiquitin. In the *Xenopus* egg extract sample, K6-only ubiquitin was added to the extract. This mutant of ubiquitin allows formation of K6 linked chains, but terminates formation of other chains, thus promoting short chain and mono-ubiquitylation. In contrast, wild-type ubiquitin was expressed in the mammalian cells used for the mass spectrometry sample, which would be unlikely to bias chain formation. Contrasting the chain types seen in the *Xenopus* sample with the tissue culture

sample (Table 3.1 and Table 3.2) highlights the differences seen between samples. Recent work from Swatek et al. (2019) revealed that pS65 ubiquitin is primarily found on mono-ubiquitin or short polyubiquitin chains. If pT66 ubiquitin follows a similar pattern, then the K6-only ubiquitin would be more likely to increase the amount of this modification for detection.

The way the damage was induced was also changed between samples. DSBs in egg extract were induced with the endonuclease EcoR1, which gives rise to clean DSBs with limited overhangs. Ionising radiation was used to induce damage in the tissue culture sample. IR gives rise to many different types of DNA damage, including single-stranded lesions and base alterations, as well as DSBs (Mavragani et al., 2019). This activates multiple DDR pathways, not just the DSB response, and so increases the complexity of ubiquitin signalling within the sample, potentially limiting detection of pT66 ubiquitin. Increasing the dose of IR increases the amount of DSBs induced within the sample, and may aid detection of pT66 ubiquitin.

Other optimisations to explore include using different pulldown techniques, perhaps using FLAG tag pulldown which is generally “cleaner” than the HIS-pulldown originally used. Phospho-peptide enrichment could also be of benefit, either at the whole protein level or after tryptic digestion at the peptide level. Whilst this would enrich for all phosphorylated peptides, not just phospho-ubiquitin, it would help decrease the overall complexity of the sample, potentially aiding detection of the low-abundance pT66 peptide. There are many optimisations and considerations for further work for mass spectrometry, but there is confidence that this modification will be detected in tissue culture.

Chapter 4: Expression of ubiquitin that cannot be phosphorylated at T66 causes phenotypes indicative of an impaired DDR

4.1 Introduction

In chapter 3, pT66-ubiquitin was observed to form foci after cells were exposed to ionising radiation, and these foci co-localised well with a known marker of DSBs, 53BP1. Strikingly, expression of a mutant of ubiquitin that cannot be phosphorylated at T66 (T66A) showed reduced numbers of 53BP1 foci after damage, indicating that pT66-ubiquitin may be involved in the DDR pathway that recruits this protein.

This led to the next aim of my thesis – to determine whether pT66-ubiquitin has a role in the DDR by observing the phenotypes caused by replacing endogenous ubiquitin with mutants of ubiquitin.

4.2 Results

4.2.1 Creating the ubiquitin mutants used in this study

To investigate the impact of loss of pT66-ubiquitin, a number of ubiquitin mutants were created. T66A ubiquitin prevents phosphorylation at this site, allowing us to determine the phenotypes that occur in the absence of pT66-ubiquitin. Conversely, mutation to T66D acts a phospho-mimic, as the aspartic acid carries a strong electro-negative charge that partially recapitulates the electro-negativity of the phosphate group. A mutant with the adjacent serine mutated to alanine, S65A, was also created. This residue is known to be phosphorylated, but is not known to play a role in the DNA damage response, so should show that any phenotypes identified can be attributed to phosphorylation at T66 specifically. Mutant K63R was created as a negative control,

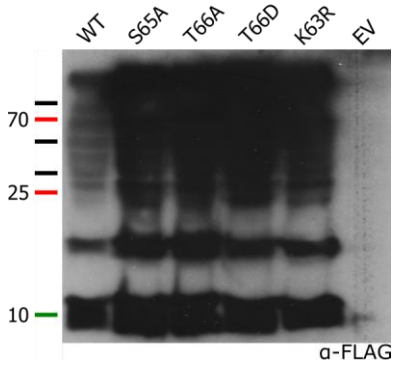

Figure 4.1: Transfected cells show expression of FLAG-tagged ubiquitin mutants. Example blot from cells transiently expressing FLAG-ubiquitin mutants 48 hours after transfection. "Free" non-conjugated ubiquitin is detected around 10 kDa, and a characteristic ubiquitin smear is seen at higher molecular weights. EV: empty vector control plasmid.

as K63 linked ubiquitin chains are known to be important in the DDR, and mutation to arginine prevents these chains from forming.

A FLAG-tagged, siRNA resistant form of ubiquitin in a pcDNA3.1 plasmid backbone from the Penengo lab was used as the base for site-directed mutagenesis to create the FLAG-tagged mutants used in this study. The primers used are listed in table 2.2.

Once the mutants of ubiquitin had been created, they were transfected into U2OS cells to test that they were expressed and able to be conjugated. The cells were harvested 48 hours after transfection, and the samples prepared for immunoblotting with an anti-FLAG antibody. The resulting blot in Figure 4.1 shows that the ubiquitin mutants are transiently expressed within the cells and conjugated to substrates. The "free pool" of non-conjugated ubiquitin, used for the majority of new ubiquitin signalling, is detected as a band at around 10 kDa, consistent with ubiquitin's predicted molecular weight of 8.6 kDa. Interestingly, the ubiquitin mutants show two bands – one just under 10 kDa, and an additional band just over 10 kDa. Despite this anomaly, the presence of a characteristic "ubiquitin smear" at higher molecular weights indicates that the expressed ubiquitin mutants are all able to be conjugated to substrates, and so are suitable for further use.

4.2.2 Replacement of endogenous ubiquitin with siRNA

As ubiquitin is abundant within the cell, overexpression of exogenous ubiquitin alone may not be sufficient to detect phenotypes. Knockdown of endogenous ubiquitin by siRNA is possible by using two siRNAs that target their respective poly-ubiquitin precursor gene, UBA52 or RPS27A, as well as the poly-ubiquitin genes UBB and UBC (Gatti et al., 2015)(Figure 4.2a). By knocking down endogenous ubiquitin and replacing it with our siRNA resistant ubiquitin mutants, a clearer picture of the phenotypes may be possible. To test whether this was a viable method of replacing ubiquitin for our cells, U2OS cells were transfected with wild-type ubiquitin or left un-transfected, and subsequently treated with anti-ubiquitin siRNA or a non-targeting control siRNA. Samples were run

on a 4-12% SDS PAGE gel, and the membrane probed for ubiquitin using the P4D1 antibody. The resulting immunoblot is shown in Figure 4.2b.

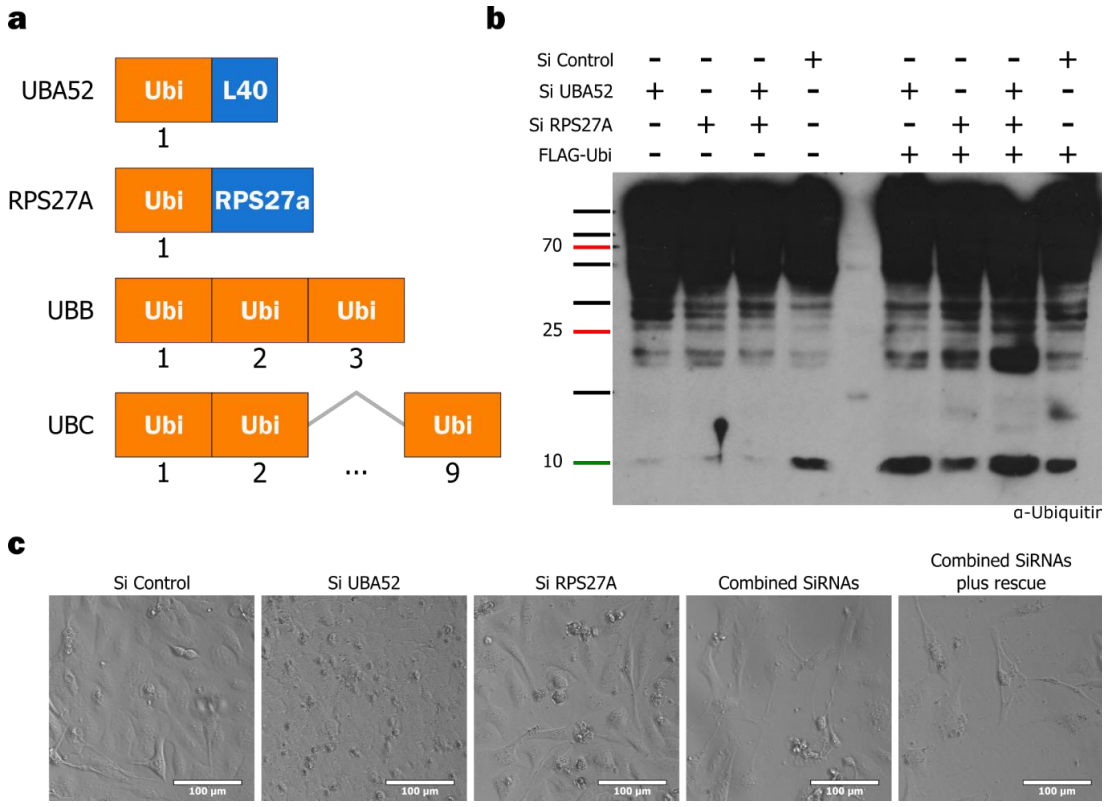

Figure 4.2: Replacing endogenous ubiquitin through siRNA knockdown leads to reduced cellular viability. (a) Diagram of the 4 genes expressing ubiquitin in human cells. **(b)** U2OS cells treated with siRNA and optionally transfected with WT-ubiquitin were harvested, and the samples prepared for immunoblotting. An example blot is shown. **(c)** Representative images of the cells from (b) prior to harvest.

In cells transfected with anti-ubiquitin siRNA alone, the ubiquitin free pool (band at 10 kDa) is greatly reduced compared with the non-targeting siRNA control. The ubiquitin smear is still present, which is expected with short term knockdown of ubiquitin. In cells transfected with the siRNA resistant wild-type ubiquitin, the free pool remains. suggesting that the overexpression of ubiquitin from the plasmid is sufficient to replace the endogenous ubiquitin in this pool. However, the viability of these cells is low, and they exhibit morphology indicative of stress and apoptosis, such as cell shrinking and membrane blebbing (Saraste and Pulkki, 2000)(Figure 4.2c). This reduction in viability makes this method of ubiquitin replacement unsuitable for use in further experiments.

4.2.3 Creation of stable cell lines to express mutants of ubiquitin

Transfecting cells can be toxic and lead to a decrease in cell viability. There is also the complication of determining which cells have been successfully transfected. These complications can be avoided by using cell lines that have exogenous gene coding for ubiquitin stably incorporated into cell genome so that cells can be induced to express mutants of ubiquitin, rather than through transient transfection. Flp-In U2OS cells were gifted from the Morris lab, alongside a plasmid (pcDNA5 FRT/TO) that expressed an siRNA-resistant, HIS-tagged ubiquitin. The Flp-In system uses a recombinase to incorporate a gene on the pCDNA5 FRT/TO plasmid into the cells genome. The recombinase site puts the incorporated gene under the control of a tet-operon, which allows for expression of the gene in the presence of tetracycline or tetracycline derivatives, such as doxycycline.

Site-directed mutagenesis was used to create the ubiquitin mutants in the pcDNA5 FRT/TO plasmid. The plasmids were first tested for use through transient transfection. Expression testing was carried out as described previously, and the samples were probed for expression of the HIS-tag. The immunoblot didn't show the free pool of ubiquitin, however the smear at higher molecular weights detected with anti-His antibody was a positive indicator that HIS-tagged ubiquitin was expressed, and the plasmids could be used for transient transfection (Figure 4.3a).

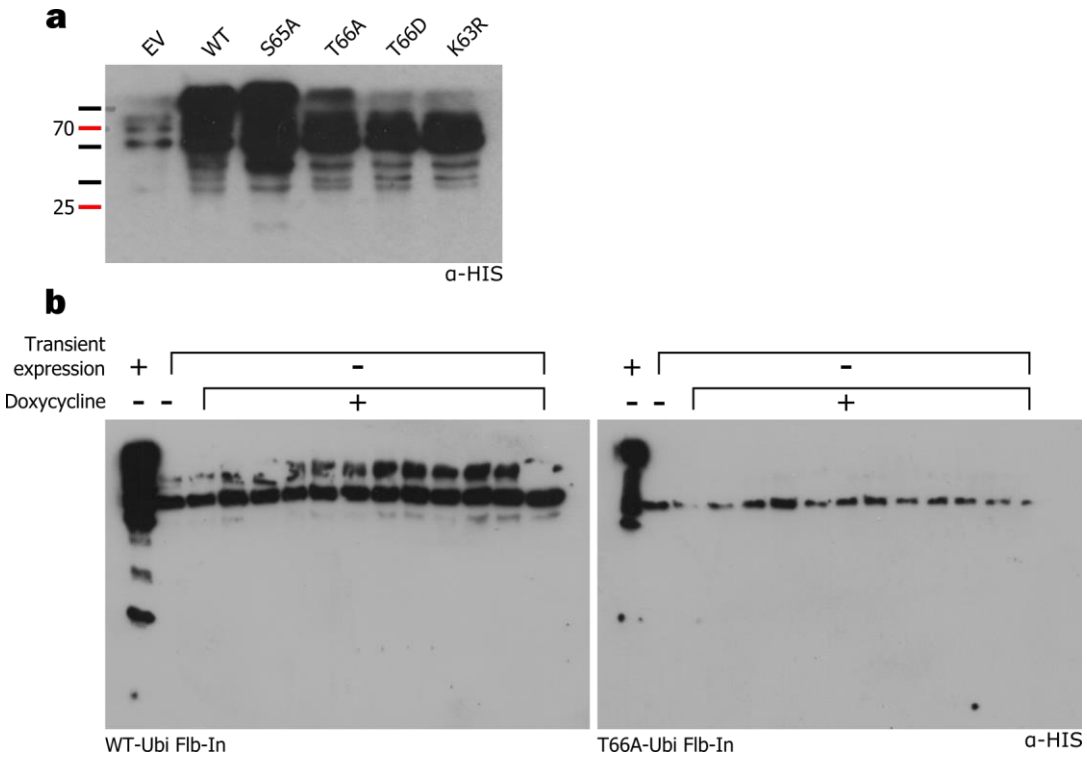

Figure 4.3: HIS-tagged ubiquitin can be transiently expressed from pcDNA5 FRT/TO plasmids, but cannot be used to create inducible cell lines. **(a)** Example blot showing transient expression of the HIS-tagged ubiquitin mutants. Using the anti-His antibody, the free pool of ubiquitin is not always detected. **(b)** Example blot showing transient and doxycycline-induced expression of HIS-tagged ubiquitin.

The first cell lines were created using the WT and T66A plasmids, using the method described in section 2.3.5. Clonal populations that showed resistance to hygromycin B and sensitivity to Zeocin were carried forward for expression testing. Cells were seeded in duplicate onto 6 well plates and incubated in tetracycline free medium in the presence or absence of doxycycline. Unmodified U2OS cells were also seeded, and transfected with either the ubiquitin mutant or an empty vector control, to show expression from the vector. Flp-In U2OS cells cannot be used for transient transfection from the vector due to the tet-operon supressing the expression. After 48 hours, cells were harvested for use in immunoblotting. Samples were run on a 12% SDS PAGE gel then transferred to PVDF membrane, which was probed for the HIS-tag. The resulting blot is shown in Figure 4.3b.

Disappointingly, the blot revealed that the cell lines created did not present the expected ubiquitin smear after induction with doxycycline – the signal observed was identical with and without doxycycline. A range of doxycycline doses were trialled, yet no expression was detected (data not

shown). The failure of the cell lines to express sufficient ubiquitin meant that they could not be used with the anti-ubiquitin siRNA to increase cell viability, making this approach to ubiquitin replacement non-viable.

4.2.4 Using proteasome inhibition to promote signalling with exogenous ubiquitin

An alternative method of ubiquitin replacement involves disrupting ubiquitin homeostasis by inhibiting proteasomal degradation of proteins. The majority of ubiquitin in cells is found conjugated to proteins, targeting the substrate proteins for degradation by the proteasome. Normally these ubiquitin chains would be targeted by DUBs after the activity of the proteasome on the substrate protein, recycling these ubiquitin chains into the free pool of ubiquitin for further signalling. MG132 is a reversible inhibitor of the proteasome, preventing degradation of substrate proteins which in turn prevents the recycling of ubiquitin into the free pool. Treatment with MG132 has been demonstrated to deplete the free pool of ubiquitin. In a background where there is overexpression of exogenous ubiquitin, this is thought to mostly impact upon the endogenous pool, ensuring that most new ubiquitin signalling occurs using the exogenously expressed ubiquitin (Figure 4.4). Use of MG132 should enable clear detection of phenotypes caused by expressing the ubiquitin mutants.

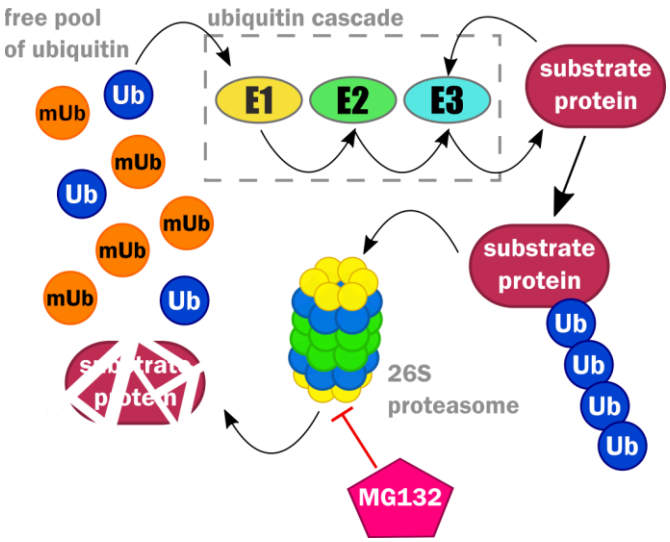

Figure 4.4: Inhibition of the proteasome by MG132 depletes the free pool of ubiquitin. This system can be exploited with ubiquitin overexpression to drive ubiquitin signalling primarily with the exogenously expressed ubiquitin.

The pcDNA3.1 plasmids, expressing the FLAG-tagged ubiquitin were carried forward for use in further testing. It had been noted during expression testing that detection of the free pool of ubiquitin was not always possible using the anti-His antibody with HIS-tagged ubiquitin expression, whereas it was consistently seen with the anti-FLAG antibody using the FLAG-tagged ubiquitin

constructs. Whether this reflected differences in antibody binding or reflected reduced expression from the HIS-tagged ubiquitin was not immediately clear. The anti-FLAG antibody also had the benefit of giving a cleaner signal for immunofluorescence, and so expression of FLAG-tagged ubiquitin had benefits for further work.

4.2.5 Expression of T66A ubiquitin reduces the number of 53BP1 foci detected after ionising radiation

In chapter 3, a reduction in the number of 53BP1 foci was noted in cells transfected with the T66A mutant of ubiquitin (Figure 3.4). To investigate this further, the ability of U2OS cells to form ionising radiation induced foci (IRIF) after transfection with mutants of ubiquitin was tested. In addition to investigating 53BP1 IRIF, the ability of cells to form γH2AX IRIF was also investigated. This mark doesn't explicitly rely on ubiquitin signalling, and so should behave relatively independently of the ubiquitin mutants. The phosphorylation of H2AX to form γH2AX occurs within moments of damage induction and is removed once damage is resolved, allowing an insight into general repair dynamics. All cells were co-stained for FLAG, to identify the cells expressing the tagged ubiquitin mutants. FLAG-negative cells were also quantified as a negative control, to show IRIF formation in cells with a depleted ubiquitin pool. These cells are referred to as "empty" in the quantification. Representative images and quantification are shown in Figure 4.5.

Cell expressing WT ubiquitin showed the expected rapid increase in γH2AX fluorescence intensity after induction of DNA damage, with a decrease in signal by 1 hour, corresponding with resolution of DNA damage. The number of 53BP1 IRIF also followed this same pattern. "Empty" cells showed an increase in γH2AX intensity at 30 minutes, consistent with γH2AX formation being independent of ubiquitin signalling . In contrast, by 8 hours post-IR, γH2AX intensity was higher in cells not expressing exogenous ubiquitin (empty) than in the WT expressing cells, consistent with a defect in resolution of DNA damage in the absence of ubiquitin signalling. The level of 53BP1 foci in these cells is notably lower at all time points, reflecting the necessity of ubiquitin for recruitment of 53BP1.

Strikingly, the number of 53BP1 IRIF in T66A expressing cells is also greatly reduced at 30 minutes and 1-hour post-IR. This defect in 53BP1 recruitment is not seen in the S65A mutant, showing that this defect is specific to the T66A mutant. However, both the T66A and S65A mutants show an increase in γH2AX IRIF at 1-hour post-IR compared to the WT ubiquitin. In both T66A and S65A mutants, the γH2AX intensity and number of 53BP1 IRIF return to wild-type levels by 8 hours, in contrast to both the K63R mutants and “empty” cells, which still show abnormal IRIF levels.

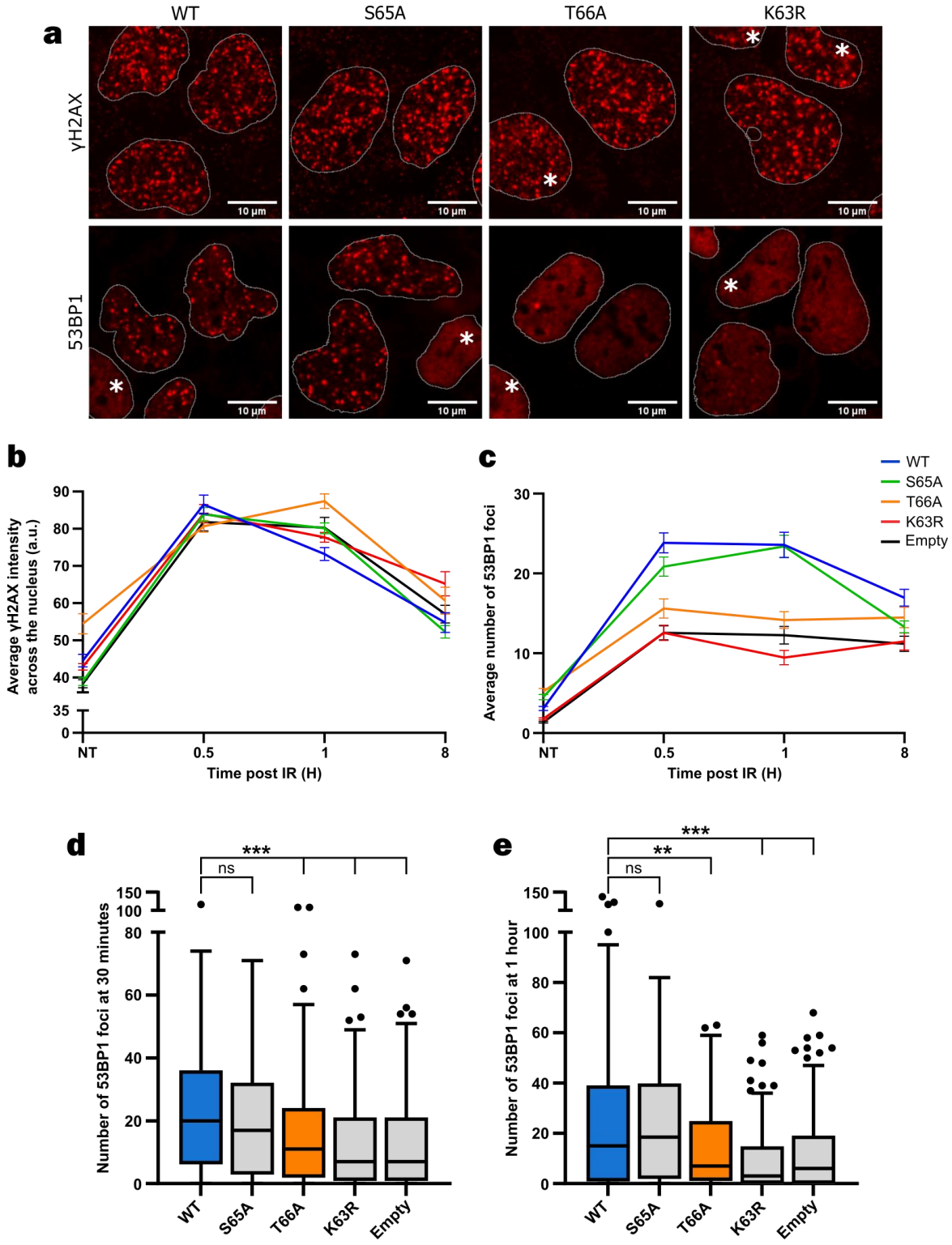

Figure 4.5: T66A ubiquitin shows reduced 53BP1 IRIF formation with a corresponding increase in γH2AX fluorescence intensity. U2OS cells treated with MG132 and then irradiated, were fixed at the indicated times post-IR and stained for γH2AX or 53BP1 and FLAG. Data from 3 repeated experiments. **(a**) Representative images of cells expressing T66A or K63R, fixed at 1-hour post-IR and stained for FLAG and either γH2AX or 53BP1. Cells marked with an asterisk (*) are FLAG-negative (quantified as "empty"). **(b)** Quantification of γH2AX fluorescence intensity across the nucleus. Mean intensity with SEM is represented. **(c)** Quantification of the number of 53BP1 foci in each condition. Mean foci number with SEM is shown. **(d)** and **(e)** Tukey boxplots of 53BP1 IRIF at 30 minutes and 1-hour post-IR respectively. Data shown is from 3 repeats, and statistical analysis was carried out using a Kruskal-Wallis one way ANOVA with Dunn's multiple comparisons test, comparing each condition to WT. p-values are displayed as shown: **, p<0.01; ***, p<0.001

4.2.6 Discovery and correction of a missing stop codon in the pcDNA3.1 plasmid

As these experiments were being carried out, work to create additional mutations at ubiquitin's C-terminal was underway. It was at this point that it was noticed that the stop-codon was missing from the FLAG-tagged ubiquitin plasmids, leading to the expression of ubiquitin with an additional 18 amino acids at the C-terminal (Figure 4.6). A similar addition has been seen to affect ubiquitin dynamics with clinical impact (Lindsten et al., 2002). To eliminate any complications from this C-terminal addition, SDM was used to introduce a stop codon after the di-glycine motif to allow expression of a normal length ubiquitin, and the experiment quantifying the 53BP1 and γH2AX foci was repeated with these new "fixed" plasmids.

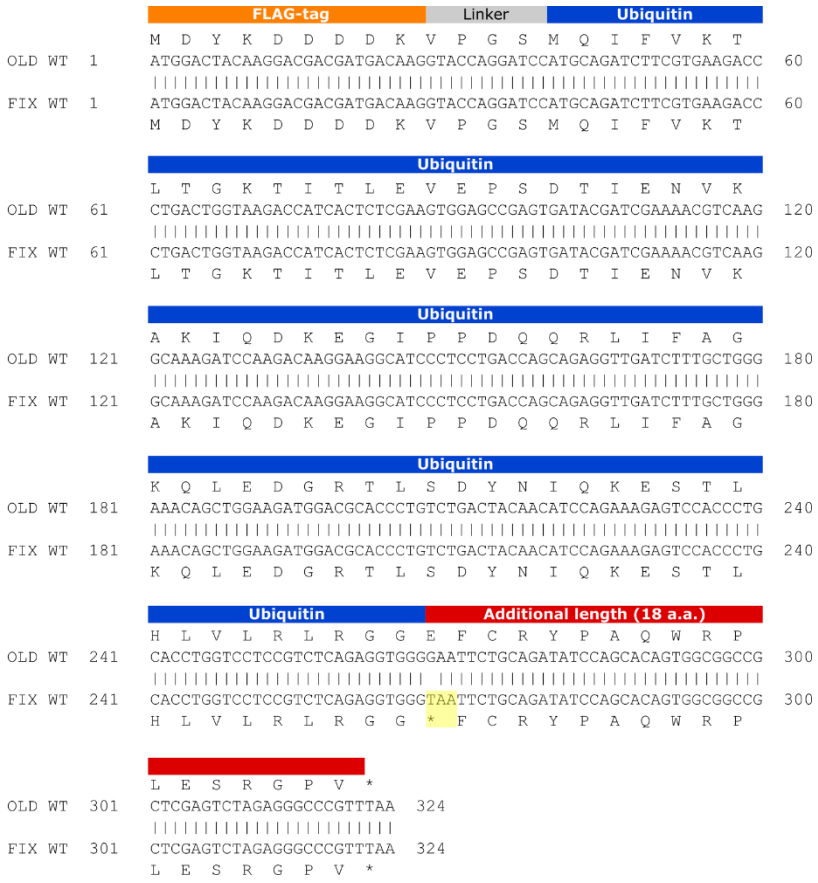

Figure 4.6: The original FLAG-ubiquitin expressing plasmid has a missed stop codon, leading to an additional 18 amino acids at the C-terminal tail of ubiquitin. Sequencing of the original WT ubiquitin plasmid (top) compared with the fixed stop-codon plasmid (bottom). The newly introduced stop codon is highlighted in yellow.

4.2.7 Expression of ubiquitin mutants with the appropriate stop codon confirms the 53BP1 phenotype

Whilst introducing the stop codon with SDM, new antibodies were sourced for FLAG and γH2AX, enabling co-staining by all three antibodies on the same sample. Example images and quantification using the corrected plasmids are shown in Figure 4.7. The staining with the new γH2AX antibody was clearer, enabling quantitation of the number of foci rather than using fluorescence intensity as a proxy for γH2AX.

The peak number of γH2AX foci was detected 30 minutes after treatment with IR (Figure 4.7b), consistent with the peak in fluorescence intensity at 30 minutes post IR observed previously (Figure 4.5b) The number of γH2AX foci remains constant at 1 hour post IR, in contrast to the reduction in fluorescence intensity seen previously. It is not clear whether this difference can be attributed to the change in ubiquitin plasmid, or the change in experimental set up and detection. This makes direct comparison of the two experiments difficult, though comparisons of the differences between ubiquitin mutants in each experiment is appropriate.

Differences in the number of γH2AX foci detected between ubiquitin mutants are apparent by 30 minutes post IR. Cells expressing S65A ubiquitin showed comparable numbers of foci to WT ubiquitin, with all other mutants of ubiquitin and “empty” cells showing elevated numbers of foci. This increase in γH2AX foci is also seen at later timepoints, and may reflect persistence of unrepaired DSBs, indicative of a repair defect (Siddiqui et al., 2015).

By 8 hours post-IR, a decrease in the number of γH2AX foci relative to the number at 1 hour is observed in all ubiquitin mutants. Interestingly, a difference between WT and S65A ubiquitin can be observed at this time, with S65A ubiquitin showing a higher number of γH2AX foci relative to WT ubiquitin. This will be explored in the discussion section. Caution is needed in interpreting the results at this late time point, as MG132’s inhibition of the proteasome is reversible, and so endogenous ubiquitin is likely to be available for signalling at this time (Kisselev and Goldberg, 2001).

The number of 53BP1 foci counted in this experiment differed from what was recorded in the original experiment. Previously 53BP1 foci number peaked at 30 minutes in cells expressing WT ubiquitin (Figure 4.5c), but in this experiment the peak is seen later, at 1-hour post-IR (Figure 4.7c). As seen previously, cells expressing S65A ubiquitin were able to form 53BP1 foci in response to IR, with levels not significantly different from WT ubiquitin at 30 minutes or 1-hour post-IR. Unexpectedly, the levels of 53BP1 foci in cells expressing S65A ubiquitin remained high at 8 hours post-IR, and didn't reduce to the numbers seen in WT ubiquitin expressing cells, reflecting the elevated levels of γH2AX also seen in this mutant. Cells expressing K63R ubiquitin, or not expressing exogenous ubiquitin both showed fewer 53BP1 foci than WT expressing cells, as observed with the previous ubiquitin plasmid.

Cells expressing T66A ubiquitin formed the fewest 53BP1 foci at both 30 minutes and 1 hour after IR, despite comparable numbers of γH2AX foci (Figure 4.7b and c). This confirms the reduction in 53BP1 foci upon expression of T66A observed previously (Figure 4.5c), and suggests that this reduction is not due to impaired detection of DSBs. The phospho-mimetic mutant T66D was added to this experiment. Although able to recruit 53BP1 at a comparable level to WT and S65A ubiquitin at 30 minutes post-IR, there is a reduction in 53BP1 foci observed at 1 hour (4.7c, d and e). As γH2AX foci don't decrease over the same time in this mutant (Figure 4.7b), this is unlikely to be a reflection of completed repair, but an inability to retain 53BP1. This observation raises the possibility of multiple readers of pT66 ubiquitin, with the phospho-mimetic T66D mutant sufficient for initial recruitment of 53BP1, in contrast to the lack of recruitment by T66A, but insufficient for subsequent retention of 53BP1 at damage sites.

One unexpected result in this experiment is that the number of 53BP1 foci observed in "empty" cells is comparable to the number seen upon expression of WT ubiquitin at 30 minutes post-IR (Figure 4.7c and d). As recruitment of 53BP1 is ubiquitin dependent, and "empty" cells should have a depleted pool of free ubiquitin, it was expected that there should be fewer 53BP1 foci in these

“empty” cells. This result is explored further in the discussion section of this chapter, but is likely to reflect a low level of free ubiquitin present in these cells, sufficient for 53BP1 recruitment at 30 minutes, but not by 1 hour.

Together, this data confirms the loss of 53BP1 foci upon expression of T66A ubiquitin, and further indicates the possibility of a DNA repair defect, as suggested by the elevated levels of γH2AX foci. Expression of T66D ubiquitin was able to recruit 53BP1 at 30 minutes, suggesting that mutation of T66 alone is not responsible for the loss of 53BP1 recruitment.

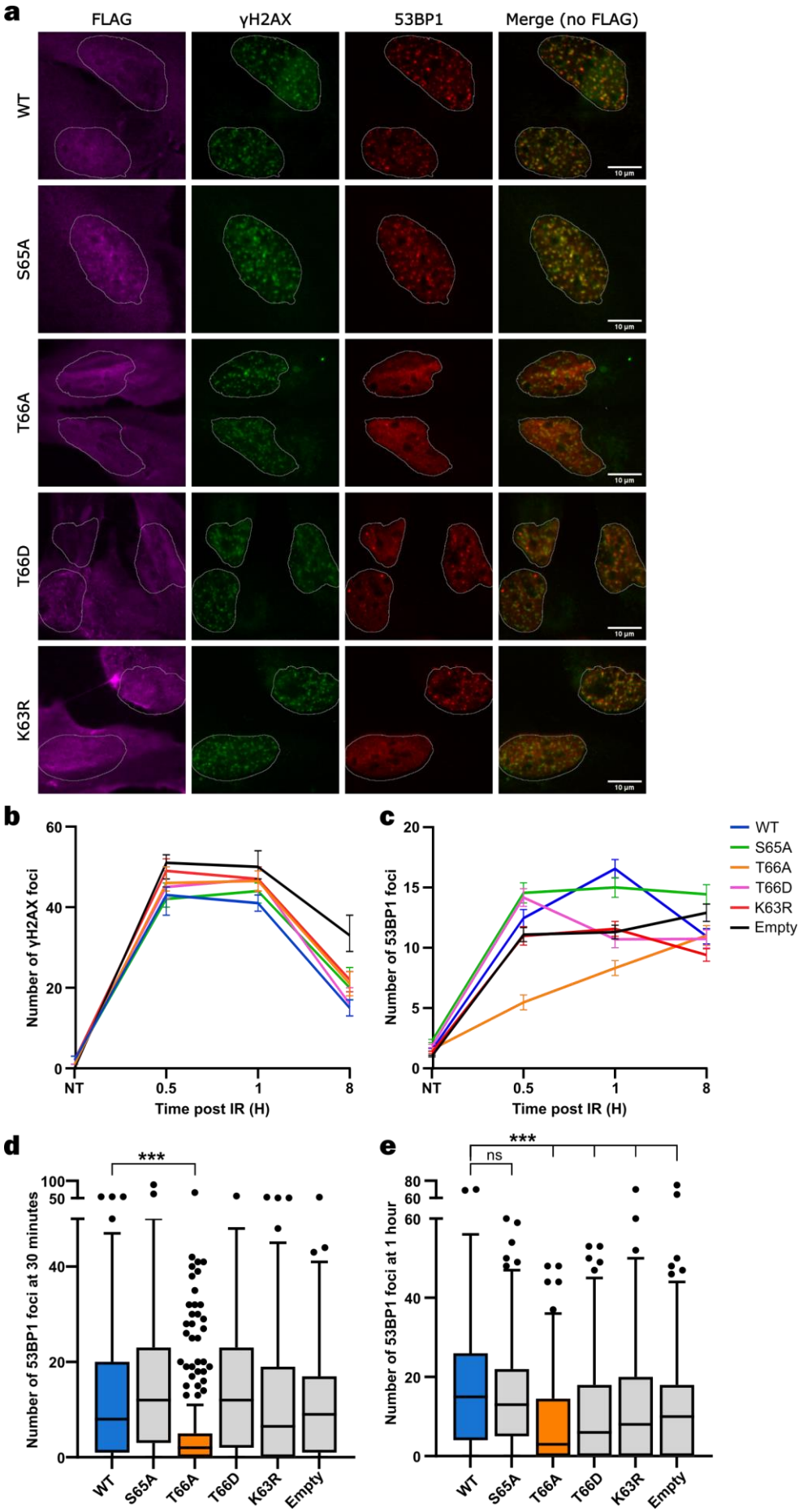
a
FLAG
γH2AX
53BP1
Merge (no FLAG)
WT
S65A
T66A
T66D
K63R
10 μm
b
Number of γH2AX foci
Time post IR (H)
NT
0.5
1
8
c
Number of 53BP1 foci
WT
S65A
T66A
T66D
K63R
Empty
d
Number of 53BP1 foci at 30 minutes
***
e
Number of 53BP1 foci at 1 hour
ns
***

Figure 4.7: The reduction in 53BP1 foci in cells expressing T66A ubiquitin is still seen when an appropriate stop codon is introduced to the expression plasmid. The previous experimental set up was repeated using the plasmids with the correct ed stop codon. **(a)** Representative images of γH2AX and 53BP1 foci in cells fixed 1-hour post-IR in cells expressing the corrected ubiquitin mutants. **(b)** Quantification of the number of γH2AX and 53BP1 foci. Mean foci number with SEM is shown **(c)** Comparison of 53BP1 foci at 30 minutes and 1 hour after damage across ubiquitin mutants. Data displayed as Tukey boxplots, with statistical analysis carried out using a Kruskal-Wallis one way ANOVA with Dunn's multiple comparisons test to compare all samples to WT ubiquitin. P values are represented as follows: ns, p>0.05; ***, p<0.001

4.2.8 T66A ubiquitin shows an opposing phenotype to T12A ubiquitin

At this time, work from the Penengo lab revealed a role for ubiquitin phosphorylated at T12 in the DNA damage response (Walser et al., 2020). Their paper demonstrated that phosphorylation at T12 prevents 53BP1 recruitment, and that blocking phosphorylation by using a phospho-dead T12A ubiquitin mutant leads to an increase in 53BP1 recruitment. A T12A and T12D mutant were created using SDM and added to the experiment, with quantification shown in Figure 4.8.

The T12A mutant showed a small but statistically significant increase in 53BP1 foci in undamaged conditions compared to WT ubiquitin (T12A: mean 2.5, range 38; WT: mean 1.5, range 12. p=0.03). However, we could not recapitulate the increase in 53BP1 foci after damage in T12A ubiquitin compared to WT ubiquitin seen by the previous authors. T12A showed fewer 53BP1 foci after damage compared to WT ubiquitin, although this did not reach the threshold for statistical significance. The T12D phospho-mimic showed a strong reduction in the number of 53BP1 foci, comparable to the numbers seen in the T66A ubiquitin mutant. Unlike the T66A mutant however, the levels of 53BP1 foci did not increase at 8 hours, remaining low. This result gives confidence to the hypothesis that phosphorylated T66 ubiquitin plays a role in the DDR, and raises the possibility that phosphorylation at different sites drives different pathways in the DDR.

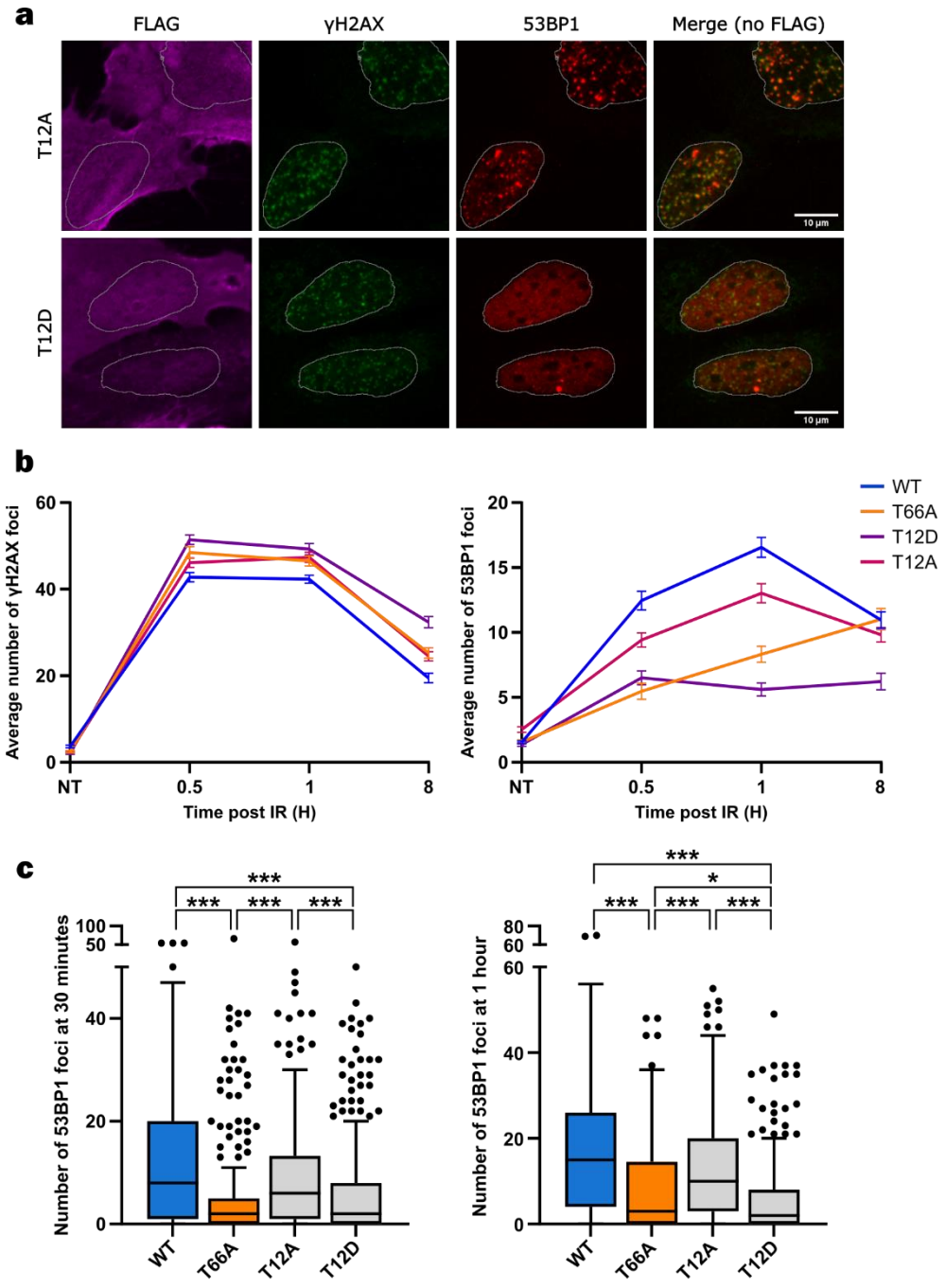

Figure 4.8: T66A ubiquitin prevents 53BP1 IRIF formation with different kinetics to the phospho-mimic T12D. Two additional ubiquitin mutants, T12A and T12D were added to the previous experiment. **(a)** Representative images of cells expressing the T12A and T12D ubiquitin mutant, fixed 1 hour after IR and stained for FLAG, γH2AX and 53BP1. **(b)** Quantification of the number of 53BP1 and γH2AX foci detected in cells expressing the T12 ubiquitin mutants, displayed with the quantification of the WT and T66A ubiquitin mutants previously shown in Figure 4.5. **(c)** Tukey boxplots of the number of 53BP1 foci detected at 30 minutes and 1-hour post-IR in cells expressing ubiquitin mutants. WT and T66A data shown from previous experiment, as before. Data collected from 3 repeats, with statistical analysis carried out using a Kruskal-Wallis one way ANOVA with Dunn's multiple comparisons test. p-values are represented as shown: *, $p<0.05$ to $p>0.01$; ***, $p<0.001$

4.2.9 Expression of T66A does not impact BRCA1 foci formation after damage

The early DDR contributes to recruitment of both 53BP1 and BRCA1 to break sites, with multiple factors contributing to whether the break is ultimately repaired by HR, NHEJ or an alternative pathway. If the absence of pT66 ubiquitin is causing defective recruitment early in the DDR, then recruitment of BRCA1 may be affected too. Alternatively, if BRCA1 is recruited normally, then the reduction of 53BP1 IRIF suggests that pT66-ubiquitin may be a factor in NHEJ repair. To test this, BRCA1 foci formation was quantified 1 hour after treatment with IR. However, BRCA1 foci cannot be detected in the presence of MG132, so detecting the phenotype had to be done without proteasome inhibition. In chapter 3, when looking at pT66-ubiquitin foci and using 53BP1 as a control, a decrease in 53BP1 foci was detected even in the absence of MG132. This gives confidence that a change to BRCA1 IRIF should be detected using overexpression of ubiquitin mutants, even in the absence of MG132.

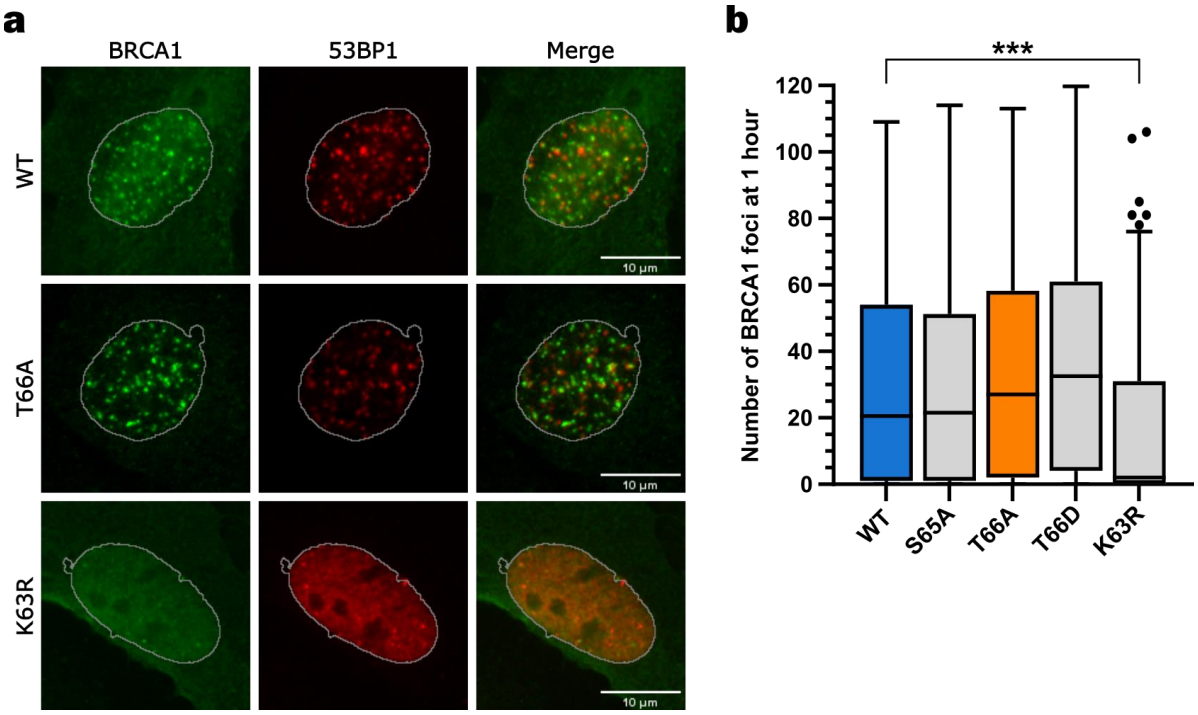

Figure 4.9: Cells expressing T66A ubiquitin do not show differences in BRCA1 IRIF formation. U2OS cells expressing mutants of ubiquitin were treated with 4 Gy of IR and fixed 1-hour post-treatment. Cells were stained for BRCA1, 53BP1, and FLAG. **(a)** Representative images from the experiment are shown. **(b)** Tukey boxplot of the number of BRCA1 IRIF formed 1-hour post-IR. Statistical analysis was carried out using a Kruskal-Wallis one way ANOVA with Dunn's multiple comparisons test to compare all samples to WT ubiquitin. P-values are represented as follows: ***, p<0.001

Mutants of ubiquitin were expressed in U2OS cells grown on coverslips for 48 hours, then treated with 4 Gy of IR from an X-ray source. Cells were fixed 1 hour following IR. Representative images and the quantification are shown in Figure 4.9.

Both T66A and T66D ubiquitin expressing cells show a slight increase in the number of BRCA1 foci detected post IR compared to WT ubiquitin. However, this increase was not found to be statistically significant. In contrast, cells expressing K63R showed a significant reduction in the number of BRCA1 foci detected, consistent with the role of K63 linked ubiquitin chains recruiting BRCA1 to sites of damage (Lee et al., 2017a).

4.2.10 Cells expressing ubiquitin mutants show little variation in their cell cycle profiles

Unlike 53BP1, which is recruited throughout the cell cycle, BRCA1 recruitment is largely limited to late S/G2 phase. As such, it is important to verify that transfecting cells with ubiquitin mutants does not give rise to cell cycle changes that could mask changes to the number of BRCA1 foci detected after damage. Using FACS, cells expressing FLAG tagged mutants of ubiquitin were identified, and their DNA content estimated using Hoechst staining intensity. Fluorescence profiles, as well as quantification from the gates used to identify G1 and G2 cells are shown in Figure 4.10. No significant differences could be found between cells expressing different ubiquitin mutants, suggesting that expressing the ubiquitin mutants does not lead to cell cycle changes, and that the number of BRCA1 foci detected previously reflects the use of the ubiquitin mutants and not alterations to the cell cycle.

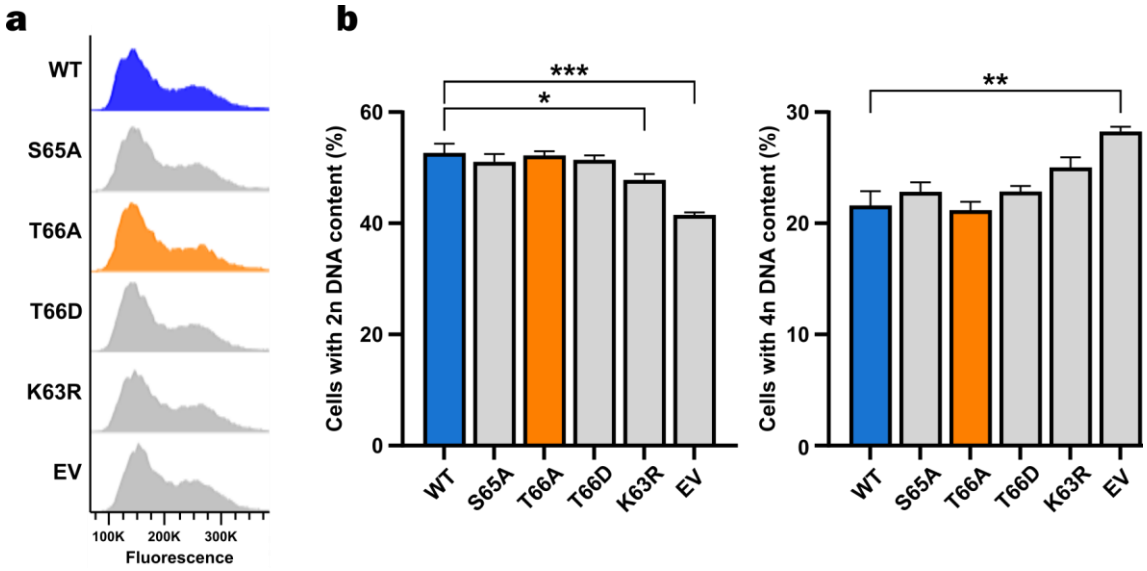

Figure 4.10: Expression of ubiquitin alters the cell cycle compared to an empty-vector control, but changes between ubiquitin mutants are minimal. (a) Representative FACS profile of U20S cells expressing FLAG-tagged mutants of ubiquitin, or transfected with an empty vector control, 48 hours after transfection. **(b)** Gates were drawn to quantify G1/0 and G2 populations based on Hoechst fluorescence intensity. Results displayed as mean percentage, with SEM. Data is from three repeats, and statistical analysis was carried out using a Kruskal-Wallis one way ANOVA with Dunn's multiple comparisons test. *, $p<0.05$ to $p>0.01$; **, $p<0.01$ to $p>0.001$; ***, $p<0.001$

4.2.11 Cell viability is increased in T66A and T12D mutants after damage

So far, we have evidence that ubiquitin that cannot be phosphorylated at T66 leads to a decrease in 53BP1 IRIF, without affecting BRCA1 IRIF. What is the impact of this altered DNA damage response on the whole cell? Clonogenic assays can be used to determine the ability of individual cells to survive treatment and subsequently proliferate to form a colony. Using cells transfected with mutants of ubiquitin will enable us to see viability of cells overall, as well as viability of cells treated with ionising radiation, both in the presence and absence of MG132. Quantification from the clonogenic assays is shown in Figure 4.11.

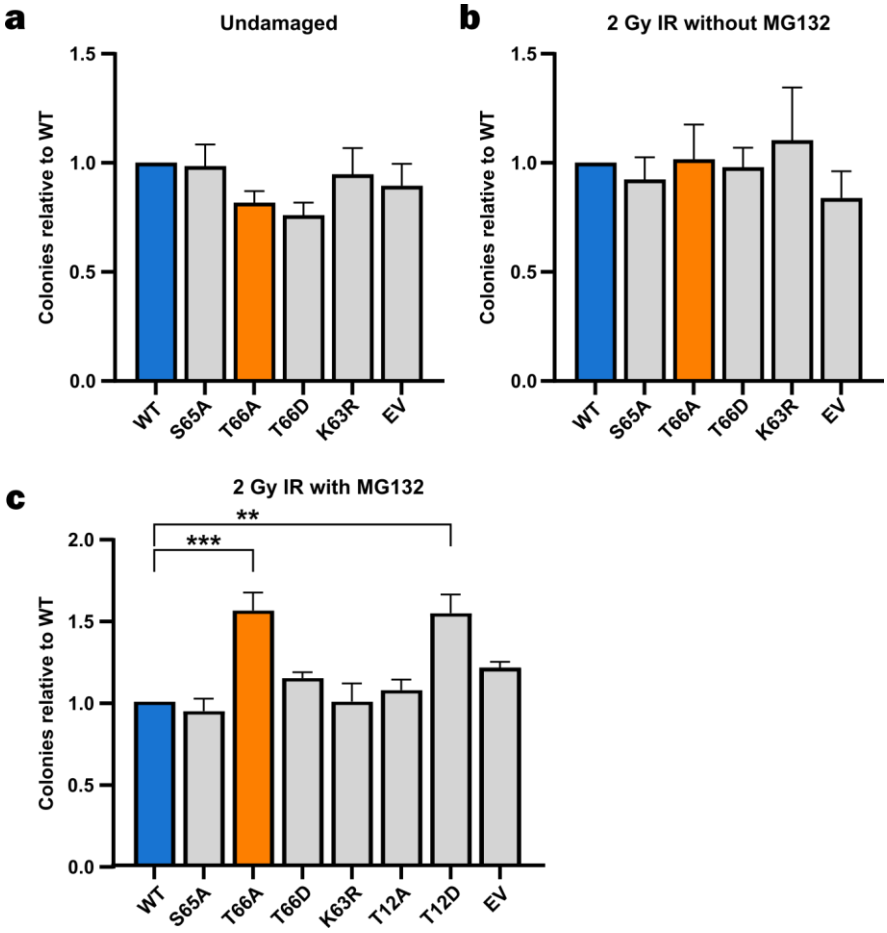

Figure 4.11: T66A ubiquitin does not significantly alter colony formation in unperturbed cells, but increases colony formation after IR after treatment with MG132. U2OS cells were transfected with ubiquitin mutants, treated as indicated, then plated and maintained for 7 days. Colony numbers from the clonogenic assay were normalised to the WT sample. Results are displayed are the mean of these normalised values from 3 repeats, with SEM. **(a)** Cells plated without damage. **(b)** Cells treated with 2 Gy IR from an X-ray source prior to plating. **(c)** Cells were treated with MG132 for an hour, then treated with 2 Gy IR prior to plating. Statistical analysis was carried out using a Kruskal-Wallis one way ANOVA with Dunn's multiple comparisons test. p-values are shown as follows: **, $p<0.01$ to $p>0.001$; ***, $p<0.001$

In the absence of MG132 or irradiation, there were no significant differences in colony number between any of the ubiquitin mutants, or cells transfected with the empty vector plasmid. When cells were treated with ionising radiation alone (2 Gy from an X-ray source), again no significant differences were seen. As this experiment did not select for only cells expressing the mutants of ubiquitin, it may be that any phenotype present is masked by the presence of endogenous ubiquitin.

Cells cannot be incubated with MG132 over a long time as inhibition of the proteasome is toxic. However, MG132 is a reversible inhibitor and can be used for a short treatment prior to IR, as used before for immunofluorescence experiments. When treated with MG132 and IR, a statistically significant difference in colony number becomes apparent. Cells expressing T66A show an increase in colony number after treatment, an unexpected result given the defect in 53BP1 IRIF formation seen in cells expressing this ubiquitin mutant. Addition of the T12 ubiquitin mutants revealed that T12D, which also has a defect in 53BP1 IRIF formation, also shows an increase in colony number after treatment. This suggests that this phenotype may be a result of abnormal 53BP1 kinetics in the DDR.

4.2.12 Expression of T66A leads to PARP inhibitor sensitivity

Cells with hypomorphic mutations in BRCA1 that lead to reduced expression or impaired function are sensitive to treatment with PARP inhibitors, a phenotype that has been exploited for use in BRCA1 deficient cancers. This sensitivity to PARP inhibitors can be rescued if 53BP1 is also lost, leading to synthetic viability (Aly and Ganesan, 2011; Li et al., 2020; Rose et al., 2020). As we have seen deficient 53BP1 IRIF formation in cells expressing T66A ubiquitin, it was hypothesised that cells expressing T66A ubiquitin may be resistant to PARP inhibitors after knockdown of BRCA1. To test this, cells transfected with mutants of ubiquitin and either non-targeting (NT) siRNA or BRCA1 siRNA were seeded for use in proliferation and clonogenic assays. Cells were then incubated in the presence of varying concentrations of the PARP inhibitor, olaparib.

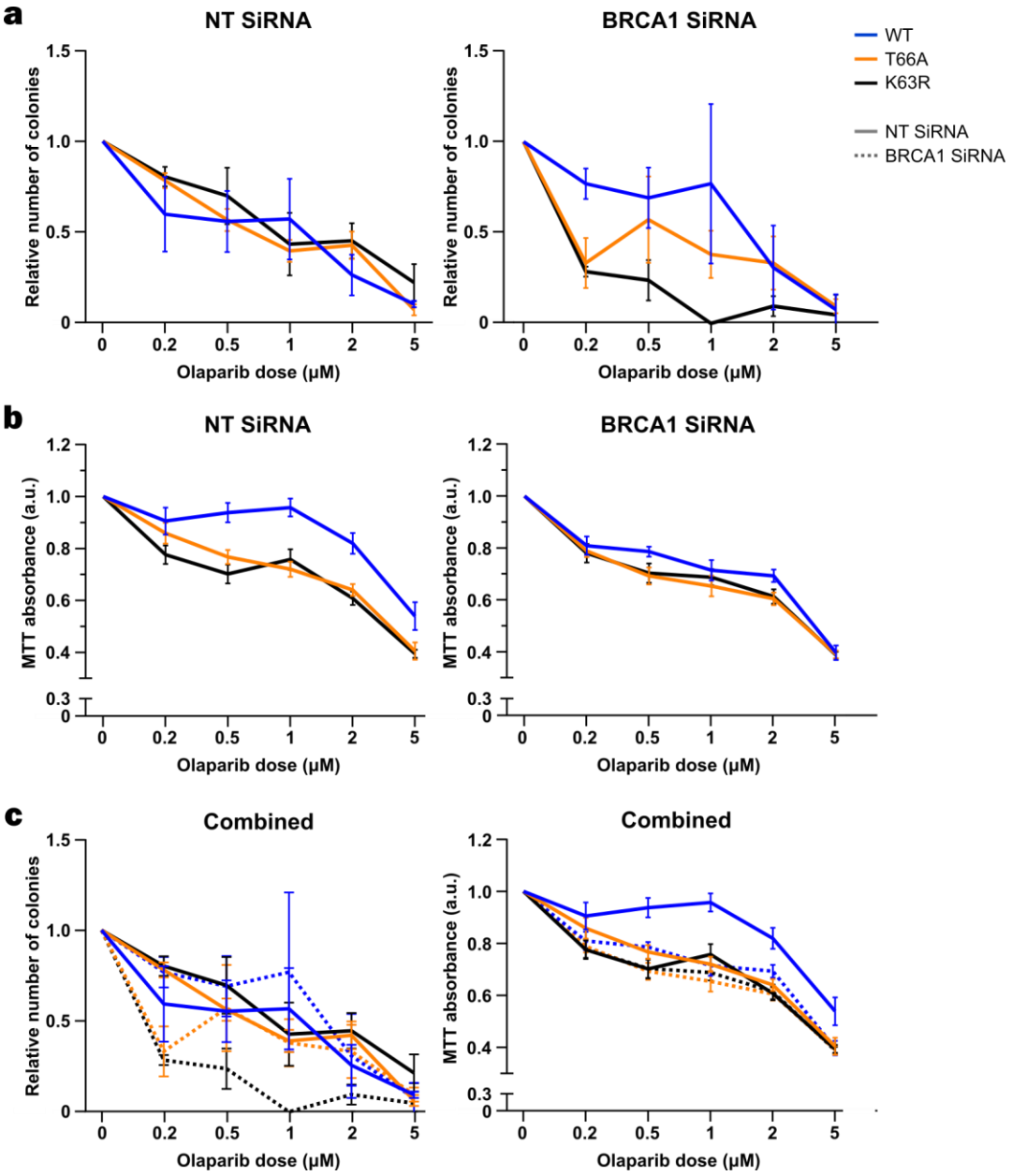

Figure 4.12: Expressing T66A ubiquitin sensitises cells to PARP inhibition. U2OS cells were transfected with mutants of ubiquitin and treated with the indicated siRNA. Cells were plated for clonogenic assay or MTT assay, as outlined in section 2.3.13. Clonogenic and MTT assays were repeated in triplicate. The MTT proliferation assays used the average of 3 wells used for each repeat. **(a)** The mean number of colonies in each condition is displayed, with SEM. **(b)** MTT absorbance is measured, with each condition normalised to the untreated condition. **(c)** Graphs directly comparing the impact of NT and BRCA1 SiRNA treatment.

Consistent with the colony assays shown previously in Figure 4.11, cells treated with NT siRNA and without olaparib showed no significant differences in colony formation between ubiquitin mutants (Figure 4.12). After treatment with BRCA1 siRNA, the number of colonies formed decreased significantly (WT, $p<0.001$; T66A, $p<0.001$; K63R, $p=0.0025$), but again no statistically significant differences were detected between ubiquitin mutants. Addition of olaparib decreased the number of colonies formed irrespective of ubiquitin mutant or siRNA treatment, with no differences detected between the ubiquitin mutants at any concentration of olaparib.

Quantification of the proliferation assay revealed a different pattern. Cells expressing WT ubiquitin and treated with NT siRNA show resistance to olaparib, up to a concentration of 2 μM, after which a decrease in proliferation is measured (Figure 4.12b). Cells expressing K63R show sensitivity to olaparib at low concentrations, as expected from the reduced recruitment of BRCA1 seen in Figure 4.9. Unexpectedly, the T66A ubiquitin mutant also induces sensitivity to olaparib. Although the reduction in proliferation is not as great as the K63R mutant, the difference between the T66A and K63R mutant was not found to be statistically significant.

Cells transfected with WT ubiquitin and BRCA1 siRNA showed sensitivity to olaparib, as expected from loss of BRCA1 (Aly and Ganesan, 2011). No further reduction in proliferation was seen when K63R transfected cells were transfected with BRCA1 siRNA compared to NT siRNA. Knockdown of BRCA1 decreased proliferation of T66A transfected cells further compared to NT siRNA alone, however this decrease was not found to be statistically significant.

4.3 Discussion

The discovery of pT66 ubiquitin foci after DNA damage in chapter 3 suggested a role for this modification in the DDR. An incidental finding, that a non-phosphorylatable mutant of ubiquitin (T66A) reduced the number of 53BP1 IRIF narrowed the focus to a specific role in the double-strand break response, with this chapter aiming to investigate pT66 ubiquitin's role in the DSB response further. Work in this chapter confirms the reduction in 53BP1 IRIF in cells expressing T66A ubiquitin, and finds that this reduction is not seen in BRCA1, another DSB response protein. There is also no reduction in γH2AX foci, indicating that the DDR is intact in these cells. Together this suggests that pT66 ubiquitin is acting specifically in the NHEJ pathways of DSB repair. Detailed interpretation of the results, including the limitations of the experimental techniques used, are discussed below.

4.3.1 T66A ubiquitin specifically impacts 53BP1 IRIF formation

The initial finding of reduced 53BP1 IRIF could have reflected a general defect in the response to DSBs, and not a specific 53BP1 defect. Analysis of γH2AX formation shows that this early part of the DSB response is intact, and is not the cause of the reduced 53BP1 IRIF. Further evidence for an intact DDR comes from the finding of comparable BRCA1 IRIF in cells expressing T66A ubiquitin compared to WT. BRCA1 recruitment is dependent on an intact DDR pathway, and is ubiquitin dependent particularly through the activity of RNF8 (Sherker et al., 2021). This indicates that RNF8 recruitment and activity is unlikely to be impacted by pT66 ubiquitin, and suggests pT66 acts downstream of RNF8, although it cannot be ruled out that substrates modified by RNF8 may be subsequently phosphorylated.

The cell cycle is a key driver of pathway choice in DSB repair, with alterations to cell cycle progression potentially impacting IRIF formation. Using FACS to determine the cell cycle profile of cells expressing ubiquitin mutants, it was determined that an alteration to cell cycle was unlikely to be the cause for the altered IRIF formation, with the ubiquitin mutants having little to no impact on cell cycle progression. The biggest difference observed was between cells expression WT ubiquitin or

transfected with the empty vector control, which may be attributed to altered ubiquitin signalling upon ubiquitin overexpression. Small alterations were seen in the K63R ubiquitin mutant, with fewer cells with a 2n DNA content (G1/G0) and more with a 4n DNA content (G2). This could be explained by the variety of roles for K63 linked chains in the cell outside of the DDR, such as replication stress signalling and during mitosis, which may contribute to an accumulation of cells in G2 (Mirsanaye et al., 2021; Zhang et al., 2015).

At 8 hours post-IR, an increase in γH2AX foci numbers in cells expressing S65A ubiquitin relative to WT is observed (Figure 4.7b), and the number of 53BP1 foci in S65A cells also remains high (Figure 4.7c). This result may be related to the role of pS65 ubiquitin in the clearance of damaged mitochondria. Ionising radiation impacts mitochondrial function through mitochondrial DNA damage, and altered metabolism, including disruption of the electron transport chain (Kam and Banati, 2013). This altered mitochondrial function leads to increased production of reactive oxygen species, which are a major source of endogenous DNA damage (Kawamura et al., 2018; Srinivas et al., 2019). Reduced clearance of these damaged mitochondria through expression of S65A ubiquitin would likely contribute to elevated levels of reactive oxygen species, leading to increased DNA damage over time. It could be that the elevated levels of γH2AX and 53BP1 foci at these late times after the initial damage are not due to impaired repair, but reflect new and ongoing DNA damage from mitochondrial dysfunction.

4.3.2 The reduction in 53BP1 IRIF formation upon expression of T66A ubiquitin is robust to changes in the experimental set up

Whilst working with the ubiquitin mutants in this chapter, work was underway to create additional mutations in the C-terminal tail. This led to the identification of the missing stop-codon, which extends the C-terminus of ubiquitin by 19 amino acids. The experiment was repeated using ubiquitin mutants with the appropriate stop codon, to determine whether the phenotype remained with more “normal” ubiquitin. The plasmids weren’t the only difference between experiments, with the

COVID19 pandemic necessitating a change to a new means of DNA damage, from a caesium IR source to an X-ray source. Despite these changes, the reduction in 53BP1 IRIF was consistent in both experiments, showing that this phenotype is robust and reproducible, lending strength to these findings.

It is unclear what impact the C-terminal extension of ubiquitin present in the first experiment may have on the ubiquitin cascade. Expression testing of the mutants showed smearing at higher molecular weights, indicating the extended ubiquitin can be used for conjugation, but this test does not identify whether the rate of conjugation or DUB activity is affected (Figure 4.1). There is evidence that suggests that the C-terminal extension is cleaved from ubiquitin entirely, restoring a normal C-terminal. Cleavage by DUBs at the di-glycine motif is required during expression of ubiquitin, to release ubiquitin from its pro-protein form, and there is evidence that this C-terminal extension is similarly cleaved. The expression testing by immunoblot (Figure 4.1) shows two bands at the bottom of the gel: one just above and one just below 10 kDa, which could correlate with "normal" ubiquitin and the extended ubiquitin, indicating cleavage of the C-terminal extension.

There is good reason for caution in proceeding with these ubiquitin mutants. Molecular misreading of the UBB gene leads to expression of ubiquitin with a C-terminal extension of ubiquitin, with an additional 19 amino acids between G75 and G76, termed UBB+1 (van Leeuwen et al., 1998a). UBB+1 has reported implications in Alzheimer's disease and other tau pathologies through altered ubiquitin signalling, and is considered clinically significant (van Leeuwen et al., 1998b). Disruption of the di-glycine motif is commonly reported as rendering UBB+1 un-conjugatable. It can still be conjugated to by other ubiquitin proteins, allowing the formation of free ubiquitin chains, capable of signalling (Lim and Hasty, 1996; Lindsten et al., 2002). Furthermore, these chains are refractory to DUB activity.

Although UBB+1 is reported as un-conjugatable, disruption of the di-glycine motif in normal length ubiquitin (G76A) is conjugatable, albeit with reduced efficiency (van Wijk and Timmers, 2010). Similarly to UBB+1, G76A ubiquitin is refractory to cleavage by DUBs, promoting ubiquitin chains.

This does raise the question of how much disruption of the di-glycine motif is interfering with normal ubiquitin signalling, vs. the role of the C-terminal extension (Schaefer and Morgan, 2011).

Comparing 53BP1 IRIF formation before and after introduction of the appropriate stop codon revealed some differences – using corrected vectors the number of 53BP1 IRIF were lower in all mutants of ubiquitin tested compared to previous results. 53BP1 IRIF in cells expressing T66A ubiquitin showed a different pattern as well – in the initial experiment 53BP1 levels remained low throughout the time course, whereas levels of 53BP1 IRIF have increased by 8 hours after introducing the stop codon. One interpretation could be that without the stop codon, the ubiquitin mutants are refractory to DUBs.

MG132 inhibition of the proteasome is rapidly reversed upon removal of the inhibitor, which was done immediately following irradiation. This allows endogenous ubiquitin to be returned to the free pool for signalling. Ubiquitin signalling is dynamic, with DUBs constantly removing ubiquitin as E2s/E3s replace the ubiquitin mark – if the ubiquitin without a stop codon is refractory to DUBs, this modification will remain in place, with little opportunity for the ubiquitin mark to be replaced with endogenous ubiquitin. The recovery of 53BP1 foci at 8 h post-IR seen after introducing the stop codon (Figure 4.7) could indicate recovery of the ubiquitin cascade and exchange of the mutant ubiquitin for endogenous one. The increase over time is not seen with the K63R ubiquitin mutant, but this is anticipated. K63R works as a chain terminator for K63 linked chains, which are essential for DSB signalling. This limits the recovery possible in the presence of this mutant.

With the appropriate stop codon, T66A expressing cells had fewer 53BP1 IRIF than K63R or “empty” cells, which is not observed with the extended C-terminus. Whilst the reason for this requires further investigation, one possibility is that phosphorylation at T66 stabilises ubiquitin signalling, and so T66A is removed to allow for adequate signalling to take place. Phosphorylation of ubiquitin at other sites often diminishes DUB activity (Huguenin-Dezot et al., 2016). If the C-terminal extension was reducing DUB activity, this may have fulfilled similar function as phosphorylation at T66 and enabled

a partial rescue of 53BP1 recruitment. This view does indicate that recognition of the pT66 site directly by 53BP1 is unlikely to be the sole driver of 53BP1 IRIF formation. This is in keeping with published structures of 53BP1 binding to the nucleosome, which do not suggest a role for ubiquitin phosphorylation in the interaction, and indeed indicate that this may be inhibitory towards 53BP1 binding (Hu et al., 2017; Walser et al., 2020; Wilson et al., 2016).

However, there is another factor complicating the interpretation of these results, as introduction of the stop codon was not the only alteration between the experimental setup. The COVID19 pandemic prevented access to the caesium source used in the first experiment, necessitating a change to an X-ray source for IR treatment. Internal validation by the Beggs group showed no difference in DNA damage markers at 1 hour post treatment between these two sources (data unpublished). However, dose rate has been observed to impact repair kinetics, and varies between the sources (Nair et al., 2019). The dose rate from the caesium source was 2 Gy min^{-1}, compared to 0.89 Gy min^{-1} from the x-ray source. This could contribute to lower levels of 53BP1 foci and altered repair kinetics in the second experiment, however the internal control of "Empty", non-transfected cells shows no differences in the number of 53BP1 foci between the caesium and X-ray source after irradiation. Although their DDR is attenuated by the MG132 treatment, comparing the values indicates that the internal validation was correct, and that changes to kinetics caused by the change in IR source is not likely to be a significant factor when interpreting the results.

Despite the differences between the two experiments, the reduction in 53BP1 IRIF in cells expressing T66A ubiquitin was observed in both experiments. Again, in both experiments mutation of the adjacent amino acid, S65 to S65A, did not affect 53BP1 IRIF formation. This gives confidence in this result being correct, and reflects the specificity of this 53BP1 phenotype for loss of ubiquitin phosphorylation at T66.

4.3.2a Interpretation of 53BP1 foci formation in "empty" cells

In the second experiment, using the corrected ubiquitin plasmids, the number of 53BP1 foci observed in "empty" cells was comparable to the number of foci observed in cells expressing WT ubiquitin at 30 minutes post-IR (Figure 4.7c and d). This was unexpected, as MG132 treatment was expected to deplete the free pool of ubiquitin, preventing the ubiquitin signalling required for recruitment of 53BP1 after damage. The number of 53BP1 foci present at 1 hour was significantly reduced in "empty" cells compared to WT. This suggests that the free pool of ubiquitin is reduced, but not completely depleted, in "empty" cells at 30 minutes, sufficient for early 53BP1 recruitment but not enough to reach the peak 53BP1 recruitment at 1 hour. This result contrasts with the first experiment, where "empty" cells showed fewer 53BP1 foci compared to WT at both 30 minutes and 1 hour post-IR (Figure 4.5c).

There was a considerable gap in time between the first and second experiments, in part due to the need to correct the c-terminal extensions of the original ubiquitin plasmids, and due to the COVID19 pandemic preventing access to the laboratory. This means that a different aliquot of U20S cells were used, a new order of MG132, and additional changes to the experimental set up were required due to ongoing access issues caused by the pandemic, as discussed previously. All these incremental changes have impacted the experimental set up, and it is possible that the MG132 treatment optimised for the first experiment is not sufficiently optimised for the second experiment, leading to incomplete depletion of the free ubiquitin pool.

This result, whilst unexpected, does not impact the overall interpretation of the results. There is still a clear difference in the number of 53BP1 foci observed in cells expressing the T66A ubiquitin compared to the WT ubiquitin at 30 minutes and 1 hour, and the results from this experiment are consistent with the other data collected in this thesis, adding confidence in the interpretation of this data.

4.3.3 Interpreting results using a phospho-mimetic mutation

After introducing the stop codon, a phospho-mimetic mutant (T66D) was added for testing. This mutant showed an unexpected pattern, with normal 53BP1 foci formation at 30 minutes post-IR, then a reduction in foci numbers to levels comparable to "empty" or K63R ubiquitin. This finding suggests that there are multiple interactors with pT66-ubiquitin, driving an initial recruitment of 53BP1, and then a second interaction that stabilises 53BP1 at damage sites. The loss of 53BP1 foci at 1 hour compared to 30 minutes post-IR could indicate that pT66 is dynamic at break sites, and that removal of the phosphorylation is as important as its placement at damage sites. However, another possibility is that the loss of 53BP1 foci at 1 hour in cells expressing T66D is a result of the phospho-mimetic mutation only partly mimicking phosphorylation at this site, disrupting onward signalling.

Phospho-mimetic mutations do not perfectly recapitulate phosphorylation at a residue. They introduce a negative charge (as an electronegative amino acid) that broadly mimics the charge associated with phosphorylation, although a phosphate group is capable of a greater negative charge than is possible with an amino acid. These negative charges are often sufficient for conformational changes in proteins, leading to downstream effects, or some recognition by phospho-recognition motifs. However, phospho-mimetics may not capture the full function of phosphorylation, leading to incomplete conformational changes or missed recognition by specific phospho-receptors (Chen et al., 2014; Chen and Cole, 2015; Dephoure et al., 2013; Kozeleková et al., 2022)

For ubiquitin, the phospho-mimetic mutation is not sufficient to stabilise the C-terminal retracted minor conformation of ubiquitin, either at S65 or T66 (Dong et al., 2017). Phospho-mimetic mutations, however, are sufficient to drive localisation and activity of the Parkin E3 ligase in the absence of PINK1 activity, so looking into the impact of T66D mutation has relevance. Phospho-mimetic mutations at other sites of ubiquitin limit the activity of DUBs, recapitulating what has been seen with phosphorylation at these sites (Swaney et al., 2015; Wauer et al., 2015b). It could be that

pT66 ubiquitin is used in several ways within the DNA damage response, and the phospho-mimetic mutation is capable of rescuing only part of the pathway. If this is the case, then T66D could be used as a separation of function mutation in further work, allowing identification of the different roles for phospho-ubiquitin in the DDR.

Another phospho-mimetic mutation commonly used is glutamic acid. This mutation is commonly used to mimic phospho-serine, but it has been used to mimic phospho-threonine as well. Importantly, the different phospho-mimics can lead to different phenotypes. T12D and T12E mutations of ubiquitin showed differing phenotypes in the paper by Walser et al. (2020). Future work incorporating the T66E mutation should be considered, to see if alternative phenotypes are present with this other mutation.

4.3.4 T66-ubiquitin mutants show an opposing phenotype to those observed with T12-ubiquitin mutants

During my PhD, a publication from the Penengo laboratory revealed the discovery of ubiquitin phosphorylated at T12 in the DDR (Walser et al., 2020). Strikingly, the phenotypes observed were directly opposite those observed at T66. Whereas T66A led to a decrease in 53BP1 IRIF, T12A was shown to increase these IRIF. Moreover, T12D prevented recruitment of 53BP1 after damage. The T12 phenotypes made them interesting additions to study, with the implication that differential phosphorylation of ubiquitin could be an important driver in the choice of repair pathway.

I could not fully recapitulate the findings from the Penengo laboratory during my study. A small increase in 53BP1 foci in cells expressing T12A compared to WT was present in undamaged cells. This difference reached the level of statistical significance, however the difference in mean and media values was small enough to raise doubt as to the biological significance (WT mean = 1.55, median = 1; T12A mean = 2.52, median= 1). The main difference detected was in the range of values, with WT cells having up to 12 53BP1 foci, and T12A having up to 38 53BP1 foci. However, an increase in 53BP1 foci with T12A compared to WT ubiquitin could not be detected after damage.

The finding that expression of a phospho-mimetic mutant of ubiquitin led to loss of 53BP1 IRIF after damage was repeatable. Use of the T12D ubiquitin mutant in my work led to a near total loss of 53BP1 IRIF which did not increase over the course of the experiment. This contrasts with the T66A ubiquitin mutant, which showed an increase in 53BP1 IRIF over the course of the experiment. This difference may be attributed to the activity of DUBs, which Walser et al. show are less able to act on the T12D ubiquitin mutant, and so cannot clear it from the substrate. DUB activity should be unaffected by the T66A mutation, and so can be cleared and replaced with endogenous ubiquitin as MG132 inhibition reverses, as part of normal dynamic ubiquitin regulation.

The inability to repeat the phenotype previously seen with the T12A ubiquitin mutant may be explained in part due to the different ubiquitin plasmids used. The original ubiquitin plasmid used in my PhD, with its C-terminal extension, was originally acquired from the Penengo laboratory. Discussion with this laboratory indicates that this is the plasmid they are using in their study. In WT-ubiquitin expressing cells in undamaged conditions, the paper reports 15-40% of cells with 5 or more 53BP1 foci (variation is large between experiments). With the stop codon introduced, only 9% of my cells met this threshold, but using the original plasmid, 26% of cells had 5 or more 53BP1 foci, more comparable to their reported results. If, as stated before, the C-terminal extension is refractory to activity to DUBs, then an increase in 53BP1 foci in cells expressing T12A may be expected, as the removal of the extended mutant would be slow, limiting the exchange of this mutant for endogenous ubiquitin. This would amplify the disruption to 53BP1 binding caused by lack of phosphorylation at T12.

Walser et al. name histone H2A as the substrate for ubiquitin phosphorylation, specifically at K13/15. This would agree with molecular models which find that ubiquitin phosphorylation would likely be inhibitory towards 53BP1 recruitment (Wilson et al., 2016). It is interesting to see an accumulation of 53BP1 foci in cells expressing T12A. This may indicate that ubiquitylation at this site occurs even in the absence of DNA damage and is dynamically regulated, rather than the common assertion that this site is only ubiquitylated as part of the DDR.

The evidence gathered so far in this thesis does not support histone H2A(X) as the substrate for pT66-ubiquitin. In chapter 3, the pT66-ubiquitin foci could not be detected when samples were pre-extracted prior to fixation, indicating that the modification is not likely to be strongly chromatin bound. Available models of 53BP1 recruitment to histone H2A also suggest that phosphorylation of this ubiquitin is likely to be inhibitory towards recruitment, rather than promote recruitment (Walser et al., 2020; Wilson et al., 2016). The phenotype caused by expression of T66D also suggests that the interaction between pT66-ubiquitin and 53BP1 is unlikely to be direct, with the recruitment of 53BP1

at 30 minutes post-IR which is not sustained at 1 hour. Nevertheless, the finding of opposing phenotypes for ubiquitin phosphorylated at different sites raises the interesting possibility of a kinase driven mechanism for driving repair pathway choice.

4.3.5 T66A ubiquitin alters cell viability and confers sensitivity to PARP inhibitors

Clonogenic assays test cell's ability to survive and subsequently proliferate. The test is limited by its inability to distinguish the reason for reduced colony formation, for example cell death by apoptosis or loss of proliferation through senescence. However, it remains a useful tool for assessing cell's sensitivity to treatment such as ionising radiation. The reduction in 53BP1 IRIF seen with expression of T66A ubiquitin was indicative of a DNA repair defect, however it was not apparent whether this would have an impact on overall cell viability. A clonogenic assay was used to determine whether T66A ubiquitin conferred a radiosensitivity phenotype (Figure 4.11).

In undamaged cells, no significant differences were observed between the ubiquitin mutants, although a slight decrease in colony formation is observed with the T66A and T66D ubiquitin mutants. This agrees with the earlier FACS data, which showed only small differences in the cell cycle between ubiquitin mutants. In the absence of MG132, treatment with IR also showed no significant differences in colony formation between the ubiquitin mutants. Treatment with MG132 an hour before IR reveals a statistically significant change in T66A and T12D, the ubiquitin mutants that show impaired 53BP1 IRIF formation. Unexpectedly, this is an increase in colony formation relative to WT ubiquitin, rather than the expected decrease. That this increase in colony formation occurs in both ubiquitin mutants with a reduced 53BP1 IRIF phenotype gives confidence in this increase being a genuine phenotype.

Like many DDR proteins, the phenotype caused by loss of 53BP1 differs from those observed with mutations of specific domains, reflecting the multiple roles of these proteins (Cuella-Martin et al., 2016; Liu and Lu, 2020; Menolfi and Zha, 2020). Loss of 53BP1 is associated with radiosensitivity and genomic instability as a result of compromised DSB repair (Chapman et al., 2013; Ward et al., 2003).

In addition to its role in NHEJ repair 53BP1 also acts more widely in the DDR, notably through its interaction with p53. p53 is a master regulator in the DDR, promoting cell cycle arrest, DNA repair and apoptosis (Lakin and Jackson, 1999). p53 is the most commonly mutated tumour suppressor in human cancers, demonstrating the importance of regulating this pathway (Zhu et al., 2020).

53BP1 promotes p53 activity at least in part by promoting deubiquitylation of p53, enhancing its stability (Cuella-Martin et al., 2016). This function of 53BP1 is separable from its role in DNA repair, as the interaction between 53BP1 and p53 requires 53BP1's BRCT domains, which are largely dispensable for DNA repair. Mutation of these BRCT domains has been found to increase cell survival after DNA damage, consistent with dysregulation of p53 (Cuella-Martin et al., 2016). This increased cell survival was noted in the colony assay with both T66A and T12A ubiquitin mutants (Figure 4.11), and may link 53BP1's role in DNA damage repair with its regulatory role with p53.

The genetic background also impacts cellular response to 53BP1 loss. One well documented example of where loss of 53BP1 confers viability is where the loss coincides with a BRCA1 mutation. BRCA1 mutations sensitise cells to PARP inhibition, termed "synthetic lethality", and has become a mainstay of cancer treatment (Rose et al., 2020). With the additional loss of 53BP1, PARP sensitivity is decreased, with tumours showing resistance to treatment. This idea was taken forward to observe colony formation and cell proliferation in cells expressing ubiquitin mutants in the presence of the PARP inhibitor, olaparib. The expectation was that expression of T66A, with its reduced 53BP1 IRIF, should lead to reduced sensitivity to PARP inhibition in cells with reduced BRCA1.

There is little difference between WT and T66A expressing cells with any concentration of PARP inhibitor when assessing colony formation in either NT or BRCA1 siRNA conditions (Figure 4.12). However, interpretation of the assay is complicated by the very low number of colonies identified in all conditions after treatment with BRCA1 siRNA. Assessing cell proliferation reveals a clear difference in sensitivity to PARP inhibitor in cells expressing WT ubiquitin, with BRCA1 siRNA causing a clear reduction in proliferation. Expression of K63R ubiquitin showed sensitivity to PARP inhibitor

without BRCA1 siRNA. This would be expected given the role of K63 linked chains in recruitment of BRCA1, which was observed in the reduction of BRCA1 IRIF in Figure 4.9. T66A ubiquitin in the absence of BRCA1 siRNA also caused sensitivity to PARP inhibition, despite forming normal BRCA1 IRIF. Unlike with K63R ubiquitin, addition of BRCA1 siRNA further sensitised T66A cells to PARP inhibition, suggesting BRCA1 recruitment alone was not the cause of the sensitivity.

One of the mechanisms for resistance to PARP inhibitors is by removal of restrictions to DNA end resection, which promotes repair by HR (Li et al., 2020). Loss of 53BP1 removes a barrier to end resection, leading to PARP inhibitor resistance. However, this resistance is mediated at least in part by the downstream effectors of 53BP1, such as the shieldin complex (Gupta et al., 2018). 53BP1 is not the only barrier to end resection. The Ku complex itself is a barrier to long range DNA resection, with removal required for HR progression (Marini et al., 2019). Chromatin remodelling around break sites is also required, as compact chromatin itself is a barrier to nuclease activity (Chen and Symington, 2013). This thesis shows evidence for pT66-ubiquitin in 53BP1 IRIF formation, but so far has not provided a mechanism. As expression of T66A ubiquitin fails to rescue PARP inhibitor sensitivity upon knockdown of BRCA1, and shows increased sensitivity in a WT BRCA1 background, there may be a role for pT66-ubiquitin beyond recruitment and retention of 53BP1 to damage sites.

4.3.6 Ubiquitin replacement methods impose limitations on the study of mutant ubiquitin

The use of MG132 to promote the use of exogenously expressed ubiquitin is not without drawbacks. It cannot be used for long term studies, as inhibition of the proteasome is toxic. Inhibition of the proteasome potentially impacts on other cellular processes, for example BRCA1 cannot be viewed when cells are treated with MG132, although the mechanism for this is unknown (unpublished data from the Morris laboratory). Other techniques were trialled to replace endogenous ubiquitin with ubiquitin mutants, but these were not carried forward for use in my PhD, and are discussed below.

4.3.6a Use of siRNA knockdown for ubiquitin

A variety of techniques are available to replace endogenous proteins with mutant variants, allowing the study of resulting phenotypes. However, ubiquitin's expression from multiple genes and as a pro-protein makes ubiquitin replacement complicated. Endogenous ubiquitin can be knocked down using two siRNAs targeting UBA52 and RPS27A, which also prevents expression from UBB and UBC genes (Gatti et al., 2015). UBA52 and RPS27A also encode for essential ribosomal subunits, L40 and S27A respectively, knockdown of which impacts cell viability (Zhou et al., 2015).

Published papers have used siRNA knockdown and replacement of ubiquitin, with brief mention of steps taken to mitigate reduced cell viability (Adam et al., 2013; Gatti et al., 2015). In trying to replicate this method, I found that the introduction of plasmid DNA in conjunction with siRNA to rescue the knockdown led to the greatest reduction in viability, whilst siRNA alone was tolerated. This limitation was shown in Figure 4.2, where despite successful knockdown and rescue of ubiquitin, seen in the depletion and re-introduction of the free pool of ubiquitin, cell viability was too low to use this method in experiments.

4.3.6b Creation of inducible cell lines to express ubiquitin

To avoid the reduction in viability associated with plasmid transfection, the Flp-In™ T-REx™ system (ThermoFisher) was used to create U2OS cell lines that could express ubiquitin in the presence of doxycycline. The plasmids used were capable of transient expression of HIS-tagged ubiquitin, with ubiquitin smearing seen at higher molecular weights (Figure 4.3). Immunoblots using the anti-His antibody didn't show ubiquitin at lower molecular weights, and the free pool of ubiquitin was not consistently detected. The reason for this was unclear – although it could have been possible that expression from this plasmid was reduced compared to the FLAG-ubiquitin plasmid, the presence of ubiquitin smearing at higher molecular weights indicated that there was sufficient ubiquitin being expressed for rescue. It was possible also that the anti-His antibody is less sensitive and cannot detect the lower level of signal from unconjugated ubiquitin. The decision was made to continue to

create cell lines with the HIS-ubiquitin plasmid. Clonal populations that demonstrated incorporation of the vector into the correct site (both hygromycin resistant and Zeocin sensitive) were carried forward to test inducible expression of ubiquitin mutants.

Despite testing a range of doxycycline doses, expression of ubiquitin was very low, being undetectable in the T66A cell lines. Transient transfection generally results in more protein being expressed than from cell lines, on account of translation from multiple plasmids vs a single incorporation site. This is likely the primary cause in the discrepancy between transient and inducible expression. Additionally, the pcDNA5 FRT/TO vector used contained and incorporated only a single ubiquitin gene to facilitate site directed mutagenesis to create mutants. It is possible that by modifying the vector to express a poly-ubiquitin protein, the protein levels would increase to a usable level. A plasmid exists to create cell lines that inducibly knocks down endogenous ubiquitin, expresses two copies of ubiquitin and replaces the lost ribosomal proteins, preventing the need for any transfections (Xu et al., 2009). However, this plasmid is not widely available, and it was not possible to acquire for use in this project. It remains a possible avenue for ubiquitin replacement in future work.

Chapter 5: Characterising pT66-ubiquitin in the DNA damage response

5.1 Introduction

Chapter 3 of this thesis provided evidence that ubiquitin phosphorylated at T66 is localised to sites of damage after cells are exposed to ionising radiation. Chapter 4 demonstrated that expression of a mutant of ubiquitin that cannot be phosphorylated at this site leads to a decrease in 53BP1 foci after IR compared to expression of WT ubiquitin. What remains unclear is how pT66-ubiquitin and 53BP1 are linked, and where in the DNA repair pathway pT66-ubiquitin is acting. This chapter aims to more fully characterise the pT66-ubiquitin modification, by exploring its relation to other proteins in the DDR.

5.2 Results

5.2.1 pT66-ubiquitin foci numbers after damage peak later than 53BP1 foci

Establishing the kinetics of pT66-ubiquitin recruitment to, and dissolution of, ionising radiation induced foci in comparison with 53BP1 foci dynamics, may help us understand the interplay between the two factors and shed light on when in the DNA damage response pT66-ubiquitin is required. U2OS cells were treated with 4 Gy of IR from an X-ray source, and fixed at various times post-IR treatment. The samples were subsequently stained for pT66-ubiquitin and 53BP1, and the number of foci per cell was counted.

After treatment with IR, most cells make 53BP1 foci, with 76% of cells having 10 or more 53BP1 foci 30 minutes post-IR, rising to 95% at 1-hour post-IR (Figure 5.1b). The median number of foci also peaks at 1-hour post-IR, with a median of 37 foci per cell. This contrasts with pT66-ubiquitin foci, with only 50% of cells with 10 or more pT66-ubiquitin foci at 1 hour, rising to 75% of cells at 4 hours post-IR. The median number of pT66-ubiquitin foci at 1 hour is only 12, although this number is

skewed by a low value in one of the replicates of this experiment. By 4 hours, the median number of pT66-ubiquitin foci is 20, still below the median number of 53BP1 foci observed (32, Figure 5.1a).

Using 10 or more foci as a cut off for a "positive" response to IR, Figure 5.1c shows that cells that were positive for 53BP1 foci were only positive for pT66-ubiquitin foci approximately half the time (56% at 1 hour post-IR). In contrast, almost every cell classed as positive for pT66-ubiquitin foci was also positive for 53BP1 (99% at 1-hour post-IR). An exception to this is seen at 30 minutes post-IR, where a proportion of cells positive for pT66-ubiquitin foci do not show more than 10 53BP1 foci. An example image of these cells is seen in Figure 5.1e.

These findings suggest that 53BP1 foci formation may be independent of pT66-ubiquitin foci formation, as 53BP1 foci form in cells without observable pT66-ubiquitin foci. This is an unexpected finding given the reduction in 53BP1 foci seen in all cells upon expression of T66A ubiquitin. In the cells that do have both pT66 and 53BP1 foci, clear co-localisation of the foci is seen, establishing that there is a link, at least in a subset of cells, between 53BP1 and pT66-ubiquitin.

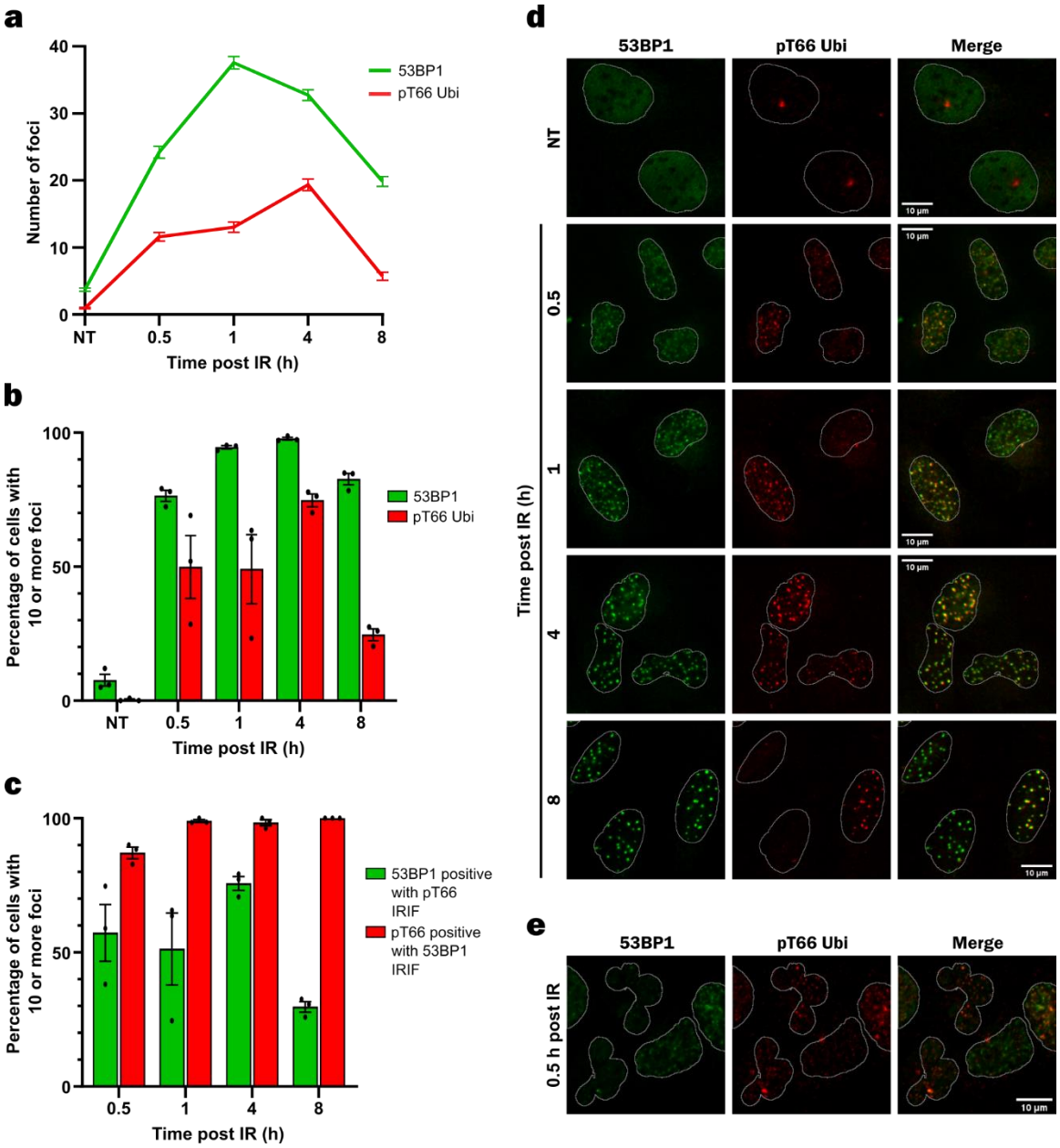

Figure 5.1: 53BP1 and pT66-ubiquitin form foci with different kinetics. U2OS cells were treated with 4 Gy IR and fixed at the indicated timepoints post-IR. Graphs show means from three experiments, with error bars reflecting the standard error of the mean. **(a)** Mean number of foci at each timepoint is shown. **(b)** The mean percentage of cells with 10 or more foci is shown. **(c)** The percentage of cells positive for one foci type that are also positive for the second foci type. At 1-hour post-IR. **(d)** Representative images from the three repeats showing 53BP1 and pT66-ubiquitin foci at each timepoint with **(e)** showing an example of a pT66-ubiquitin positive cell that is 53BP1 negative, 30-minutes post-IR.

5.2.2 pT66-ubiquitin is linked to the cell cycle

The large variability in whether cells formed pT66-ubiquitin foci after damage raised questions as to how pT66-ubiquitin foci formation may be regulated. The cell cycle is known to be an important driver of different DNA repair pathways, so the impact of the cell cycle on pT66-ubiquitin was investigated. An experiment using mutants of ubiquitin with the incorrect stop codon (Figure 5.2) had previously been performed using CldU incorporation as a marker of cell cycle. In addition to treatment with MG132, cells were also incubated with CldU for 20 minutes before treatment with 4

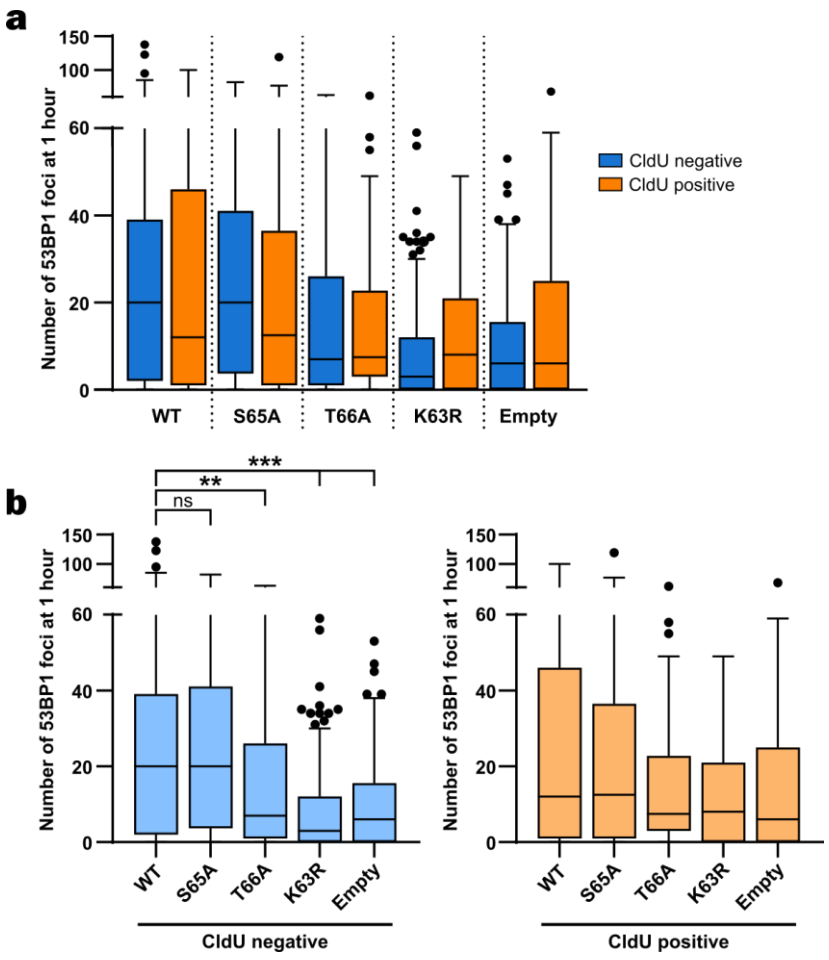

Figure 5.2: T66A ubiquitin causes a greater decrease in 53BP1 foci in cells without CldU staining. U2OS cells transfected with FLAG-tagged ubiquitin mutants were treated with CldU 20 minutes prior to treatment with 4 Gy IR. Cells were fixed 1 hour following IR and stained for CldU, 53BP1 and FLAG. The ubiquitin mutants used contain a C-terminal extension. Data shown is from 3 replicates. **(a)** Comparison of 53BP1 foci in cells with or without CldU staining. **(b)** Data from (a) displayed to directly compare changes in 53BP1 foci numbers between ubiquitin mutants in CldU positive or negative cells. Statistical analysis comparing ubiquitin mutants to WT ubiquitin was performed using Kruskal-Wallis one-way ANOVA. **, $p<0.01$; ***, $p<0.001$. No statistically significant differences were observed in CldU positive cells.

Gy IR from a caesium source. Positive staining for CldU indicated incorporation of the thymidine analogue into DNA, indicating a cell in S-phase stage of the cell cycle just before the irradiation treatment. Co-staining for 53BP1 revealed that the reduction in 53BP1 foci in all ubiquitin mutants was primarily seen in cells without CldU staining (Figure 5.2). Although a reduction in 53BP1 foci numbers between T66A and WT ubiquitin expressing cells was seen in CldU positive cells, this decrease did not reach the threshold for statistical significance.

The difference in 53BP1 foci numbers between CldU positive and negative cells upon expression of T66A indicated that pT66-ubiquitin may be more important in certain cell cycle phases. To investigate this further, pT66-ubiquitin was observed directly in different phases of the cell cycle. CENPF rather than CldU was used as a cell cycle marker, to better identify the cell cycle stage at the time of fixing. CENPF, also known as mitosin, accumulates in the nucleus during S/G2 phase and reaches its maximum expression in G2/M, after which it is rapidly degraded. This allows identification of G0/G1 cells as those without CENPF staining. U2OS cells treated with 4 Gy of IR from an X-ray source were fixed 1-hour post-IR, and stained for CENPF and pT66-ubiquitin.

At 1 hour, 28% of cells had positive staining for CENPF (Figure 5.3a). This is consistent with the FACS data from chapter 2, where 28% of cells transfected with an empty vector control were found to have a 4n DNA content, indicating late S/G2/M which would be expected to be CENPF positive (Figure 4.10). Of these CENPF positive cells, 29% had 10 or more pT66-ubiquitin foci, compared to 57% of CENPF negative cells (Figure 5.3b). After 4 hours, 40% of U2OS cells were CENPF positive, of which 55% had 10 or more pT66-ubiquitin foci. An average of 85% of CENPF negative cells had 10 or more pT66-ubiquitin foci at this time (Figure 5.3c and d). This data indicates that the cell cycle imparts a large influence over the formation of pT66-ubiquitin foci, but is unlikely to be the sole factor governing pT66-ubiquitin foci formation. More work is needed to fully characterise pT66-ubiquitin foci formation during the cell cycle, and the factors responsible.

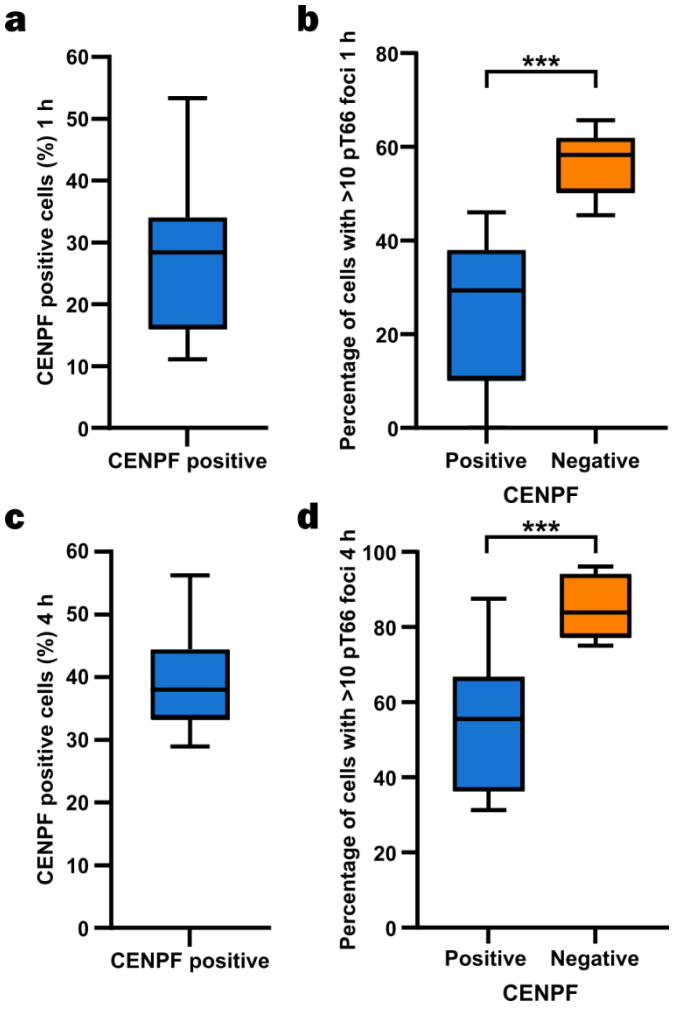

Figure 5.3: pT66-ubiquitin foci formation occurs primarily in CENPF negative cells. U2OS cells treated with 4 Gy IR were fixed at 1- or 4-hours post-IR and stained for pT66-ubiquitin and CENPF. Quantification from each imaged over 3 repeats is shown. **(a)** Percentage of cells with CENPF staining, 1-hour post-IR. **(b)** Percentage of CENPF positive or negative cells with 10 or more pT66-ubiquitin foci 1-hour post-IR. **(c)** and **(d)** are as in (a) and (b), at 4-hours post-IR. Statistical analysis uses the Mann-Whitney t-test. *** = p<0.001

5.2.3 MDC1 foci numbers after IR are not affected by expression of ubiquitin mutants

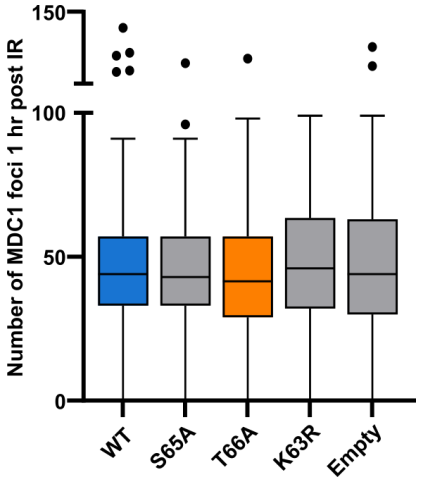

Figure 5.4: Expression of ubiquitin mutants does not alter numbers of MDC1 foci at 1 hour after damage. U2OS cells were treated with MG132 1 hour prior to irradiation with 4 Gy. Cells were fixed 1 hour after IR, then stained for MDC1 and FLAG. Quantification from 3 repeats is shown. No statistically significant differences were detected between samples using Kruskal-Wallis one-way ANOVA.

Recruitment of 53BP1 to sites of damage is tightly regulated, with many factors contributing to its recruitment to and eviction from DSB sites. To try to identify where pT66-ubiquitin is acting in the DDR pathway, proteins upstream of 53BP1 were explored.

MDC1 is a very early responder to DNA damage, serving as a major recruiting platform for other DDR proteins. A direct interaction between MDC1 and 53BP1 has been reported as essential for 53BP1 recruitment to sites of damage (Eliezer et al., 2009), therefore MDC1 recruitment in cells expressing ubiquitin mutants was investigated. U2OS cells expressing mutants of ubiquitin were treated with MG132, then exposed to 4 Gy of IR from a caesium source. The cells were fixed 1-hour post-IR, and the number of MDC1 foci were counted. No differences were found in the numbers of MDC1 foci in any of the ubiquitin mutants tested (Figure 5.4), indicating that the reduction in 53BP1 foci seen in cells expressing T66A ubiquitin was not due to a reduction in MDC1 recruitment to DSBs.

5.2.4 pT66-ubiquitin IRIF are dependent on RNF168

MDC1 recruits the canonical DSB E3 ligases, RNF8 and RNF168, to sites of damage. RNF168 ubiquitylates many targets, but is particularly notable as it ubiquitylates histone H2A at K15, which is strictly required for 53BP1 recruitment to sites of damage (Fradet-Turcotte et al., 2013; Mattiroli et al., 2012). As RNF168 has a direct link to 53BP1 recruitment, this protein was selected for further investigation.

Directly visualising RNF168 was not possible during my thesis. Antibodies against RNF168 and used for immunofluorescence in published literature were no longer giving clear staining. Other labs reported the same issue, and a suitable alternative had not been sourced. Using tagged RNF168 proteins to overcome the lack of an antibody against endogenous protein was also unsuccessful. Using transient expression of a FLAG-tagged RNF168 vector allowed for RNF168 foci to be detected, however the overexpression was toxic to cells. A doxycycline inducible cell line was also trialled, expressing Myc-tagged, siRNA resistant RNF168. Induced cells could form 53BP1 foci after treatment with RNF168 siRNA, suggesting that the tagged RNF168 was expressed. However, RNF168 foci could not be visualised by immunofluorescence in most of these cells, and so the cell line was not taken further.

Although directly detecting RNF168 was not possible, using the siRNA against RNF168 it would be possible to see whether pT66-ubiquitin foci formation was RNF168 dependent. U2OS cells were treated with non-targeting siRNA or RNF168 siRNA, then 48 hours later treated with 4 Gy of IR from an X-ray source. Cells were fixed at 1-hour post-IR. Samples were stained for pT66-ubiquitin and 53BP1. As 53BP1 recruitment is dependent on RNF168, 53BP1 foci can be used as an indicator of the efficacy of the siRNA treatment.

When treated with NT siRNA, 92% of cells were positive (have 10 or more foci) for 53BP1 foci, with 18% positive for pT66-ubiquitin foci (Figure 5.5). Treatment with RNF168 siRNA reduces this to 9% of cells positive for 53BP1, and 1% positive for pT66-ubiquitin foci. This reduction in pT66-ubiquitin foci demonstrates that this mark is downstream of RNF168, although it is not yet determined whether RNF168 used pT66-ubiquitin directly, or the phosphorylation is after ligation to a substrate.

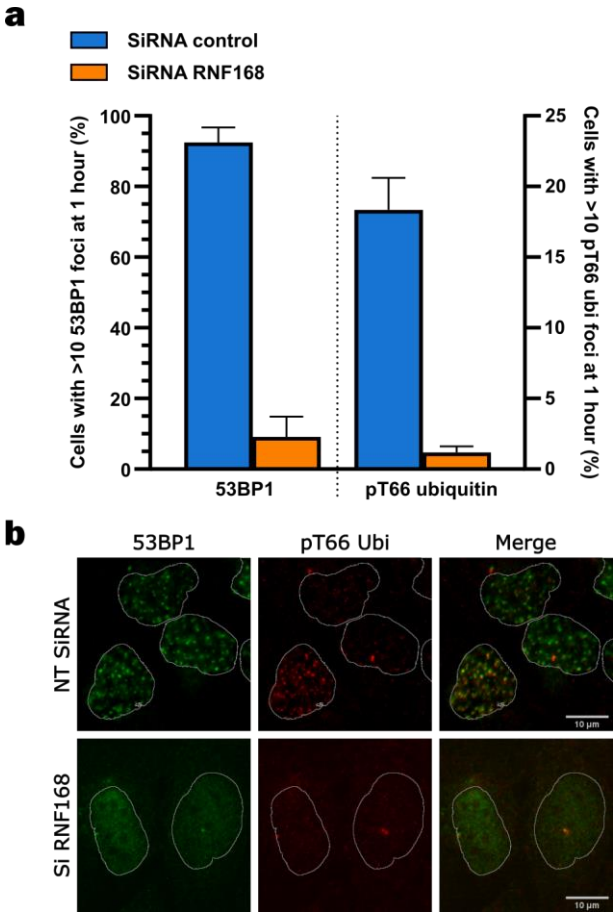

Figure 5.5: pT66-ubiquitin foci are dependent on RNF168. U2OS cells transfected with either NT or RNF168 siRNA were treated with 4 Gy IR, then fixed after 1 hour. Quantification from three repeats is shown. **(a)** Percentage of cells with 10 or more foci after transfection with NT or RNF168 siRNA. Representative images are shown in **(b).**

5.2.5 pT66-ubiquitin IRIF formation is dependent on ATM kinase activity

A major remaining question about pT66-ubiquitin is the identity of the kinase responsible for this phosphorylation. The three major kinases in the DDR: ATM, ATR, and DNA-PK, are unlikely to be responsible for phosphorylating ubiquitin at T66, as this site does not fit with the consensus motif for these kinases. Observing pT66-ubiquitin IRIF formation when they are inhibited can however establish whether pT66-ubiquitin IRIF formation is dependent on these canonical kinases, and indicate whether this modification is specific to the DSB response. Different responses to the kinase inhibitors may also be used to narrow down potential kinases, directing future work to identify the ubiquitin kinase involved.

U2OS cells were incubated in media containing kinase inhibitors, treated with 4 Gy of IR, and fixed 1-hour post-IR. Samples were stained for γH2AX, as a general indicator of kinase inhibition, and pT66-ubiquitin. Image J was used to quantify the fluorescence intensity across the nucleus of both proteins, and the number of pT66-ubiquitin foci were counted. The data is shown in Figure 5.6, with representative images of the samples. A large reduction in γH2AX fluorescence intensity was seen in cells treated with either ATM or DNA-PK inhibitors, in keeping with published literature establishing the importance of these kinases in formation and spreading of γH2AX foci after damage (An et al., 2010; Stiff et al., 2004). A small reduction in γH2AX fluorescence intensity is seen with the ATR inhibitor. This reduction does not meet the threshold for statistical significance, but is expected due to the minor role of ATR in γH2AX formation and the redundancy of the DDR kinases.

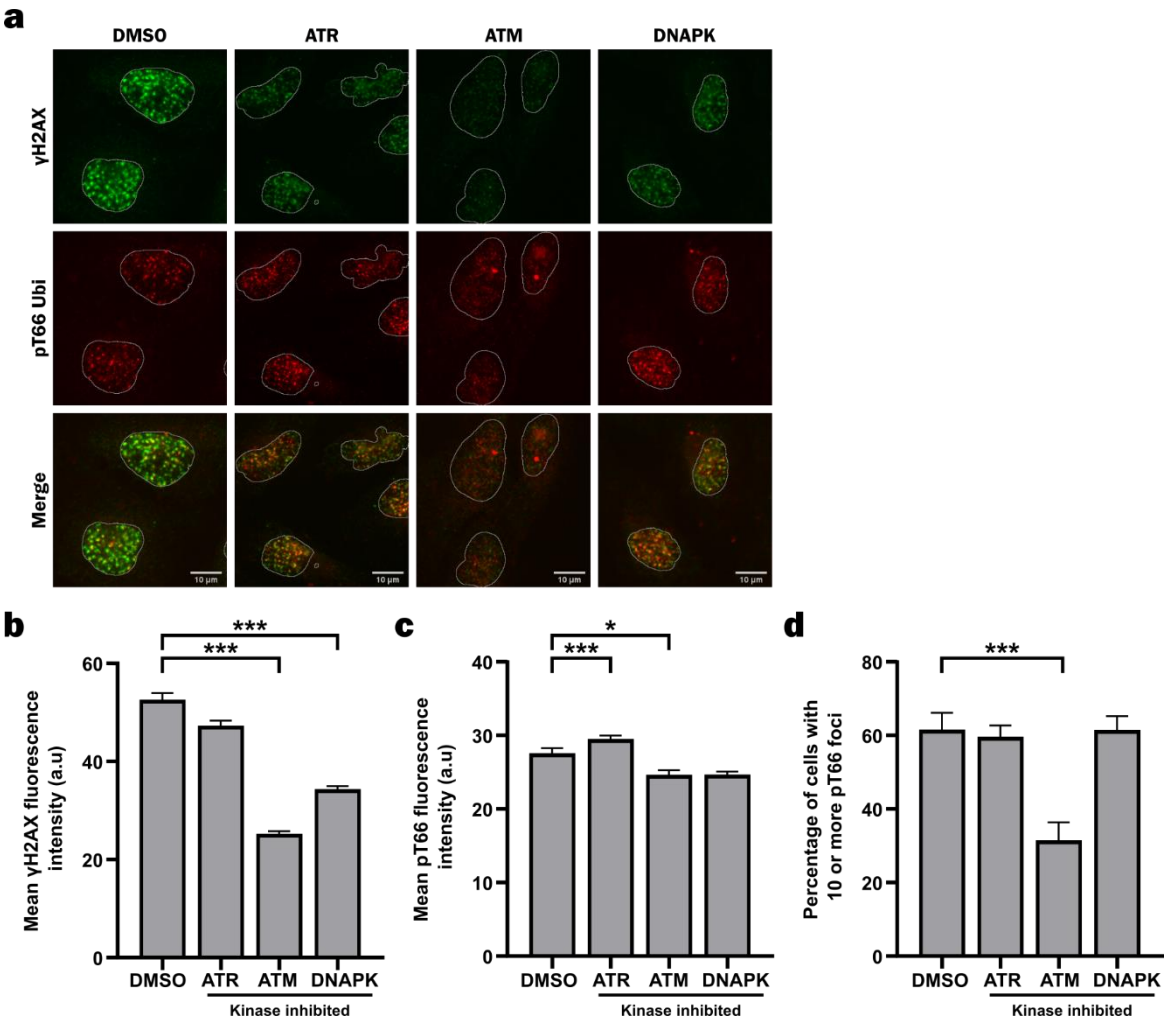

Figure 5.6: Inhibition of ATM kinase, but not ATR or DNA-PK causes a loss of pT66-ubiquitin foci. U2OS cells grown on coverslips were treated with inhibitors of DNA damage kinases, then treated with 4 Gy of IR. Cells were fixed 1 hour after IR and stained for pT66-ubiquitin and γH2AX. **(a)** representative images showing γH2AX and pT66-ubiquitin foci formation in response to IR in the presence of indicated kinase inhibitors. **(b)** Quantification of fluorescence intensity from the nucleus, and the percentage of cells with 10 or more pT66-ubiquitin foci.

The differences in mean pT66-ubiquitin fluorescence intensity between kinase inhibitors was very small, with a range of just 4.8 units of fluorescence intensity been the brightest and dimmest samples. This very small difference did not reflect what was seen in the microscope – see the example images in Figure 5.6a. The samples were re-analysed to identify the number of cells with 10 or more pT66-ubiquitin foci, and using this metric a reduction in the number of cells positive for pT66-ubiquitin foci was identified in cells treated with an inhibitor of ATM (Figure 5.6d).

The reduction in pT66-ubiquitin positive cells when treated with ATM inhibitor, but not ATR inhibitor, is strong evidence that formation of pT66-ubiquitin foci is a DSB specific response. It is important to note, that whilst the DNA-PK inhibitor did not reduce the number of cells with a positive pT66-ubiquitin foci response, there are qualitative differences in the pT66-ubiquitin staining that are not reflected in the data. The pT66-ubiquitin foci formed in cells treated with DMSO or ATR inhibitor were clear and discrete with low background fluorescence. Cells treated with DNA-PK inhibitor have high background fluorescence, which is speckled rather than uniform. This suggests that DNA-PK may impact localisation of pT66-ubiquitin to damage foci, although more work is needed to definitively draw that conclusion.

5.3 Discussion

So far in this thesis, our understanding of pT66-ubiquitin has been shaped by observing the phenotypes caused by its absence, through the T66A-ubiquitin mutant. By using the pT66-ubiquitin antibody characterised in chapter 3, direct observation of pT66-ubiquitin foci is possible, allowing study of the relationship between pT66-ubiquitin and 53BP1 directly.

5.3.1 pT66-ubiquitin foci formation is part of the canonical DSB response

5.3.1a pT66-ubiquitin foci formation is downstream of the DSB response kinase

Although pT66-ubiquitin foci have been demonstrated to be DNA damage dependent in chapter 3 of this thesis, it has not been established whether this modification is dependent on the canonical proteins of the DSB response. Through investigating key DSB response proteins, RNF168 and the principal DDR kinases, there is clear evidence that formation of pT66-ubiquitin foci is part of the canonical DSB response pathway. A remaining question is whether the pT66-ubiquitin foci are a result of ubiquitin phosphorylated at the break site, either as free ubiquitin or already conjugated to a substrate, or caused by re-localisation of this modification from other sites.

In the kinase inhibitor screen (Figure 5.6), inhibition of ATM, the apical kinase in the DSB response, but not ATR or DNA-PK leads to a decrease in the number of cells with pT66-ubiquitin IRIF. This places pT66-ubiquitin foci formation downstream of ATM, indicating that the role of this modification is specific to the DSB response. This ATM kinase dependence does not necessarily mean that ATM is the kinase responsible for T66 phosphorylation, with the T66 phosphorylation site being a poor fit for ATM's consensus motif (Johnson et al., 2022). ATM is known to activate many downstream kinases, which could account for the dependence on ATM activity.

ATM and ATR have many overlapping substrates, with some redundancy in activity. However, they also have unique substrates, which give rise to the different phenotypes observed in ATM vs ATR deficiency models. As ATR did not affect pT66-ubiquitin foci formation, it is likely that one of the

ATM specific substrates is key to the formation of pT66-ubiquitin foci. This information can be used to narrow down potential kinase candidates, which will be discussed in chapter 6.

The same separation cannot be made for ATM and DNA-PK activity, with increasing evidence that both ATM and DNA-PK activity are required to repair a subset of DSBs (Beucher et al., 2009; Gapud and Sleckman, 2011). Although not quantified, it was noted that cells treated with the DNA-PK inhibitor had less "defined" pT66 foci with an increased background compared to other inhibitors. This could indicate that both kinases are important for pT66-ubiquitin signalling, but it could also indicate retention of pT66-ubiquitin when c-NHEJ is impaired. Further work is needed to confirm this observation, and determine how these kinases impact pT66-ubiquitin signalling.

5.3.1b Limitations of the kinase assay

The first measurements taken in the kinase inhibitor screen were of fluorescence intensity across the nucleus. This measurement had previously been used in characterising the antibody, and showed induction of signal after DNA damage, however this was done in the presence of ubiquitin peptides (Figure 3.3). Measuring fluorescence intensity across the nucleus in the kinase inhibitor assay did not detect any differences between the samples, despite a clear difference in pT66-ubiquitin foci formation. There was a relatively high background staining present in all samples, irrespective of treatment, that was likely obscuring the detection of localised signal. In characterising the antibody, competition with a peptide corresponding to the epitope, optionally phosphorylated was used. It may have been that the non-phosphorylated peptide was limiting the non-specific binding of the pT66-ubiquitin antibody, reducing the background signal, thus enabling detection of the induction of signal. It is possible that processing the samples with the addition of the non-phosphorylated peptide may enable detection of differences in fluorescence intensity between the samples.

Changes to fluorescence intensity can be small, even in cells where the formation of foci is clear. For example, this measurement is of limited use in monitoring 53BP1 response, as 53BP1 has a high

background in undamaged cells, with the background reducing as 53BP1 re-localises to sites of damage. This can make the difference in mean fluorescence intensity across the nucleus negligible or even negative between damaged and undamaged cells (Hu et al., 2014). It remains to be seen whether pT66-ubiquitin is formed and then localised to sites of damage, or this modification is created directly at sites of damage.

5.3.1c pT66-ubiquitin foci formation is downstream of a canonical DSB E3-ligase

In addition to the requirement for ATM activity, knockdown of the E3 ligase RNF168 also caused the near-total loss of pT66-ubiquitin foci. The dependence of pT66-ubiquitin foci on RNF168 is further confirmation that pT66-ubiquitin foci formation is part of the canonical DSB response pathway.

The dependence on RNF168 suggests that pT66-ubiquitin foci formation is downstream of RNF168's activity. This could be through direct use of pT66-ubiquitin by RNF168, phosphorylation of ubiquitin after it has been ligated to a substrate by RNF168, or through recruitment of a pT66-ubiquitin modified substrate in an RNF168 dependent manner. Outside of histone H2AK13/15 (where phosphorylated ubiquitin would likely inhibit recruitment of 53BP1), RNF168 ubiquitylates 53BP1 itself, JMJD2A, and L3MBTL1 (Acs et al., 2011; Bohgaki et al., 2013; Mallette et al., 2012). Ubiquitylation of all these substrates contributes to 53BP1 recruitment to damage sites. Given this direct link between RNF168 activity and 53BP1 recruitment, if free ubiquitin is phosphorylated at T66, RNF168 is the most likely candidate to utilise such a phosphorylated ubiquitin to regulate 53BP1 recruitment. More work is needed to establish the relationship between RNF168 and pT66-ubiquitin.

In all repeats of this experiment, the percentage of cells with pT66-ubiquitin foci was lower than seen in other experiments, with less than 20% of the population positive for pT66-ubiquitin foci, compared with approximately 50% across other experiments. This is a result of staining optimisation in subsequent experiments, which reduced background staining and improved detection of damage induced foci. This reduction in pT66-ubiquitin positive cells does not change the interpretation of the results from this experiment, and so it has not been repeated with the optimised staining.

5.3.2 pT66-ubiquitin foci form primarily, but not exclusively, in G1

It was apparent during characterisation of the pT66-ubiquitin antibody that a significant proportion of cells show little to no pT66 foci in response to DNA damage. This finding is quantified in Figure 5.1, where at 1-hour post-IR over 90% of cells are 53BP1 positive, whereas approximately 50% are pT66 positive. Visually, there is little to distinguish the cells that are pT66 positive from those that fail to make foci, such as chromatin condensation or membrane blebbing that would have indicated mitosis or apoptosis respectively. Cell cycle has an impact on repair pathway choice, so the impact of the cell cycle on pT66-ubiquitin foci formation was investigated.

CENPF (also known as mitosin) accumulates throughout the cell cycle reaching a peak in G2/M, and is then rapidly degraded after mitosis (Liao et al., 1995). This allows for the identification of cells with absent CENPF staining as likely G1 cells. Cells without CENPF staining (likely G0/G1) were more likely to be pT66 positive after damage than CENPF positive cells 1 hour after damage induction. By 4 hours, the percentage of cells with pT66-ubiquitin foci increased in both CENPF positive and negative cells, compared to at 1 hour. This demonstrates that although cell cycle has an impact on pT66-ubiquitin foci formation, these foci are not exclusive to a single stage of the cell cycle.

This finding fits with pT66-ubiquitin being a PTM in the NHEJ pathway. C-NHEJ can occur throughout the cell cycle, but repair by HR is largely limited to S/G2. This is also reflected in the variability in the percentage of pT66 positive cells in CENPF positive vs. negative cells. There is less variability in G1, where most repair will be channelled through c-NHEJ pathways, but in S/G2, other repair pathways are available, introducing larger variability into the results.

The impact of cell cycle is reflected further when evaluating the impact of expressing mutants of ubiquitin on 53BP1 foci after damage, whilst co-staining for CldU as a marker of cell cycle. Cells with CldU staining were assigned as S/G2 phase at the time of foci analysis, whereas cells without CldU staining were assigned as G1. 53BP1 IRIF were found to be reduced in both CldU positive and negative cells expressing T66A ubiquitin, compared to WT ubiquitin. However, the difference

between T66A and WT was found to be greatest in CldU negative cells, in line with a role for pT66-ubiquitin primarily in G1. Also of note, is the reduction in the median number of 53BP1 foci in CldU positive vs negative cells when expressing WT ubiquitin. This reduction was not seen in cells expressing T66A ubiquitin. This may suggest that even when present, pT66-ubiquitin is not as critical for 53BP1 recruitment outside of G1.

5.3.3 Peak pT66-ubiquitin foci levels are later than observed for 53BP1

Both the kinetics data and CENPF data show that 1 hour after damage, approximately 50% of cells don't show robust pT66-ubiquitin foci formation, with peak foci numbers and percentage of cells with 10 or more foci occurring later, at 4 hours post-IR. This late peak in pT66-ubiquitin IRIF is seemingly at odds with the reduction of 53BP1 IRIF observed shortly after IR when expressing T66A ubiquitin. The early impact of the T66A mutation suggests pT66-ubiquitin is involved in 53BP1 IRIF formation, but 53BP1 IRIF in cells without clearly visible pT66-ubiquitin IRIF would suggest that this is not the case.

A PhD thesis by Zuzanna Kozik (2019) demonstrated that histone modifications reach peak levels at different times, even when associated with the "early" DDR. H2A(X)K15 ubiquitylation for example was found to reach peak levels at DSB sites at 4-8 hours after damage, despite this modification being necessary for 53BP1 recruitment which shows peak foci numbers much earlier. Other research indicates that foci formation is not necessarily an indicator of activity at a break site. RNF168 is critical for 53BP1 foci formation, and can be observed co-localising at damage sites. However, a mutant of RNF168 (N221*) which doesn't form foci is still capable of forming 53BP1 IRIF when endogenous RNF168 has been knocked down, demonstrating that localisation at foci is not key to its role in the DDR (Muñoz et al., 2014). Unpublished work from the Morris lab has shown that expression of tagged RNF168 rescues 53BP1 IRIF after knockdown of endogenous RNF168, including in cells without tagged-RNF168 foci.

This highlights a limitation of interpreting DDR foci, as localisation to damage sites and activity at damage sites are not mutually inclusive (Markova et al., 2007). In the case of pT66-ubiquitin, it could be that there is enough of this modification to signal in the DDR pathway without being sufficient for detection by widefield fluorescence microscopy, and that the foci that are detected are where there is accumulation of pT66-ubiquitin. This would fit with the increased detection of pT66-ubiquitin foci at later timepoints (Figure 5.1), although additional work is required to determine whether pT66-ubiquitin is accumulating at break sites, or only marking specific break sites.

There are an increasing number of methods to improve the resolution of DNA damage foci, which may be of benefit in future work with pT66-ubiquitin. These include super-resolution microscopy and single molecule techniques, and expansion microscopy, all of which can improve understanding of the organisation of proteins directly at break sites (Schaich and Van Houten, 2021). These techniques have already been used to demonstrate the interplay between BRCA1 and 53BP1 at damage sites, and reinforce that a "focus" seen by widefield fluorescence microscopy, as used in this thesis, may not be fully representative of the underlying repair of the break site (Chapman et al., 2012a; Faulkner et al., 2022; Rothkamm et al., 2015). Future work incorporating super-resolution techniques may help determine whether pT66-ubiquitin is present at all break sites and accumulating in only some cells, as well as provide further detailed information into its role at DSBs.

If the assumption is that accumulation at damage foci is not required for pT66 signalling, then the question changes from "why don't all cells show pT66-ubiquitin foci" to "what drives accumulation of pT66-ubiquitin at foci". pT66-ubiquitin foci are visible at 30 minutes post-IR (earlier timepoints have not been examined) and similar numbers are present at 30 minutes and 1-hour post-IR, indicating that time alone is not a sufficient explanation for pT66 foci formation. IRIF formation cannot be attributed to cell cycle alone either, as CENPF negative cells (broadly G0/G1) had approximately 40% of cells without 10 or more pT66-ubiquitin foci at 1 hour after damage.

Answers for what drives pT66-ubiquitin foci formation are unlikely to be easy to come by, given the complexity of the DDR signalling pathway. Cell cycle, break complexity, chromatin environment and other factors complicate the study of DDR pathways. The factors governing pT66-ubiquitin foci formation are likely to be factors that affect the whole cell, as most cells either do or do-not display robust IRIF. There are many avenues for further work into not only pT66-ubiquitin, but factors governing DSB repair pathways more generally.

5.3.4 Conclusion

Results presented in this chapter using the pT66 antibody establish pT66-ubiquitin as a modification in the canonical DSB response, and give further confidence in this modification being part of the NHEJ pathway. These results also confirm a link between 53BP1 and pT66-ubiquitin, although suggest that this link is unlikely to be a direct interaction between the two proteins, implicating an as-of-yet unidentified substrate for pT66-ubiquitin.

Chapter 6: Thesis discussion

6.1 Discussion

At the start of this project, three questions were set out to guide work into pT66-ubiquitin:

1. Is phosphorylation of ubiquitin at T66 in response to DNA damage conserved in mammalian cells?
2. What is the role of pT66-ubiquitin in the DNA damage response?
3. How is this modification regulated in the DNA damage response?

The extent to which these questions have been addressed in this thesis is outlined below.

6.1.1a Is phosphorylation of ubiquitin at T66 in response to DNA damage conserved in mammalian cells?

Evidence gathered in this thesis shows that pT66-ubiquitin is conserved between human and *Xenopus laevis*, and localises in the nucleus in response to DNA damage. Using a raised and characterised antibody against pT66-ubiquitin, a signal can be detected by IF and IB that is distinct from an anti-ubiquitin antibody (Figure 3.6) or FLAG-tagged ubiquitin (Figure 3.4). By IF, pT66-ubiquitin can be observed to form foci in the nucleus after DNA damage in U2OS cells, and these foci co-localise with 53BP1, a known marker of double-strand breaks (Figures 3.1 and 5.1). Further evidence for pT66-ubiquitin in the DNA damage response is through the dependence of foci formation on the established DNA damage proteins, ATM and RNF168 (Figures 5.5 and 5.6). Phenotypes caused by expression of the non-phosphorylatable mutant of ubiquitin, T66A, also support a role for pT66-ubiquitin in the normal progression of the DDR by reducing the recruitment of 53BP1 (Figures 4.5 and 4.7)

This study does not exclude a role for pT66-ubiquitin outside of the DDR. In undamaged U2OS cells, the pT66-ubiquitin antibody stains extra-nuclear foci, which are thought to be centrosomes (Figure 3.9). This suggests pT66-ubiquitin may have a role in other aspects of cell homeostasis regulated by

the centrosomes, such as the cell cycle. It also raises the possibility that pT66-ubiquitin is not formed in response to DNA damage, but relocates from the centrosomes. However, the signal from the extra-nuclear foci was found to not be as sensitive to competition from the phosphorylated peptide as the DNA damage induced foci, which may indicate that this signal is caused by non-specific antibody binding. This is an interesting avenue for future work, which could create another link between centrosomes and the DDR if this signal is found to be specific.

6.1.1b What is the role of pT66-ubiquitin in the DNA damage response?

We have identified that pT66-ubiquitin foci formation is part of the double-strand break response, with evidence that it is involved in the NHEJ repair pathway through recruitment of 53BP1. However, as the proteins responsible for the formation of pT66-ubiquitin have not been identified, its exact role and mechanism is unknown. pT66-ubiquitin foci formation is reduced upon inhibition of ATM, but not ATR (Figure 5.6), placing pT66-ubiquitin foci formation downstream of the master DSB kinase. Further evidence for pT66-ubiquitin in the DSB response is seen with the loss of pT66-ubiquitin foci upon knockdown of RNF168, a key ubiquitin ligase in this pathway (Figure 5.5).

Expression of T66A ubiquitin was found to reduce the number of 53BP1 foci after damage, whilst BRCA1 foci numbers were unaffected (Figures 4.5, 4.7, and 4.9). Recruitment of 53BP1 to damage sites is associated with repair of DSBs by NHEJ, whereas BRCA1 drives repair by HR. The reduction in 53BP1 foci indicates pT66-ubiquitin is important in the NHEJ pathway. The impact of cell cycle also indicates pT66 is likely to be part of the NHEJ pathway. The reduction in 53BP1 foci upon T66A ubiquitin expression was largest in CldU negative cells (Figure 5.2), and pT66-ubiquitin foci were more common in CENPF negative cells (Figure 5.3). This is indicative of pT66-ubiquitin signalling being more prevalent in G0/G1 stages of the cell cycle, consistent with a role in NHEJ.

6.1.1c How is this modification regulated in the DNA damage response?

The final question investigated in this thesis has only been partially answered. We have established that the formation of pT66-ubiquitin foci is dependent on canonical DDR proteins (Figures 5.5 and 5.6), so can infer that factors that regulate the early DSB response are likely to impact pT66-ubiquitin foci formation as well. However, the substrate protein for pT66-ubiquitin and the proteins that interact with this modification have not been identified. This means it is impossible to place pT66-ubiquitin accurately within the DDR signalling pathway, which would give clues as to the regulatory mechanisms that write, read, and remove this mark.

Work in this thesis does narrow down the scope of possible proteins involved. As pT66-ubiquitin foci formation is largely ATM dependent, this can be used to identify the first subset of proteins involved. The loss of pT66-ubiquitin foci upon RNF168 knockdown further narrows this scope, with either RNF168 substrates, or proteins that interact with these substrates as strong candidates for the pT66-ubiquitin substrate. These findings can be used to rationally guide future work to identify the proteins involved in pT66-ubiquitin signalling.

6.1.2 Future Work

6.1.2a Future Directions

There are several questions raised by this thesis that are avenues for future work.

1) What proteins are involved in writing, reading, and removing pT66-ubiquitin signalling?

This question offers a lot of scope for further work, with all the proteins involved in pT66-ubiquitin signalling still undiscovered. Identification of proteins by mass spectrometry is one way forward, as it can identify many proteins from a single sample. Immunoblotting with the pT66-ubiquitin antibody reveals multiple bands up to 185 kDa, the highest marker on the gel (Figure 3.6), indicating that pT66-ubiquitin is conjugated to substrate proteins. It may be possible to use the pT66-ubiquitin antibody to identify these substrates, by using the antibody for immunoprecipitation. A pull-down of pT66-ubiquitin would also pull-down conjugated proteins, which would then be identified by mass

spectrometry. Information on these substrates would also guide the search for the other proteins involved in pT66-ubiquitin signalling, such as the E2s, E3s, and kinases, as protein interactions may already be known.

Figure 3.6 suggests that free ubiquitin may be phosphorylated, with two bands thought to correspond to free ubiquitin observed with the anti-ubiquitin antibody between 10 and 15 kDa. The higher of these bands could be due to the slower migration of modified proteins compared to their unmodified counterparts, and a band of this size is seen with the pT66-ubiquitin antibody, further suggesting this top band is modified ubiquitin. Determining whether free ubiquitin is phosphorylated has important implications for the E2/E3 enzyme involved as these enzymes are likely to be regulated by the availability of pT66-ubiquitin, whether they preferentially use or are unable to conjugate pT66-ubiquitin. If ubiquitin is only phosphorylated when conjugated to a substrate, this would require a kinase capable of differentiating between free and conjugated ubiquitin, likely through additional recognition domains. Linking this information with substrates found from a pT66-ubiquitin IP could identify the kinase. Mass spectrometry of proteins under 15 kDa (to best capture free ubiquitin, both modified and not) could help confirm whether free ubiquitin is phosphorylated at T66.

No phosphorylation of ubiquitin was detected in the mass spectrometry analysis from this thesis (Table 3.2). Mass spectrometry is known to be biased against low-abundance peptides, which means that conventional mass spectrometry is unlikely to be the best approach (Peck Justice et al., 2021). SRM and PRM techniques can be used to selectively identify proteins from complex samples, which greatly increases the sensitivity of mass spectrometry towards low abundance peptides. This makes use of these techniques ideal to study post-translational modifications, and indeed SRM has been used in the detection and quantification of ubiquitin phosphorylated at S65 (Ordureau et al., 2015; Rauniyar, 2015).

Determining whether pT66-ubiquitin is newly formed or is instead re-localised after damage is also key, with this information further informing which proteins are involved in pT66-ubiquitin signalling. Little difference in the amount of pT66-ubiquitin signalling has been seen between irradiated and un-treated samples by IB (Figure 3.6). Whilst this could suggest that pT66-ubiquitin is primarily re-localised after damage, if pT66-ubiquitin has multiple roles within the cell (suggested by the centrosomal staining in Figure 3.9), a basal level of pT66 may be expected. PRM mass spectrometry should enable quantification of this modification in damaged and undamaged samples, demonstrating whether there is increased pT66-ubiquitin after damage, indicating new phosphorylation, or if the levels remain steady, indicating re-localisation of existing pT66-ubiquitin.

2) What is the impact of pT66-ubiquitin on repair outcomes?

Up to 80% of DSBs are repaired with rapid kinetics by NHEJ, which requires only the core NHEJ proteins (Ingram et al., 2019; Shibata and Jeggo, 2020). The remaining breaks are repaired with additional proteins, depending on factors such as cell cycle stage, break site, and damage complexity (Chang et al., 2016; Shen et al., 2021). Expression of T66A ubiquitin was observed to reduce 53BP1 IRIF formation, but does this lead to a significant alteration to DNA repair outcomes? Expression of T66A may direct DSB repair to HR or alt-EJ pathways, or render them irreparable. DNA repair deficits could also manifest as genomic instability, as is seen with deficiencies in other DDR proteins (Gorodetska et al., 2019; Sishc and Davis, 2017). Exploring the impact of T66A ubiquitin expression on DNA repair outcomes could highlight biologically important roles for pT66-ubiquitin in the DDR.

Study into the impact of T66A ubiquitin on DNA repair outcomes has been limited by the issues surrounding replacement of endogenous ubiquitin with ubiquitin mutants. A stable cell line created in a U2OS background has been used to replace endogenous ubiquitin, including in the study of pT12-ubiquitin (Walser et al., 2020; Xu et al., 2009). Use of this cell line would be beneficial in studying the impact of T66A ubiquitin over longer time periods, without concern for toxicity caused by proteasome inhibition, or endogenous ubiquitin potentially masking phenotypes. However, some

groups using this cell line have reported in private correspondence that this cell line has its own issues, with viability and unexpected sensitivity in experiments (unpublished data). Additional methods to study DNA repair outcomes should also be considered.

Finally, the work carried out in this thesis has used the U2OS cell line, a well characterised human cancer line. Expanding the cell lines used in future studies to include cell lines from different tissues and non-cancerous backgrounds would strengthen the confidence in the findings of this thesis, demonstrating that any repair outcomes caused by altering pT66-ubiquitin signalling is not tissue or cancer specific. Cell lines with known DNA repair or response defects could also be beneficial, enabling characterisation of pT66-ubiquitin signalling when the DDR is altered.

3) Is there a link between pT12- and pT66-ubiquitin?

Walser et al. (2020) discovered ubiquitin phosphorylated at T12 in the DDR, which has opposing roles to phosphorylation at T66. Can both modifications exist on the same ubiquitin, or localise to the same damage sites? Does phosphorylation at one site regulate phosphorylation at the other? The interplay of these two modifications of ubiquitin may be important in driving DNA repair pathway choice. Repair pathway choice is an area of interest in cancer therapeutics, which may make these modifications clinically relevant (Trenner and Sartori, 2019).

Although of interest, this work is likely to be a lower priority for future work, as both pT66- and pT12-ubiquitin modifications are not well characterised. Work into characterising the individual modification a more immediate priority. Exactly how to approach this question is also unclear – T66 and T12 are spatially close on ubiquitin (Figure 1.3), which could impede antibody binding if antibodies against these phospho-sites are used together (Abdiche et al., 2017). Mass spectrometry would also not determine whether these two modifications occur on the same protein, as the peptides would not overlap. Better characterisation of either of these modifications is likely to open up more avenues for exploring this question in the future.

4) Does pT66-ubiquitin have a role outside of the DDR?

A question outside the scope of this thesis was whether the extra-nuclear foci visualised with the pT66-ubiquitin antibody could be confirmed as centrosomes (Figure 3.9). Centrosomes have multiple roles within cells, including in the DNA damage response, and may serve to link the local DNA damage response at break sites to the global cell changes after DNA damage (Mullee and Morrison, 2016). Proteins linked to the DNA damage response often have other roles within cells, and many have been found localised to centrosomes at various stages of the cell cycle (Luna-Maldonado et al., 2021), so a link between the centrosome and DNA damage response would not be unexpected.

6.1.3 Speculation on where pT66 ubiquitin could be acting in the DDR

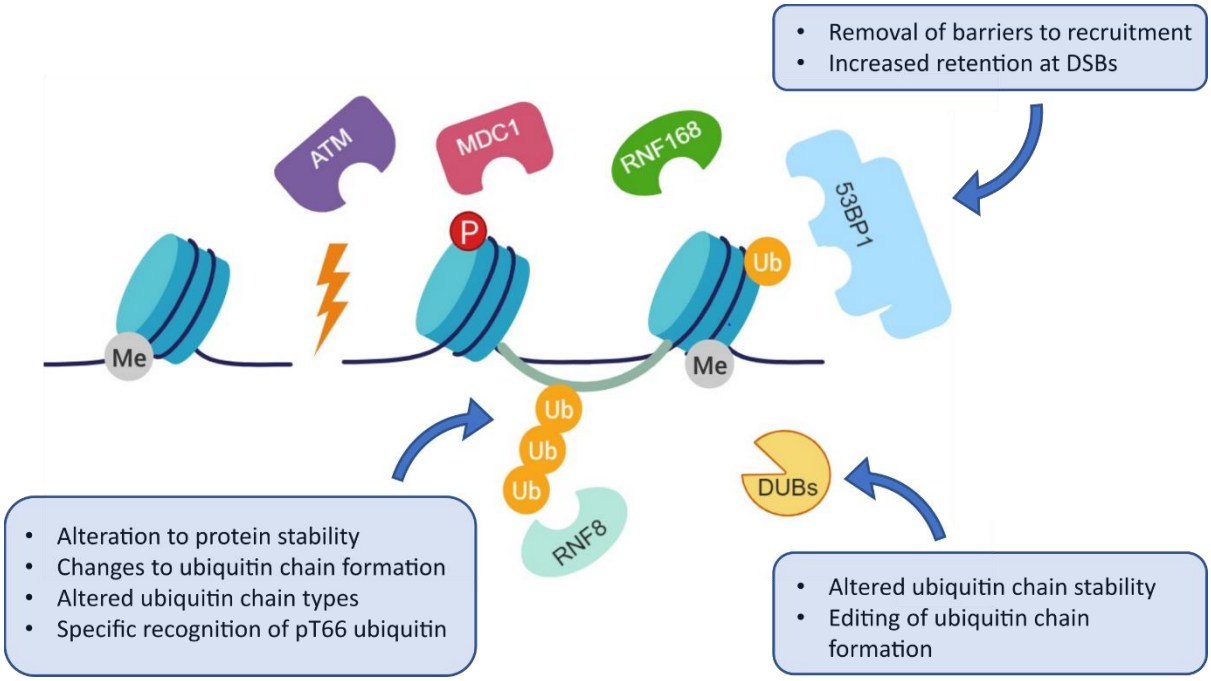

Figure 6.1: Ubiquitin phosphorylated at T66 could regulate the DDR in multiple ways. Phosphorylated ubiquitin could alter ubiquitin chain formation, either through E2/E3 enzymes or DUBs, or the phosphorylated ubiquitin itself could serve as a recruitment motif for recruiting proteins in the DDR pathway.

Ubiquitin signalling is generally viewed in terms of its conjugation to a substrate protein. However, ubiquitin signalling can also occur without this conjugation, either as unanchored ubiquitin chains or through allosteric interactions (Wiener et al., 2012; Xia et al., 2009). These different forms of

ubiquitin signalling are observed with pS65 ubiquitin, where free ubiquitin and ubiquitin already incorporated into ubiquitin chains on proteins of the outer mitochondrial membrane is phosphorylated by PINK1 (Kane et al., 2014). Free pS65 ubiquitin acts allosterically on Parkin to promote its subsequent phosphorylation and enzymatic activity (Kazlauskaite et al., 2015). Parkin can also use the free pS65 ubiquitin to build unanchored ubiquitin chains, or ubiquitin chains conjugated to proteins on the surface of mitochondria. These phosphorylated ubiquitin chains promote additional recruitment of Parkin in a feed forward mechanism that drives mitophagy (Dunkerley et al., 2022).

With pT66 ubiquitin, it is unclear whether free ubiquitin can be phosphorylated, or if the phosphorylation is limited to ubiquitin already conjugated to a substrate. This distinction has many implications for the regulation of this signalling pathway, as well as how to approach research into pT66 ubiquitin. If ubiquitin is only phosphorylated when conjugated to a substrate protein, emphasis is placed on the identity of the kinase, and how its activity is regulated. Phosphorylation of only conjugated ubiquitin implies specific recognition by the kinase, either through recognition of the substrate protein and ubiquitin, or specific conformations of ubiquitin arising from chain types. This limits the use of pT66 ubiquitin to a specific step in the DDR pathway. This regulation may be the case with pT12 ubiquitin, where tight control of the signalling is likely to be necessary (Walser et al., 2020).

In contrast, if free ubiquitin is phosphorylated, a greater importance is given to the E2 and E3 enzymes involved. Ubiquitin chain formation may be altered, both in terms of chain building activity and in the chain types formed (Wauer et al., 2015b). In unpublished data, RNF168 is said to be able to build chains using pT12 ubiquitin, raising the possibility that it may be able to use ubiquitin phosphorylated at other residues as well (Walser et al., 2020). RNF168 is commonly associated with building K63 linked ubiquitin chains, but has also been demonstrated to build K27 linked ubiquitin chains, with both chain types contributing to the DDR and recruitment of 53BP1 to sites of damage

(Gatti et al., 2015). Phosphorylation of ubiquitin at T66 could represent one way to modulate which chain types are built by RNF168 during the DDR.

Phosphorylated ubiquitin conjugated to a substrate impacts the "readers" of the ubiquitin mark. As seen with T12 phosphorylation, some ubiquitin binding domains remain able to interact with the modified ubiquitin (such as BRCA1 and RNF169), whilst 53BP1 is unable to interact with pT12 ubiquitin mark, hindering its recruitment. Phosphorylation of ubiquitin may bring about new interactions through phospho-binding domains, which are common in DDR proteins. pT66 ubiquitin could be a signal for factors surrounding 53BP1 recruitment, such as removal of L3MBTL and JMJD2A from masking H4K20Me2 sites (Acs et al., 2011; Mallette et al., 2012) or for recruiting chromatin remodellers that regulate 53BP1's access to and stability at DSB sites (Chapman et al., 2012a; Rother et al., 2020).

Deubiquitinating enzymes are also affected by ubiquitin phosphorylation, and play a significant role in moderating the DDR (Le et al., 2019). Many DUBs are observed to be hindered in their ability to remove phosphorylated ubiquitin, stabilising ubiquitin signalling (Huguenin-Dezot et al., 2016; Wauer et al., 2015b). This can impact on repair pathway choice, as is the case with USP14. Overexpression of USP14 counteracts ubiquitin signalling by RNF168, limiting NHEJ and instead promoting repair by HR. Conversely, depletion of USP14 promotes repair by NHEJ (Sharma and Almasan, 2020). USP14 is less active against pS65 ubiquitin than WT ubiquitin (Stuber et al., 2021), demonstrating that it is affected by ubiquitin phosphorylation, and that ubiquitin phosphorylation may be a mechanism to promote stability of RNF168 ubiquitin signalling.

Unconjugated pT66 ubiquitin could affect the DDR through allosteric modulation of ubiquitin cascade proteins, as has been observed with the allosteric activation of Parkin by pS65 ubiquitin (Kazlauskaite et al., 2015). The DUB OTUB1, in addition to its enzymatic activity also acts in a non-canonical manner to inhibit the E2 enzyme UBC13. OTUB1 binds to UBC13 in complex with ubiquitin, preventing ubiquitin transfer through the cascade, and this interaction is strengthened by free

ubiquitin binding allosterically to OTUB1 (Nakada et al., 2010). UBC13 facilitates K63-linked ubiquitin chain formation in the DDR in collaboration with E3 ligases including RNF8 and RNF168 (Campbell et al., 2012; Mattiroli et al., 2012), so inhibition of this E2 limits the activity of RNF8 and RNF168, likely limiting recruitment of 53BP1. If free pT66 ubiquitin alters this allosteric interaction, this would be an interesting mechanism for controlling ubiquitin signalling in the DDR.

6.2 Conclusion

Post-translational modifications of ubiquitin are emerging as important signals in a diverse set of pathways, expanding the already complex ubiquitin code. Work in this thesis establishes a role for another ubiquitin PTM, phosphorylation at T66, in the DDR, and gives evidence that this modification may be involved in DNA repair by NHEJ. pT66-ubiquitin is observed to form nuclear foci after DNA damage, with the formation of these foci dependent on known DSB response proteins. This modification is also important for 53BP1 foci formation after damage with a phospho-dead mutant limiting foci formation, although the mechanism for this is unknown. This effect on 53BP1 foci formation is opposite to that observed with phosphorylation of ubiquitin at T12, which suggests that differential phosphorylation of ubiquitin may be important in DNA repair pathway choice. Further research into the roles and mechanism of pT66-ubiquitin signalling are required for complete characterisation of this modification, but research into modulating the DNA damage response is important in areas such as cancer therapeutics and gene-editing, making pT66-ubiquitin a valuable target for onward research.

Bibliography

Abdiche, Y., A. Yeung, I. Ni, D. Stone, A. Miles, W. Morishige, A. Rossi, and P. Strop, 2017, Antibodies Targeting Closely Adjacent or Minimally Overlapping Epitopes Can Displace One Another: PloS one, v. 12.

Acs, K., M. Luijsterburg, L. Ackermann, F. Salomons, T. Hoppe, and N. Dantuma, 2011, The AAA-ATPase VCP/p97 promotes 53BP1 recruitment by removing L3MBTL1 from DNA double-strand breaks: Nature structural & molecular biology, v. 18.

Adam, K., and T. Hunter, 2017, Histidine kinases and the missing phosphoproteome from prokaryotes to eukaryotes: Laboratory Investigation, v. 98, p. 233-247.

Adam, S., S. Polo, and G. Almouzni, 2013, Transcription recovery after DNA damage requires chromatin priming by the H3.3 histone chaperone HIRA: Cell, v. 155.

Aguirre, J., K. Dunkerley, P. Mercier, and G. Shaw, 2017, Structure of phosphorylated UBL domain and insights into PINK1-orchestrated parkin activation: Proceedings of the National Academy of Sciences of the United States of America, v. 114.

Aly, A., and S. Ganesan, 2011, BRCA1, PARP, and 53BP1: conditional synthetic lethality and synthetic viability: Journal of molecular cell biology, v. 3.

An, J., Y. Huang, Q. Xu, L. Zhou, Z. Shang, B. Huang, Y. Wang, X. Liu, D. Wu, and P. Zhou, 2010, DNA-PKcs plays a dominant role in the regulation of H2AX phosphorylation in response to DNA damage and cell cycle progression: BMC molecular biology, v. 11.

Ardito, F., M. Giuliani, D. Perrone, G. Troiano, and L. Lo Muzio, 2017, The crucial role of protein phosphorylation in cell signaling and its use as targeted therapy (Review): Int J Mol Med, v. 40, p. 271-280.

Aschner, Y., and G. Downey, 2018, The Importance of Tyrosine Phosphorylation Control of Cellular Signaling Pathways in Respiratory Disease: pY and pY Not: American journal of respiratory cell and molecular biology, v. 59.

Awasthi, P., M. Foiani, and A. Kumar, 2015, ATM and ATR signaling at a glance: J Cell Sci, v. 128, p. 4255-62.

Balmus, G., A. Barros, P. Wijnhoven, C. Lescale, H. Hasse, K. Boroviak, C. le Sage, B. Doe, A. Speak, A. Galli, M. Jacobsen, L. Deriano, D. Adams, A. Blackford, and S. Jackson, 2016, Synthetic lethality between PAXX and XLF in mammalian development: Genes & development, v. 30.

Baudat, F., Y. Imai, and B. de Massy, 2013, Meiotic recombination in mammals: localization and regulation: Nature reviews. Genetics, v. 14.

Becker, J., G. Clifford, C. Bonnet, A. Groth, M. Wilson, and J. Chapman, 2021, BARD1 reads H2A lysine 15 ubiquitination to direct homologous recombination: Nature, v. 596.

Becker, J., R. Cuella-Martin, M. Barazas, R. Liu, C. Oliveira, A. Oliver, K. Bilham, A. Holt, A. Blackford, J. Heierhorst, J. Jonkers, S. Rottenberg, and J. Chapman, 2018, The ASCIZ-DYNLL1 axis promotes 53BP1-dependent non-homologous end joining and PARP inhibitor sensitivity: Nature communications, v. 9.

Bennardo, N., A. Cheng, N. Huang, and J. Stark, 2008, Alternative-NHEJ is a mechanistically distinct pathway of mammalian chromosome break repair: PLoS genetics, v. 4.

Bennetzen, M., D. Larsen, J. Bunkenborg, J. Bartek, J. Lukas, and J. Andersen, 2010, Site-specific phosphorylation dynamics of the nuclear proteome during the DNA damage response: Molecular & cellular proteomics : MCP, v. 9.

Berginski, M. E., N. Moret, C. Liu, D. Goldfarb, P. K. Sorger, and S. M. Gomez, 2021, The Dark Kinase Knowledgebase: an online compendium of knowledge and experimental results of understudied kinases: Nucleic Acids Res, v. 49, p. D529-D535.

Bergmann, L., A. Lang, C. Bross, S. Altinoluk-Hambüchen, I. Fey, N. Overbeck, A. Stefanski, C. Wiek, A. Kefalas, P. Verhülsdonk, C. Mielke, D. Sohn, K. Stühler, H. Hanenberg, R. Jänicke, J. Scheller, A. Reichert, M. Ahmadian, and R. Piekorz, 2020, Subcellular Localization and Mitotic

Interactome Analyses Identify SIRT4 as a Centrosomally Localized and Microtubule Associated Protein: Cells, v. 9.
Beucher, A., J. Birraux, L. Tchouandong, O. Barton, A. Shibata, S. Conrad, A. Goodarzi, A. Krempler, P. Jeggo, and M. Löbrich, 2009, ATM and Artemis promote homologous recombination of radiation-induced DNA double-strand breaks in G2: The EMBO journal, v. 28.
Blackford, A. N., and S. P. Jackson, 2017, ATM, ATR, and DNA-PK: The Trinity at the Heart of the DNA Damage Response: Mol Cell, v. 66, p. 801-817.
Boboila, C., C. Yan, D. Wesemann, M. Jankovic, J. Wang, J. Manis, A. Nussenzweig, M. Nussenzweig, and F. Alt, 2010, Alternative end-joining catalyzes class switch recombination in the absence of both Ku70 and DNA ligase 4: The Journal of experimental medicine, v. 207.
Bohgaki, M., T. Bohgaki, S. El Ghamrasni, T. Srikumar, G. Maire, S. Panier, A. Fradet-Turcotte, G. S. Stewart, B. Raught, A. Hakem, and R. Hakem, 2013, RNF168 ubiquitylates 53BP1 and controls its response to DNA double-strand breaks: Proc Natl Acad Sci U S A, v. 110, p. 20982-7.
Boisvert, F., A. Rhie, S. Richard, and A. Doherty, 2005, The GAR motif of 53BP1 is arginine methylated by PRMT1 and is necessary for 53BP1 DNA binding activity: Cell cycle (Georgetown, Tex.), v. 4.
Bothmer, A., D. Robbiani, M. Di Virgilio, S. Bunting, I. Klein, N. Feldhahn, J. Barlow, H. Chen, D. Bosque, E. Callen, A. Nussenzweig, and M. Nussenzweig, 2011, Regulation of DNA end joining, resection, and immunoglobulin class switch recombination by 53BP1: Molecular cell, v. 42.
Bouwman, P., A. Aly, J. Escandell, M. Pieterse, J. Bartkova, H. van der Gulden, S. Hiddingh, M. Thanasoula, A. Kulkarni, Q. Yang, B. Haffty, J. Tommiska, C. Blomqvist, R. Drapkin, D. Adams, H. Nevanlinna, J. Bartek, M. Tarsounas, S. Ganesan, and J. Jonkers, 2010, 53BP1 loss rescues BRCA1 deficiency and is associated with triple-negative and BRCA-mutated breast cancers: Nature structural & molecular biology, v. 17.
Braten, O., I. Livneh, T. Ziv, A. Admon, I. Kehat, L. H. Caspi, H. Gonen, B. Bercovich, A. Godzik, S. Jahandideh, L. Jaroszewski, T. Sommer, Y. T. Kwon, M. Guharoy, P. Tompa, and A. Ciechanover, 2016, Numerous proteins with unique characteristics are degraded by the 26S proteasome following monoubiquitination: Proc Natl Acad Sci U S A, v. 113, p. E4639-47.
Brzovic, P., P. Rajagopal, D. Hoyt, M. King, and R. Klevit, 2001, Structure of a BRCA1-BARD1 heterodimeric RING-RING complex: Nature structural biology, v. 8.
Bunting, S., E. Callén, M. Kozak, J. Kim, N. Wong, A. López-Contreras, T. Ludwig, R. Baer, R. Faryabi, A. Malhowski, H. Chen, O. Fernandez-Capetillo, A. D'Andrea, and A. Nussenzweig, 2012, BRCA1 functions independently of homologous recombination in DNA interstrand crosslink repair: Molecular cell, v. 46.
Bétermier, M., P. Bertrand, and B. Lopez, 2014, Is non-homologous end-joining really an inherently error-prone process?: PLoS genetics, v. 10.
Callen, E., D. Zong, W. Wu, N. Wong, A. Stanlie, M. Ishikawa, R. Pavani, L. Dumitrache, A. Byrum, C. Mendez-Dorantes, P. Martinez, A. Canela, Y. Maman, A. Day, M. Kruhlak, M. Blasco, J. Stark, N. Mosammaparast, P. McKinnon, and A. Nussenzweig, 2020, 53BP1 Enforces Distinct Pre- and Post-resection Blocks on Homologous Recombination: Molecular cell, v. 77.
Campbell, S., R. Edwards, C. Leung, D. Neculai, C. Hodge, S. Dhe-Paganon, and J. Glover, 2012, Molecular insights into the function of RING finger (RNF)-containing proteins hRNF8 and hRNF168 in Ubc13/Mms2-dependent ubiquitylation: The Journal of biological chemistry, v. 287.
Ceccaldi, R., J. Liu, R. Amunugama, I. Hajdu, B. Primack, M. Petalcorin, K. O'Connor, P. Konstantinopoulos, S. Elledge, S. Boulton, T. Yusufzai, and A. D'Andrea, 2015, Homologous-recombination-deficient tumours are dependent on Polθ-mediated repair: Nature, v. 518.
Cejka, P., 2015, DNA End Resection: Nucleases Team Up with the Right Partners to Initiate Homologous Recombination: The Journal of biological chemistry, v. 290.

Chang, H., G. Watanabe, C. Gerodimos, T. Ochi, T. Blundell, S. Jackson, and M. Lieber, 2016, Different DNA End Configurations Dictate Which NHEJ Components Are Most Important for Joining Efficiency: The Journal of biological chemistry, v. 291.

Chang, H. H. Y., N. R. Pannunzio, N. Adachi, and M. R. Lieber, 2017, Non-homologous DNA end joining and alternative pathways to double-strand break repair: Nat Rev Mol Cell Biol, v. 18, p. 495-506.

Chapman, J., P. Barral, J. Vannier, V. Borel, M. Steger, A. Tomas-Loba, A. Sartori, I. Adams, F. Batista, and S. Boulton, 2013, RIF1 is essential for 53BP1-dependent nonhomologous end joining and suppression of DNA double-strand break resection: Molecular cell, v. 49.

Chapman, J., A. Sossick, S. Boulton, and S. Jackson, 2012a, BRCA1-associated exclusion of 53BP1 from DNA damage sites underlies temporal control of DNA repair: Journal of cell science, v. 125.

Chapman, J., M. Taylor, and S. Boulton, 2012b, Playing the end game: DNA double-strand break repair pathway choice: Molecular cell, v. 47.

Chau, V., J. Tobias, A. Bachmair, D. Marriott, D. Ecker, D. Gonda, and A. Varshavsky, 1989, A multiubiquitin chain is confined to specific lysine in a targeted short-lived protein: Science (New York, N.Y.), v. 243.

Chen, C., B. Ha, A. Thévenin, H. Lou, R. Zhang, K. Yip, J. Peterson, M. Gerstein, P. Kim, P. Filippakopoulos, S. Knapp, T. Boggon, and B. Turk, 2014, Identification of a Major Determinant for Serine-Threonine Kinase Phosphoacceptor Specificity: Mol Cell, v. 53, p. 140-7.

Chen, H., and L. Symington, 2013, Overcoming the chromatin barrier to end resection: Cell research, v. 23.

Chen, J., E. Bae, L. Zhang, K. Hughes, G. Parmigiani, D. Braun, and T. Rebbeck, 2020, Penetrance of Breast and Ovarian Cancer in Women Who Carry a BRCA1/2 Mutation and Do Not Use Risk-Reducing Salpingo-Oophorectomy: An Updated Meta-Analysis: JNCI cancer spectrum, v. 4.

Chen, Z., and P. Cole, 2015, Synthetic approaches to protein phosphorylation: Current opinion in chemical biology, v. 28.

Chen, Z., H. Jiang, W. Xu, X. Li, D. Dempsey, X. Zhang, P. Devreotes, C. Wolberger, L. Amzel, S. Gabelli, and P. Cole, 2017, A Tunable Brake for HECT Ubiquitin Ligases: Molecular cell, v. 66.

Chiruvella, K., Z. Liang, and T. Wilson, 2013, Repair of double-strand breaks by end joining: Cold Spring Harbor perspectives in biology, v. 5.

Chong, R., K. Wu, D. Spratt, Y. Yang, C. Lee, J. Nayak, M. Xu, R. Elkholi, I. Tappin, J. Li, J. Hurwitz, B. Brown, J. Chipuk, Z. Chen, R. Sanchez, G. Shaw, L. Huang, and Z. Pan, 2014, Pivotal role for the ubiquitin Y59-E51 loop in lysine 48 polyubiquitination: Proceedings of the National Academy of Sciences of the United States of America, v. 111.

Clouaire, T., V. Rocher, A. Lashgari, C. Arnould, M. Aguirrebengoa, A. Biernacka, M. Skrzypczak, F. Aymard, B. Fongang, N. Dojer, J. Iacovoni, M. Rowicka, K. Ginalski, J. Côté, and G. Legube, 2018, Comprehensive Mapping of Histone Modifications at DNA Double-Strand Breaks Deciphers Repair Pathway Chromatin Signatures: Molecular cell, v. 72.

Cruz-Garcia, A., A. Lopez-Saavedra, and P. Huertas, 2014, BRCA1 accelerates CtIP-mediated DNA-end resection: Cell Rep, v. 9, p. 451-9.

Cuella-Martin, R., C. Oliveira, H. E. Lockstone, S. Snellenberg, N. Grolmusova, and J. R. Chapman, 2016, 53BP1 Integrates DNA Repair and p53-Dependent Cell Fate Decisions via Distinct Mechanisms: Mol Cell, v. 64, p. 51-64.

d'Adda di Fagagna, F., 2008, Living on a break: cellular senescence as a DNA-damage response: Nature reviews. Cancer, v. 8.

Daley, J., N. Tomimatsu, G. Hooks, W. Wang, A. Miller, X. Xue, K. Nguyen, H. Kaur, E. Williamson, B. Mukherjee, R. Hromas, S. Burma, and P. Sung, 2020, Specificity of end resection pathways for double-strand break regions containing ribonucleotides and base lesions: Nature communications, v. 11.

Daley, J., and T. Wilson, 2005, Rejoining of DNA double-strand breaks as a function of overhang length: Molecular and cellular biology, v. 25.
Daza-Martin, M., K. Starowicz, M. Jamshad, S. Tye, G. Ronson, H. MacKay, A. Chauhan, A. Walker, H. Stone, J. Beesley, J. Coles, A. Garvin, G. Stewart, T. McCorvie, X. Zhang, R. Densham, and J. Morris, 2019, Isomerization of BRCA1-BARD1 promotes replication fork protection: Nature, v. 571.
De Zio, D., V. Cianfanelli, and F. Cecconi, 2013, New insights into the link between DNA damage and apoptosis: Antioxidants & redox signaling, v. 19.
Densham, R., A. Garvin, H. Stone, J. Strachan, R. Baldock, M. Daza-Martin, A. Fletcher, S. Blair-Reid, J. Beesley, B. Johal, L. Pearl, R. Neely, N. Keep, F. Watts, and J. Morris, 2016, Human BRCA1-BARD1 ubiquitin ligase activity counteracts chromatin barriers to DNA resection: Nat Struct Mol Biol, v. 23, p. 647-55.
Dephoure, N., K. L. Gould, S. P. Gygi, and D. R. Kellogg, 2013, Mapping and analysis of phosphorylation sites: a quick guide for cell biologists: Mol Biol Cell, v. 24, p. 535-42.
Dev, H., T. Chiang, C. Lescale, I. de Krijger, A. Martin, D. Pilger, J. Coates, M. Sczaniecka-Clift, W. Wei, M. Ostermaier, M. Herzog, J. Lam, A. Shea, M. Demir, Q. Wu, F. Yang, B. Fu, Z. Lai, G. Balmus, R. Belotserkovskaya, V. Serra, M. O'Connor, A. Bruna, P. Beli, L. Pellegrini, C. Caldas, L. Deriano, J. Jacobs, Y. Galanty, and S. Jackson, 2018, Shieldin complex promotes DNA end-joining and counters homologous recombination in BRCA1-null cells: Nature cell biology, v. 20.
Doil, C., N. Mailand, S. Bekker-Jensen, P. Menard, D. Larsen, R. Pepperkok, J. Ellenberg, S. Panier, D. Durocher, J. Bartek, J. Lukas, and C. Lukas, 2009, RNF168 binds and amplifies ubiquitin conjugates on damaged chromosomes to allow accumulation of repair proteins: Cell, v. 136.
Dong, X., Z. Gong, Y. Lu, K. Liu, L. Qin, M. Ran, C. Zhang, Z. Liu, W. Zhang, and C. Tang, 2017, Ubiquitin S65 phosphorylation engenders a pH-sensitive conformational switch: Proceedings of the National Academy of Sciences of the United States of America, v. 114.
Dove, K. K., and R. E. Klevit, 2017, RING-Between-RING E3 Ligases: Emerging Themes amid the Variations: J Mol Biol, v. 429, p. 3363-3375.
Drané, P., M. Brault, G. Cui, K. Meghani, S. Chaubey, A. Detappe, N. Parnandi, Y. He, X. Zheng, M. Botuyan, A. Kalousi, W. Yewdell, C. Münch, J. Harper, J. Chaudhuri, E. Soutoglou, G. Mer, and D. Chowdhury, 2017, TIRR regulates 53BP1 by masking its histone methyl-lysine binding function: Nature, v. 543.
Dunkerley, K., A. Rintala-Dempsey, G. Salzano, R. Tadayon, D. Hadi, K. Barber, H. Walden, and G. Shaw, 2022, Distinct phosphorylation signals drive acceptor versus free ubiquitin chain targeting by parkin: The Biochemical journal, v. 479.
Elbakry, A., and M. Löbrich, 2021, Homologous Recombination Subpathways: A Tangle to Resolve: Frontiers in genetics, v. 12.
Eliezer, Y., L. Argaman, A. Rhie, A. Doherty, and M. Goldberg, 2009, The direct interaction between 53BP1 and MDC1 is required for the recruitment of 53BP1 to sites of damage: The Journal of biological chemistry, v. 284.
Faulkner, E., J. Pike, R. Densham, E. Garlick, S. Thomas, R. Neely, and J. Morris, 2022, Imaging nanoscale nuclear structures with expansion microscopy: Journal of cell science, v. 135.
Feng, L., and J. Chen, 2012, The E3 ligase RNF8 regulates KU80 removal and NHEJ repair: Nature structural & molecular biology, v. 19.
Fernandez-Vidal, A., J. Vignard, and G. Mirey, 2017, Around and beyond 53BP1 Nuclear Bodies: International journal of molecular sciences, v. 18.
Finley, D., S. Sadis, B. Monia, P. Boucher, D. Ecker, S. Crooke, and V. Chau, 1994, Inhibition of proteolysis and cell cycle progression in a multiubiquitination-deficient yeast mutant: Molecular and cellular biology, v. 14.
Fouad, S., O. Wells, M. Hill, and V. D'Angiolella, 2019, Cullin Ring Ubiquitin Ligases (CRLs) in Cancer: Responses to Ionizing Radiation (IR) Treatment: Frontiers in physiology, v. 10.

Fradet-Turcotte, A., M. D. Canny, C. Escribano-Diaz, A. Orthwein, C. C. Leung, H. Huang, M. C. Landry, J. Kitevski-LeBlanc, S. M. Noordermeer, F. Sicheri, and D. Durocher, 2013, 53BP1 is a reader of the DNA-damage-induced H2A Lys 15 ubiquitin mark: Nature, v. 499, p. 50-4.

Fugger, K., and S. West, 2016, Keeping homologous recombination in check: Cell research, v. 26.

Gapud, E., and B. Sleckman, 2011, Unique and redundant functions of ATM and DNA-PKcs during V(D)J recombination: Cell cycle (Georgetown, Tex.), v. 10.

Gatti, M., S. Pinato, A. Maiolica, F. Rocchio, M. G. Prato, R. Aebersold, and L. Penengo, 2015, RNF168 promotes noncanonical K27 ubiquitination to signal DNA damage: Cell Rep, v. 10, p. 226-38.

George, A., Y. Hoffiz, A. Charles, Y. Zhu, and A. Mabb, 2018, A Comprehensive Atlas of E3 Ubiquitin Ligase Mutations in Neurological Disorders: Frontiers in genetics, v. 9.

Gladkova, C., A. F. Schubert, J. L. Wagstaff, J. N. Pruneda, S. M. Freund, and D. Komander, 2017, An invisible ubiquitin conformation is required for efficient phosphorylation by PINK1: Embo j, v. 36, p. 3555-3572.

Gorodetska, I., I. Kozeretska, and A. Dubrovska, 2019, BRCA Genes: The Role in Genome Stability, Cancer Stemness and Therapy Resistance: Journal of Cancer, v. 10.

Grice, G. L., and J. A. Nathan, 2016, The recognition of ubiquitinated proteins by the proteasome: Cell Mol Life Sci, v. 73, p. 3497-506.

Gu, J., H. Lu, B. Tippin, N. Shimazaki, M. F. Goodman, and M. R. Lieber, 2007, XRCC4:DNA ligase IV can ligate incompatible DNA ends and can ligate across gaps: Embo j, v. 26, p. 1010-23.

Gu, T., X. Deng, F. Huang, M. Tucker, K. Crosby, V. Rimkunas, Y. Wang, G. Deng, L. Zhu, Z. Tan, Y. Hu, C. Wu, J. Nardone, J. MacNeill, J. Ren, C. Reeves, G. Innocenti, B. Norris, J. Yuan, J. Yu, H. Haack, B. Shen, C. Peng, H. Li, X. Zhou, X. Liu, J. Rush, and M. Comb, 2011, Survey of tyrosine kinase signaling reveals ROS kinase fusions in human cholangiocarcinoma: PloS one, v. 6.

Gupta, R., K. Somyajit, T. Narita, E. Maskey, A. Stanlie, M. Kremer, D. Typas, M. Lammers, N. Mailand, A. Nussenzweig, J. Lukas, and C. Choudhary, 2018, DNA Repair Network Analysis Reveals Shieldin as a Key Regulator of NHEJ and PARP Inhibitor Sensitivity: Cell, v. 173.

H.M. Berman, J. Westbrook, Z. Feng, G. Gilliland, T. N. Bhat, H. Weissig, I. N. Shindyalov, and P. E. Bourne, 2000, The Protein Data Bank, *Nucleic Acids Research*, p. 235-242.

Hashizume, R., M. Fukuda, I. Maeda, H. Nishikawa, D. Oyake, Y. Yabuki, H. Ogata, and T. Ohta, 2001, The RING heterodimer BRCA1-BARD1 is a ubiquitin ligase inactivated by a breast cancer-derived mutation: The Journal of biological chemistry, v. 276.

Hepowit, N., K. Pereira, J. Tumolo, W. Chazin, and J. MacGurn, 2020, Identification of ubiquitin Ser57 kinases regulating the oxidative stress response in yeast: eLife, v. 9.

Her, J., and S. Bunting, 2018, How cells ensure correct repair of DNA double-strand breaks: The Journal of biological chemistry, v. 293.

Hu, Q., M. Botuyan, G. Cui, D. Zhao, and G. Mer, 2017, Mechanisms of Ubiquitin-Nucleosome Recognition and Regulation of 53BP1 Chromatin Recruitment by RNF168/169 and RAD18: Molecular cell, v. 66.

Hu, Y., C. Wang, K. Huang, F. Xia, J. Parvin, and N. Mondal, 2014, Regulation of 53BP1 protein stability by RNF8 and RNF168 is important for efficient DNA double-strand break repair: PloS one, v. 9.

Huguenin-Dezot, N., C. V. De, J. Peltier, A. Knebel, Y. Kristaryianto, D. Rogerson, Y. Kulathu, M. Trost, and J. Chin, 2016, Synthesis of Isomeric Phosphoubiquitin Chains Reveals that Phosphorylation Controls Deubiquitinase Activity and Specificity: Cell reports, v. 16.

Hung, P., B. Chen, R. George, C. Liberman, A. Morales, P. Colon-Ortiz, J. Tyler, B. Sleckman, and A. Bredemeyer, 2017, Deficiency of XLF and PAXX prevents DNA double-strand break repair by non-homologous end joining in lymphocytes: Cell cycle (Georgetown, Tex.), v. 16.

Hunter, T., 2009, Tyrosine phosphorylation: thirty years and counting: Current opinion in cell biology, v. 21.

Ingram, S., J. Warmenhoven, N. Henthorn, E. Smith, A. Chadwick, N. Burnet, R. Mackay, N. Kirkby, K. Kirkby, and M. Merchant, 2019, Mechanistic modelling supports entwined rather than exclusively competitive DNA double-strand break repair pathway: Scientific reports, v. 9.

Irminger-Finger, I., M. Ratajska, and M. Pilyugin, 2016, New concepts on BARD1: Regulator of BRCA pathways and beyond: Int J Biochem Cell Biol, v. 72, p. 1-17.

Ismail, I. H., J. P. Gagne, M. M. Genois, H. Strickfaden, D. McDonald, Z. Xu, G. G. Poirier, J. Y. Masson, and M. J. Hendzel, 2015, The RNF138 E3 ligase displaces Ku to promote DNA end resection and regulate DNA repair pathway choice: Nat Cell Biol, v. 17, p. 1446-57.

Johnson, J. L., T. M. Yaron, E. M. Huntsman, A. Kerelsky, J. Song, A. Regev, T.-Y. Lin, K. Liberatore, D. M. Cizin, B. M. Cohen, N. Vasan, Y. Ma, K. Krismer, J. T. Robles, B. van de Kooij, A. E. van Vlimmeren, N. Andrée-Busch, N. Käufer, M. V. Dorovkov, A. G. Ryazanov, Y. Takagi, E. R. Kastenhuber, M. D. Goncalves, O. Elemento, D. J. Taatjes, A. Maucuer, A. Yamashita, A. Degterev, R. Linding, J. Blenis, P. V. Hornbeck, B. E. Turk, M. B. Yaffe, and L. C. Cantley, 2022, A global atlas of substrate specificities for the human serine/threonine kinome: bioRxiv, p. 2022.05.22.492882.

Joo, W., P. Jeffrey, S. Cantor, M. Finnin, D. Livingston, and N. Pavletich, 2002, Structure of the 53BP1 BRCT region bound to p53 and its comparison to the Brca1 BRCT structure: Genes & development, v. 16.

Kakarougkas, A., A. Ismail, Y. Katsuki, R. Freire, A. Shibata, and P. Jeggo, 2013, Co-operation of BRCA1 and POH1 relieves the barriers posed by 53BP1 and RAP80 to resection: Nucleic acids research, v. 41.

Kam, W., and R. Banati, 2013, Effects of ionizing radiation on mitochondria: Free radical biology & medicine, v. 65.

Kane, L. A., M. Lazarou, A. I. Fogel, Y. Li, K. Yamano, S. A. Sarraf, S. Banerjee, and R. J. Youle, 2014, PINK1 phosphorylates ubiquitin to activate Parkin E3 ubiquitin ligase activity: J Cell Biol, v. 205, p. 143-53.

Kanshin, E., L. P. Bergeron-Sandoval, S. S. Isik, P. Thibault, and S. W. Michnick, 2015, A cell-signaling network temporally resolves specific versus promiscuous phosphorylation: Cell Rep, v. 10, p. 1202-14.

Kawamura, K., F. Qi, and J. Kobayashi, 2018, Potential relationship between the biological effects of low-dose irradiation and mitochondrial ROS production: Journal of radiation research, v. 59.

Kazlauskaite, A., R. J. Martinez-Torres, S. Wilkie, A. Kumar, J. Peltier, A. Gonzalez, C. Johnson, J. Zhang, A. G. Hope, M. Peggie, M. Trost, D. M. van Aalten, D. R. Alessi, A. R. Prescott, A. Knebel, H. Walden, and M. M. Muqit, 2015, Binding to serine 65-phosphorylated ubiquitin primes Parkin for optimal PINK1-dependent phosphorylation and activation: EMBO Rep, v. 16, p. 939-54.

Kciuk, M., A. Gielecińska, S. Mujwar, M. Mojzych, and R. Kontek, 2022, Cyclin-dependent kinases in DNA damage response: Biochim Biophys Acta Rev Cancer, v. 1877, p. 188716.

Keeney, S., J. Lange, and N. Mohibullah, 2014, Self-organization of meiotic recombination initiation: general principles and molecular pathways: Annual review of genetics, v. 48.

Kelliher, J., G. Ghosal, and J. Leung, 2022, New answers to the old RIDDLE: RNF168 and the DNA damage response pathway: The FEBS journal, v. 289.

Kettenbach, A., D. Schweppe, B. Faherty, D. Pechenick, A. Pletnev, and S. Gerber, 2011, Quantitative phosphoproteomics identifies substrates and functional modules of Aurora and Polo-like kinase activities in mitotic cells: Science signaling, v. 4.

Kisselev, A., and A. Goldberg, 2001, Proteasome inhibitors: from research tools to drug candidates: Chemistry & biology, v. 8.

Kitada, T., S. Asakawa, N. Hattori, H. Matsumine, Y. Yamamura, S. Minoshima, M. Yokochi, Y. Mizuno, and N. Shimizu, 1998, Mutations in the parkin gene cause autosomal recessive juvenile parkinsonism: Nature, v. 392, p. 605-8.

Kleiner, R., P. Verma, K. Molloy, B. Chait, and T. Kapoor, 2015, Chemical proteomics reveals γH2AX-53BP1 interaction in the DNA damage response: Nature chemical biology, v. 11.
Kocyłowski, M. K., A. J. Rey, G. S. Stewart, and T. D. Halazonetis, 2015, Ubiquitin-H2AX fusions render 53BP1 recruitment to DNA damage sites independent of RNF8 or RNF168: Cell Cycle, v. 14, p. 1748-58.
Kolas, N., J. Chapman, S. Nakada, J. Ylanko, R. Chahwan, F. Sweeney, S. Panier, M. Mendez, J. Wildenhain, T. Thomson, L. Pelletier, S. Jackson, and D. Durocher, 2007, Orchestration of the DNA-damage response by the RNF8 ubiquitin ligase: Science (New York, N.Y.), v. 318.
Komander, D., M. J. Clague, and S. Urbe, 2009, Breaking the chains: structure and function of the deubiquitinases: Nat Rev Mol Cell Biol, v. 10, p. 550-63.
Kotnis, A., L. Du, C. Liu, S. Popov, and Q. Pan-Hammarström, 2009, Non-homologous end joining in class switch recombination: the beginning of the end: Philosophical transactions of the Royal Society of London. Series B, Biological sciences, v. 364.
Kozeleková, A., A. Náplavová, T. Brom, N. Gašparik, J. Šimek, J. Houser, and J. Hritz, 2022, Phosphorylated and Phosphomimicking Variants May Differ-A Case Study of 14-3-3 Protein: Frontiers in chemistry, v. 10.
Kozik, Z., 2019, *Investigation of DNA double-strand break-associated histone post-translational modifications using targeted mass spectrometry*, University of Sussex.
Krupina, K., A. Goginashvili, and D. Cleveland, 2021, Causes and consequences of micronuclei: Current opinion in cell biology, v. 70.
Kumar, A., V. Chaugule, T. Condos, K. Barber, C. Johnson, R. Toth, R. Sundaramoorthy, A. Knebel, G. Shaw, and H. Walden, 2017, Parkin-phosphoubiquitin complex reveals cryptic ubiquitin-binding site required for RBR ligase activity: Nature structural & molecular biology, v. 24.
Kumar, V., F. Alt, and R. Frock, 2016, PAXX and XLF DNA repair factors are functionally redundant in joining DNA breaks in a G1-arrested progenitor B-cell line: Proceedings of the National Academy of Sciences of the United States of America, v. 113.
Lacoursiere, R., D. Hadi, and G. Shaw, 2022, Acetylation, Phosphorylation, Ubiquitination (Oh My!): Following Post-Translational Modifications on the Ubiquitin Road: Biomolecules, v. 12.
Lakin, N., and S. Jackson, 1999, Regulation of p53 in response to DNA damage: Oncogene, v. 18.
Lamarche, B. J., N. I. Orazio, and M. D. Weitzman, 2010, The MRN complex in double-strand break repair and telomere maintenance: FEBS Lett, v. 584, p. 3682-95.
Lazarou, M., D. P. Narendra, S. M. Jin, E. Tekle, S. Banerjee, and R. J. Youle, 2013, PINK1 drives Parkin self-association and HECT-like E3 activity upstream of mitochondrial binding: J Cell Biol, v. 200, p. 163-72.
Le, J., E. Perez, L. Nemzow, and F. Gong, 2019, Role of deubiquitinases in DNA damage response: DNA repair, v. 76.
Lee, B. L., A. Singh, J. N. Mark Glover, M. J. Hendzel, and L. Spyracopoulos, 2017a, Molecular Basis for K63-Linked Ubiquitination Processes in Double-Strand DNA Break Repair: A Focus on Kinetics and Dynamics: J Mol Biol, v. 429, p. 3409-3429.
Lee, H., K. Na, M. Kwon, H. Kim, K. Kim, and Y. Paik, 2009, Quantitative analysis of phosphopeptides in search of the disease biomarker from the hepatocellular carcinoma specimen: Proteomics, v. 9.
Lee, S., J. Tumolo, A. Ehlinger, K. Jernigan, S. Qualls-Histed, P. Hsu, W. McDonald, W. Chazin, and J. MacGurn, 2017b, Ubiquitin turnover and endocytic trafficking in yeast are regulated by Ser57 phosphorylation of ubiquitin: eLife, v. 6.
Lei, T., S. Du, Z. Peng, and L. Chen, 2022, Multifaceted regulation and functions of 53BP1 in NHEJ-mediated DSB repair (Review): International journal of molecular medicine, v. 50.
Li, H., Z. Liu, N. Wu, Y. Chen, Q. Cheng, and J. Wang, 2020, PARP inhibitor resistance: the underlying mechanisms and clinical implications: Molecular cancer, v. 19.
Li, Y., Q. Ruan, Y. Li, G. Ye, X. Lu, X. Lin, and G. Xu, 2012, A novel approach to transforming a non-targeted metabolic profiling method to a pseudo-targeted method using the retention time

locking gas chromatography/mass spectrometry-selected ions monitoring: Journal of chromatography. A, v. 1255.
Liang, J., Q. Gong, Y. Li, Y. Zheng, J. Zheng, C. Tian, and J. Li, 2019, Thiirane linkers directed histone H2A diubiquitination suggests plasticity in 53BP1 recognition: Chemical communications (Cambridge, England), v. 55.
Liao, H., R. Winkfein, G. Mack, J. Rattner, and T. Yen, 1995, CENP-F is a protein of the nuclear matrix that assembles onto kinetochores at late G2 and is rapidly degraded after mitosis: The Journal of cell biology, v. 130.
Lieber, M. R., 2010, The mechanism of double-strand DNA break repair by the nonhomologous DNA end-joining pathway: Annu Rev Biochem, v. 79, p. 181-211.
Lim, D. S., and P. Hasty, 1996, A mutation in mouse rad51 results in an early embryonic lethal that is suppressed by a mutation in p53: Mol Cell Biol, v. 16, p. 7133-43.
Limbo, O., C. Chahwan, Y. Yamada, R. de Bruin, C. Wittenberg, and P. Russell, 2007, Ctp1 is a cell-cycle-regulated protein that functions with Mre11 complex to control double-strand break repair by homologous recombination: Molecular cell, v. 28.
Lindsten, K., F. de Vrij, L. Verhoef, D. Fischer, F. van Leeuwen, E. Hol, M. Masucci, and N. Dantuma, 2002, Mutant ubiquitin found in neurodegenerative disorders is a ubiquitin fusion degradation substrate that blocks proteasomal degradation: The Journal of cell biology, v. 157.
Liu, C., D. Wang, J. Wu, J. Keller, T. Ma, and X. Yu, 2013, RNF168 forms a functional complex with RAD6 during the DNA damage response: Journal of cell science, v. 126.
Liu, Y., and L. Lu, 2020, BRCA1 and homologous recombination: implications from mouse embryonic development: Cell & bioscience, v. 10.
Long, Q., Z. Liu, and M. Gullerova, 2021, Sweet Melody or Jazz? Transcription Around DNA Double-Strand Breaks: Frontiers in molecular biosciences, v. 8.
Lottersberger, F., A. Bothmer, D. Robbiani, M. Nussenzweig, and T. de Lange, 2013, Role of 53BP1 oligomerization in regulating double-strand break repair: Proceedings of the National Academy of Sciences of the United States of America, v. 110.
Luna-Maldonado, F., M. Andonegui-Elguera, J. Díaz-Chávez, and L. Herrera, 2021, Mitotic and DNA Damage Response Proteins: Maintaining the Genome Stability and Working for the Common Good: Frontiers in cell and developmental biology, v. 9.
Löbrich, M., and P. Jeggo, 2017, A Process of Resection-Dependent Nonhomologous End Joining Involving the Goddess Artemis: Trends in biochemical sciences, v. 42.
Ma, C., B. Gibb, Y. Kwon, P. Sung, and E. Greene, 2017, Protein dynamics of human RPA and RAD51 on ssDNA during assembly and disassembly of the RAD51 filament: Nucleic acids research, v. 45.
Ma, S., Z. Rong, C. Liu, X. Qin, X. Zhang, and Q. Chen, 2021, DNA damage promotes microtubule dynamics through a DNA-PK-AKT axis for enhanced repair: The Journal of cell biology, v. 220.
Mallette, F., F. Mattiroli, G. Cui, L. Young, M. Hendzel, G. Mer, T. Sixma, and S. Richard, 2012, RNF8- and RNF168-dependent degradation of KDM4A/JMJD2A triggers 53BP1 recruitment to DNA damage sites: The EMBO journal, v. 31.
Mandemaker, I., L. van Cuijk, R. Janssens, H. Lans, K. Bezstarosti, J. Hoeijmakers, J. Demmers, W. Vermeulen, and J. Marteijn, 2017, DNA damage-induced histone H1 ubiquitylation is mediated by HUWE1 and stimulates the RNF8-RNF168 pathway: Scientific reports, v. 7.
Mann, M., S. E. Ong, M. Gronborg, H. Steen, O. N. Jensen, and A. Pandey, 2002, Analysis of protein phosphorylation using mass spectrometry: deciphering the phosphoproteome: Trends Biotechnol, v. 20, p. 261-8.
Marini, F., C. Rawal, G. Liberi, and A. Pellicioli, 2019, Regulation of DNA Double Strand Breaks Processing: Focus on Barriers: Frontiers in molecular biosciences, v. 6.

Markova, E., N. Schultz, and I. Y. Belyaev, 2007, Kinetics and dose-response of residual 53BP1/gamma-H2AX foci: co-localization, relationship with DSB repair and clonogenic survival: Int J Radiat Biol, v. 83, p. 319-29.
Maspero, E., S. Mari, E. Valentini, A. Musacchio, A. Fish, S. Pasqualato, and S. Polo, 2011, Structure of the HECT:ubiquitin complex and its role in ubiquitin chain elongation: EMBO reports, v. 12.
Matthews, H., C. Bertoli, and R. de Bruin, 2022, Cell cycle control in cancer: Nature reviews. Molecular cell biology, v. 23.
Mattiroli, F., J. H. Vissers, W. J. van Dijk, P. Ikpa, E. Citterio, W. Vermeulen, J. A. Marteijn, and T. K. Sixma, 2012, RNF168 ubiquitinates K13-15 on H2A/H2AX to drive DNA damage signaling: Cell, v. 150, p. 1182-95.
Mavragani, I., Z. Nikitaki, S. Kalospyros, and A. Georgakilas, 2019, Ionizing Radiation and Complex DNA Damage: From Prediction to Detection Challenges and Biological Significance: Cancers, v. 11.
Menolfi, D., and S. Zha, 2020, ATM, ATR and DNA-PKcs kinases-the lessons from the mouse models: inhibition ≠ deletion: Cell & bioscience, v. 10.
Mirman, Z., F. Lottersberger, H. Takai, T. Kibe, Y. Gong, K. Takai, A. Bianchi, M. Zimmermann, D. Durocher, and T. de Lange, 2018, 53BP1-RIF1-shieldin counteracts DSB resection through CST- and Polα-dependent fill-in: Nature, v. 560.
Mirsanaye, A., D. Typas, and N. Mailand, 2021, Ubiquitylation at Stressed Replication Forks: Mechanisms and Functions: Trends in cell biology, v. 31.
Moritz, A., Y. Li, A. Guo, J. Villén, Y. Wang, J. MacNeill, J. Kornhauser, K. Sprott, J. Zhou, A. Possemato, J. Ren, P. Hornbeck, L. Cantley, S. Gygi, J. Rush, and M. Comb, 2010, Akt-RSK-S6 kinase signaling networks activated by oncogenic receptor tyrosine kinases: Science signaling, v. 3.
Moynahan, M., A. Pierce, and M. Jasin, 2001, BRCA2 is required for homology-directed repair of chromosomal breaks: Molecular cell, v. 7.
Mullee, L., and C. Morrison, 2016, Centrosomes in the DNA damage response--the hub outside the centre: Chromosome research : an international journal on the molecular, supramolecular and evolutionary aspects of chromosome biology, v. 24.
Muñoz, M., D. Yanez, and J. Stark, 2014, An RNF168 fragment defective for focal accumulation at DNA damage is proficient for inhibition of homologous recombination in BRCA1 deficient cells: Nucleic acids research, v. 42.
Nair, S., M. Engelbrecht, X. Miles, R. Ndimba, R. Fisher, P. du Plessis, J. Bolcaen, J. Nieto-Camero, E. de Kock, and C. Vandevoorde, 2019, The Impact of Dose Rate on DNA Double-Strand Break Formation and Repair in Human Lymphocytes Exposed to Fast Neutron Irradiation: International journal of molecular sciences, v. 20.
Nakada, S., I. Tai, S. Panier, A. Al-Hakim, S. Iemura, Y. Juang, L. O'Donnell, A. Kumakubo, M. Munro, F. Sicheri, A. Gingras, T. Natsume, T. Suda, and D. Durocher, 2010, Non-canonical inhibition of DNA damage-dependent ubiquitination by OTUB1: Nature, v. 466.
Nakamura, K., G. Saredi, J. Becker, B. Foster, N. Nguyen, T. Beyer, L. Cesa, P. Faull, S. Lukauskas, T. Frimurer, J. Chapman, T. Bartke, and A. Groth, 2019, H4K20me0 recognition by BRCA1-BARD1 directs homologous recombination to sister chromatids: Nature cell biology, v. 21.
Neal, J., and K. Meek, 2011, Choosing the right path: does DNA-PK help make the decision?: Mutation research, v. 711.
Needham, E. J., B. L. Parker, T. Burykin, D. E. James, and S. J. Humphrey, 2019, Illuminating the dark phosphoproteome: Sci Signal, v. 12.
Nick McElhinny, S., C. Snowden, J. McCarville, and D. Ramsden, 2000, Ku recruits the XRCC4-ligase IV complex to DNA ends: Molecular and cellular biology, v. 20.
Noordermeer, S., S. Adam, D. Setiaputra, M. Barazas, S. Pettitt, A. Ling, M. Olivieri, A. Álvarez-Quilón, N. Moatti, M. Zimmermann, S. Annunziato, D. Krastev, F. Song, I. Brandsma, J. Frankum, R. Brough, A. Sherker, S. Landry, R. Szilard, M. Munro, A. McEwan, T. Goullet de Rugy, Z. Lin, T.

Hart, J. Moffat, A. Gingras, A. Martin, H. van Attikum, J. Jonkers, C. Lord, S. Rottenberg, and D. D, 2018, The shieldin complex mediates 53BP1-dependent DNA repair: Nature, v. 560.
Nowsheen, S., K. Aziz, A. Aziz, M. Deng, B. Qin, K. Luo, K. Jeganathan, H. Zhang, T. Liu, J. Yu, Y. Deng, J. Yuan, W. Ding, J. van Deursen, and Z. Lou, 2018, L3MBTL2 orchestrates ubiquitin signalling by dictating the sequential recruitment of RNF8 and RNF168 after DNA damage: Nature cell biology, v. 20.
Ohtake, F., Y. Saeki, K. Sakamoto, K. Ohtake, H. Nishikawa, H. Tsuchiya, T. Ohta, K. Tanaka, and J. Kanno, 2015, Ubiquitin acetylation inhibits polyubiquitin chain elongation: EMBO reports, v. 16.
Okatsu, K., F. Koyano, M. Kimura, H. Kosako, Y. Saeki, K. Tanaka, and N. Matsuda, 2015, Phosphorylated ubiquitin chain is the genuine Parkin receptor: J Cell Biol, v. 209, p. 111-28.
Ordureau, A., C. Münch, and J. Harper, 2015, Quantifying ubiquitin signaling: Molecular cell, v. 58.
Ordureau, A., J. Paulo, W. Zhang, T. Ahfeldt, J. Zhang, E. Cohn, Z. Hou, J. Heo, L. Rubin, S. Sidhu, S. Gygi, and J. Harper, 2018, Dynamics of PARKIN-Dependent Mitochondrial Ubiquitylation in Induced Neurons and Model Systems Revealed by Digital Snapshot Proteomics: Molecular cell, v. 70.
Ordureau, A., S. A. Sarraf, D. M. Duda, J. M. Heo, M. P. Jedrychowski, V. O. Sviderskiy, J. L. Olszewski, J. T. Koerber, T. Xie, S. A. Beausoleil, J. A. Wells, S. P. Gygi, B. A. Schulman, and J. W. Harper, 2014, Quantitative proteomics reveal a feedforward mechanism for mitochondrial PARKIN translocation and ubiquitin chain synthesis: Mol Cell, v. 56, p. 360-75.
Orthwein, A., A. Fradet-Turcotte, S. Noordermeer, M. Canny, C. Brun, J. Strecker, C. Escribano-Diaz, and D. Durocher, 2014, Mitosis inhibits DNA double-strand break repair to guard against telomere fusions: Science (New York, N.Y.), v. 344.
Orthwein, A., S. Noordermeer, M. Wilson, S. Landry, R. Enchev, A. Sherker, M. Munro, J. Pinder, J. Salsman, G. Dellaire, B. Xia, M. Peter, and D. Durocher, 2015, A mechanism for the suppression of homologous recombination in G1 cells: Nature, v. 528.
Paiano, J., N. Zolnerowich, W. Wu, R. Pavani, C. Wang, H. Li, L. Zheng, B. Shen, B. Sleckman, B. Chen, and A. Nussenzweig, 2021, Role of 53BP1 in end protection and DNA synthesis at DNA breaks: Genes & development, v. 35.
Pannunzio, N., G. Watanabe, and M. Lieber, 2018, Nonhomologous DNA end-joining for repair of DNA double-strand breaks: The Journal of biological chemistry, v. 293.
Park, H., M. Hohn, T. Umehara, L. Guo, E. Osborne, J. Benner, C. Noren, J. Rinehart, and D. Söll, 2011, Expanding the genetic code of Escherichia coli with phosphoserine: Science (New York, N.Y.), v. 333.
Paull, T. T., 2015, Mechanisms of ATM Activation: Annu Rev Biochem, v. 84, p. 711-38.
Peck Justice, S., N. McCracken, J. Victorino, G. Qi, A. Wijeratne, and A. Mosley, 2021, Boosting Detection of Low-Abundance Proteins in Thermal Proteome Profiling Experiments by Addition of an Isobaric Trigger Channel to TMT Multiplexes: Analytical chemistry, v. 93.
Pilarski, R., 2019, The Role of BRCA Testing in Hereditary Pancreatic and Prostate Cancer Families: Am Soc Clin Oncol Educ Book, v. 39, p. 79-86.
Polato, F., E. Callen, N. Wong, R. Faryabi, S. Bunting, H. Chen, M. Kozak, M. Kruhlak, C. Reczek, W. Lee, T. Ludwig, R. Baer, L. Feigenbaum, S. Jackson, and A. Nussenzweig, 2014, CtIP-mediated resection is essential for viability and can operate independently of BRCA1: The Journal of experimental medicine, v. 211.
Pérez Berrocal, D., K. Witting, H. Ovaa, and M. Mulder, 2020, Hybrid Chains: A Collaboration of Ubiquitin and Ubiquitin-Like Modifiers Introducing Cross-Functionality to the Ubiquitin Code: Frontiers in chemistry, v. 7.
Qiu, S., and J. Huang, 2021, MRN complex is an essential effector of DNA damage repair: Journal of Zhejiang University. Science. B, v. 22.
Ranjha , L., S. Howard, and P. Cejka, 2018, Main steps in DNA double-strand break repair: an introduction to homologous recombination and related processes: Chromosoma, v. 127.

Rauniyar, N., 2015, Parallel Reaction Monitoring: A Targeted Experiment Performed Using High Resolution and High Mass Accuracy Mass Spectrometry: International journal of molecular sciences, v. 16.
Reczek, C., M. Szabolcs, J. Stark, T. Ludwig, and R. Baer, 2013, The interaction between CtIP and BRCA1 is not essential for resection-mediated DNA repair or tumor suppression: The Journal of cell biology, v. 201.
Reinhardt, H. C., and M. B. Yaffe, 2013, Phospho-Ser/Thr-binding domains: navigating the cell cycle and DNA damage response: Nat Rev Mol Cell Biol, v. 14, p. 563-80.
Riballo, E., M. Kühne, N. Rief, A. Doherty, G. Smith, M. Recio, C. Reis, K. Dahm, A. Fricke, A. Krempler, A. Parker, S. Jackson, A. Gennery, P. Jeggo, and M. Löbrich, 2004, A pathway of double-strand break rejoining dependent upon ATM, Artemis, and proteins locating to gamma-H2AX foci: Molecular cell, v. 16.
Rikova, K., A. Guo, Q. Zeng, A. Possemato, J. Yu, H. Haack, J. Nardone, K. Lee, C. Reeves, Y. Li, Y. Hu, Z. Tan, M. Stokes, L. Sullivan, J. Mitchell, R. Wetzel, J. Macneill, J. Ren, J. Yuan, C. Bakalarski, J. Villen, J. Kornhauser, B. Smith, D. Li, X. Zhou, S. Gygi, T. Gu, R. Polakiewicz, J. Rush, and M. Comb, 2007, Global survey of phosphotyrosine signaling identifies oncogenic kinases in lung cancer: Cell, v. 131.
Rogakou, E. P., C. Boon, C. Redon, and W. M. Bonner, 1999, Megabase chromatin domains involved in DNA double-strand breaks in vivo: J Cell Biol, v. 146, p. 905-16.
Rogerson, D., A. Sachdeva, K. Wang, T. Haq, A. Kazlauskaite, S. Hancock, N. Huguenin-Dezot, M. Muqit, A. Fry, R. Bayliss, and J. Chin, 2015, Efficient genetic encoding of phosphoserine and its nonhydrolyzable analog: Nature chemical biology, v. 11.
Ronchi, V., J. Klein, D. Edwards, and A. Haas, 2014, The active form of E6-associated protein (E6AP)/UBE3A ubiquitin ligase is an oligomer: The Journal of biological chemistry, v. 289.
Rose, M., J. Burgess, K. O'Byrne, D. Richard, and E. Bolderson, 2020, PARP Inhibitors: Clinical Relevance, Mechanisms of Action and Tumor Resistance: Frontiers in cell and developmental biology, v. 8.
Rothblum-Oviatt, C., J. Wright, M. Lefton-Greif, S. McGrath-Morrow, T. Crawford, and H. Lederman, 2016, Ataxia telangiectasia: a review: Orphanet journal of rare diseases, v. 11.
Rother, M., S. Pellegrino, R. Smith, M. Gatti, C. Meisenberg, W. Wiegant, M. Luijsterburg, R. Imhof, J. Downs, A. Vertegaal, S. Huet, M. Altmeyer, and H. van Attikum, 2020, CHD7 and 53BP1 regulate distinct pathways for the re-ligation of DNA double-strand breaks: Nature communications, v. 11.
Rothkamm, K., S. Barnard, J. Moquet, M. Ellender, Z. Rana, and S. Burdak-Rothkamm, 2015, DNA damage foci: Meaning and significance: Environmental and molecular mutagenesis, v. 56.
Ruff, S., S. Logan, M. Garabedian, and T. Huang, 2020, Roles for MDC1 in cancer development and treatment: DNA repair, v. 95.
Saha, T., D. Sundaravinayagam, and M. Di Virgilio, 2021, Charting a DNA Repair Roadmap for Immunoglobulin Class Switch Recombination: Trends in biochemical sciences, v. 46.
Saraste, A., and K. Pulkki, 2000, Morphologic and biochemical hallmarks of apoptosis: Cardiovascular research, v. 45.
Schaefer, J., and D. Morgan, 2011, Protein-linked ubiquitin chain structure restricts activity of deubiquitinating enzymes: The Journal of biological chemistry, v. 286.
Schaich, M., and B. Van Houten, 2021, Searching for DNA Damage: Insights From Single Molecule Analysis: Frontiers in molecular biosciences, v. 8.
Schrödinger, L., and W. DeLano, 2020, *PyMOL* , Available at: http://www.pymol.org/pymol.
Schubert, A., C. Gladkova, E. Pardon, J. Wagstaff, S. Freund, J. Steyaert, S. Maslen, and D. Komander, 2017, Structure of PINK1 in complex with its substrate ubiquitin: Nature, v. 552.
Schwertman, P., S. Bekker-Jensen, and N. Mailand, 2016, Regulation of DNA double-strand break repair by ubiquitin and ubiquitin-like modifiers: Nature Reviews Molecular Cell Biology, v. 17, p. 379.

Setiaputra, D., and D. Durocher, 2019, Shieldin - the protector of DNA ends: EMBO reports, v. 20.
Seto, E., and M. Yoshida, 2014, Erasers of histone acetylation: the histone deacetylase enzymes: Cold Spring Harbor perspectives in biology, v. 6.
Sfeir, A., and L. Symington, 2015, Microhomology-Mediated End Joining: A Back-up Survival Mechanism or Dedicated Pathway?: Trends in biochemical sciences, v. 40.
Shah Punatar, R., M. Martin, H. Wyatt, Y. Chan, and S. West, 2017, Resolution of single and double Holliday junction recombination intermediates by GEN1: Proceedings of the National Academy of Sciences of the United States of America, v. 114.
Sharma, A., and A. Almasan, 2020, USP14 Regulates DNA Damage Response and Is a Target for Radiosensitization in Non-Small Cell Lung Cancer: International journal of molecular sciences, v. 21.
Shen, W., Y. Ma, H. Qi, W. Wang, J. He, F. Xiao, H. Zhu, and S. He, 2021, Kinetics model of DNA double-strand break repair in eukaryotes: DNA repair, v. 100.
Sherker, A., N. Chaudhary, S. Adam, A. Heijink, S. Noordermeer, A. Fradet-Turcotte, and D. Durocher, 2021, Two redundant ubiquitin-dependent pathways of BRCA1 localization to DNA damage sites: EMBO reports, v. 22.
Shibata, A., and P. Jeggo, 2020, Canonical DNA non-homologous end-joining; capacity versus fidelity: The British journal of radiology, v. 93.
Shubina, M., E. Arifulin, D. Sorokin, M. Sosina, M. Tikhomirova, M. Serebryakova, T. Smirnova, S. Sokolov, Y. Musinova, and E. Sheval, 2020, The GAR domain integrates functions that are necessary for the proper localization of fibrillarin (FBL) inside eukaryotic cells: PeerJ, v. 8.
Siddiqui, M., M. François, M. Fenech, and W. Leifert, 2015, Persistent γH2AX: A promising molecular marker of DNA damage and aging: Mutation research. Reviews in mutation research, v. 766.
Simonetta, M., I. de Krijger, J. Serrat, N. Moatti, D. Fortunato, L. Hoekman, O. Bleijerveld, A. Altelaar, and J. Jacobs, 2018, H4K20me2 distinguishes pre-replicative from post-replicative chromatin to appropriately direct DNA repair pathway choice by 53BP1-RIF1-MAD2L2: Cell cycle (Georgetown, Tex.), v. 17.
Sishc, B., and A. Davis, 2017, The Role of the Core Non-Homologous End Joining Factors in Carcinogenesis and Cancer: Cancers, v. 9.
Slatter, M., and A. Gennery, 2020, Update on DNA-Double Strand Break Repair Defects in Combined Primary Immunodeficiency: Current allergy and asthma reports, v. 20.
Smits, V. A., and D. A. Gillespie, 2015, DNA damage control: regulation and functions of checkpoint kinase 1: FEBS J, v. 282, p. 3681-92.
Srinivas, U., B. Tan, B. Vellayappan, and A. Jeyasekharan, 2019, ROS and the DNA damage response in cancer: Redox biology, v. 25.
Stewart, G., T. Stankovic, P. Byrd, T. Wechsler, E. Miller, A. Huissoon, M. Drayson, S. West, S. Elledge, and A. Taylor, 2007, RIDDLE immunodeficiency syndrome is linked to defects in 53BP1-mediated DNA damage signaling: Proceedings of the National Academy of Sciences of the United States of America, v. 104.
Stewart, G., B. Wang, C. Bignell, A. Taylor, and S. Elledge, 2003, MDC1 is a mediator of the mammalian DNA damage checkpoint: Nature, v. 421.
Stewart, G. S., S. Panier, K. Townsend, A. K. Al-Hakim, N. K. Kolas, E. S. Miller, S. Nakada, J. Ylanko, S. Olivarius, M. Mendez, C. Oldreive, J. Wildenhain, A. Tagliaferro, L. Pelletier, N. Taubenheim, A. Durandy, P. J. Byrd, T. Stankovic, A. M. Taylor, and D. Durocher, 2009, The RIDDLE syndrome protein mediates a ubiquitin-dependent signaling cascade at sites of DNA damage: Cell, v. 136, p. 420-34.
Stewart, M. D., T. Ritterhoff, R. E. Klevit, and P. S. Brzovic, 2016, E2 enzymes: more than just middle men: Cell Research, v. 26, p. 423-440.
Stiff, T., M. O'Driscoll, N. Rief, K. Iwabuchi, M. Löbrich, and P. Jeggo, 2004, ATM and DNA-PK function redundantly to phosphorylate H2AX after exposure to ionizing radiation: Cancer research, v. 64.

Stinson, B., A. Moreno, J. Walter, and J. Loparo, 2020, A Mechanism to Minimize Errors during Non-homologous End Joining: Molecular cell, v. 77.
Stracker, T., and J. Petrini, 2011, The MRE11 complex: starting from the ends: Nature reviews. Molecular cell biology, v. 12.
Stuber, K., T. Schneider, J. Werner, M. Kovermann, A. Marx, and M. Scheffner, 2021, Structural and functional consequences of NEDD8 phosphorylation: Nature communications, v. 12.
Stucki, M., J. Clapperton, D. Mohammad, M. Yaffe, S. Smerdon, and S. Jackson, 2005, MDC1 directly binds phosphorylated histone H2AX to regulate cellular responses to DNA double-strand breaks: Cell, v. 123.
Sun, Y., T. McCorvie, L. Yates, and X. Zhang, 2020, Structural basis of homologous recombination: Cellular and molecular life sciences : CMLS, v. 77.
Sundaravinayagam, D., A. Rahjouei, M. Andreani, D. Tupiņa, S. Balasubramanian, T. Saha, V. Delgado-Benito, V. Coralluzzo, O. Daumke, and M. Di Virgilio, 2019, 53BP1 Supports Immunoglobulin Class Switch Recombination Independently of Its DNA Double-Strand Break End Protection Function: Cell reports, v. 28.
Suzuki, K., P. Bose, R. Leong-Quong, D. Fujita, and K. Riabowol, 2010, REAP: A two minute cell fractionation method: BMC research notes, v. 3.
Swaney, D. L., R. A. Rodríguez-Mias, and J. Villén, 2015, Phosphorylation of ubiquitin at Ser65 affects its polymerization, targets, and proteome-wide turnover: EMBO Rep, v. 16, p. 1131-44.
Swatek, K., J. Usher, A. Kueck, C. Gladkova, T. Mevissen, J. Pruneda, T. Skern, and D. Komander, 2019, Insights into ubiquitin chain architecture using Ub-clipping: Nature, v. 572.
Swatek, K. N., and D. Komander, 2016, Ubiquitin modifications: Cell Res, v. 26, p. 399-422.
Symington, L., and J. Gautier, 2011, Double-strand break end resection and repair pathway choice: Annual review of genetics, v. 45.
Tang, Z., J. Yang, X. Wang, M. Zeng, J. Wang, A. Wang, M. Zhao, L. Guo, C. Liu, D. Li, and J. Chen, 2018, Active DNA end processing in micronuclei of ovarian cancer cells: BMC cancer, v. 18.
Thorslund, T., A. Ripplinger, S. Hoffmann, T. Wild, M. Uckelmann, B. Villumsen, T. Narita, T. K. Sixma, C. Choudhary, S. Bekker-Jensen, and N. Mailand, 2015, Histone H1 couples initiation and amplification of ubiquitin signalling after DNA damage: Nature, v. 527, p. 389-93.
Trenner, A., and A. Sartori, 2019, Harnessing DNA Double-Strand Break Repair for Cancer Treatment: Frontiers in oncology, v. 9.
Tsai, L., F. Lopezcolorado, R. Bhargava, C. Mendez-Dorantes, E. Jahanshir, and J. Stark, 2020, RNF8 has both KU-dependent and independent roles in chromosomal break repair: Nucleic acids research, v. 48.
Valente, E., P. Abou-Sleiman, V. Caputo, M. Muqit, K. Harvey, S. Gispert, Z. Ali, D. Turco, A. Bentivoglio, D. Healy, A. Albanese, R. Nussbaum, R. Gonzalez-Maldonado, T. Deller, S. Salvi, P. Cortelli, W. Gilks, D. Latchman, R. Harvey, B. Dallapiccola, G. Auberger, and N. Wood, 2004, Hereditary Early-Onset Parkinson's Disease Caused by Mutations in PINK1: Science, v. 304, p. 1158-1160.
van Leeuwen, F., J. Burbach, and E. Hol, 1998a, Mutations in RNA: a first example of molecular misreading in Alzheimer's disease: Trends in neurosciences, v. 21.
van Leeuwen, F., D. de Kleijn, H. van den Hurk, A. Neubauer, M. Sonnemans, J. Sluijs, S. Köycü, R. Ramdjielal, A. Salehi, G. Martens, F. Grosveld, J. Peter, H. Burbach, and E. Hol, 1998b, Frameshift mutants of beta amyloid precursor protein and ubiquitin-B in Alzheimer's and Down patients: Science (New York, N.Y.), v. 279.
van Wijk, S., and H. Timmers, 2010, The family of ubiquitin-conjugating enzymes (E2s): deciding between life and death of proteins: FASEB journal : official publication of the Federation of American Societies for Experimental Biology, v. 24.
Vazquez, B., J. Thackray, N. Simonet, N. Kane-Goldsmith, P. Martinez-Redondo, T. Nguyen, S. Bunting, A. Vaquero, J. Tischfield, and L. Serrano, 2016, SIRT7 promotes genome integrity and modulates non-homologous end joining DNA repair: The EMBO journal, v. 35.

Vijay-Kumar, S., C. E. Bugg, and W. J. Cook, 1987, Structure of ubiquitin refined at 1.8 A resolution: J Mol Biol, v. 194, p. 531-44.
Walser, F., M. Mulder, B. Bragantini, S. Burger, T. Gubser, M. Gatti, M. Botuyan, A. Villa, M. Altmeyer, D. Neri, H. Ovaa, G. Mer, and L. Penengo, 2020, Ubiquitin Phosphorylation at Thr12 Modulates the DNA Damage Response: Molecular cell, v. 80.
Wang, J., A. Aroumougame, M. Lobrich, Y. Li, D. Chen, J. Chen, and Z. Gong, 2014, PTIP associates with Artemis to dictate DNA repair pathway choice: Genes Dev, v. 28, p. 2693-8.
Ward, I., J. E. Kim, K. Minn, C. C. Chini, G. Mer, and J. Chen, 2006, The tandem BRCT domain of 53BP1 is not required for its repair function: J Biol Chem, v. 281, p. 38472-7.
Ward, I., K. Minn, J. van Deursen, and J. Chen, 2003, p53 Binding protein 53BP1 is required for DNA damage responses and tumor suppression in mice: Molecular and cellular biology, v. 23.
Wauer, T., M. Simicek, A. Schubert, and D. Komander, 2015a, Mechanism of phospho-ubiquitin-induced PARKIN activation: Nature, v. 524, p. 370-4.
Wauer, T., K. N. Swatek, J. L. Wagstaff, C. Gladkova, J. N. Pruneda, M. A. Michel, M. Gersch, C. M. Johnson, S. M. Freund, and D. Komander, 2015b, Ubiquitin Ser65 phosphorylation affects ubiquitin structure, chain assembly and hydrolysis: Embo j, v. 34, p. 307-25.
Weber, J., S. Polo, and E. Maspero, 2019, HECT E3 Ligases: A Tale With Multiple Facets: Front Physiol, v. 10, p. 370.
Wiener, R., X. Zhang, T. Wang, and C. Wolberger, 2012, The mechanism of OTUB1-mediated inhibition of ubiquitination: Nature, v. 483.
Wilson, M., S. Benlekbir, A. Fradet-Turcotte, A. Sherker, J. Julien, A. McEwan, S. Noordermeer, F. Sicheri, J. Rubinstein, and D. Durocher, 2016, The structural basis of modified nucleosome recognition by 53BP1: Nature, v. 536.
Woodbine, L., A. Gennery, and P. Jeggo, 2014, The clinical impact of deficiency in DNA non-homologous end-joining: DNA repair, v. 16.
Wright, W., S. Shah, and W. Heyer, 2018, Homologous recombination and the repair of DNA double-strand breaks: The Journal of biological chemistry, v. 293.
Xia, Z., L. Sun, X. Chen, G. Pineda, X. Jiang, A. Adhikari, W. Zeng, and Z. Chen, 2009, Direct activation of protein kinases by unanchored polyubiquitin chains: Nature, v. 461.
Xu, M., B. Skaug, W. Zeng, and Z. Chen, 2009, A ubiquitin replacement strategy in human cells reveals distinct mechanisms of IKK activation by TNFalpha and IL-1beta: Molecular cell, v. 36.
Yamano, H., 2019, APC/C: current understanding and future perspectives: F1000Research, v. 8.
Yan, J., and A. Jetten, 2008, RAP80 and RNF8, key players in the recruitment of repair proteins to DNA damage sites: Cancer letters, v. 271.
Yang, Q., J. Zhao, D. Chen, and Y. Wang, 2021, E3 ubiquitin ligases: styles, structures and functions: Mol Biomed, v. 2, p. 23.
Yu, X., S. Fu, M. Lai, R. Baer, and J. Chen, 2006, BRCA1 ubiquitinates its phosphorylation-dependent binding partner CtIP: Genes & development, v. 20.
Yue, X., C. Bai, D. Xie, T. Ma, and P. K. Zhou, 2020, DNA-PKcs: A Multi-Faceted Player in DNA Damage Response: Front Genet, v. 11, p. 607428.
Zannini, L., D. Delia, and G. Buscemi, 2014, CHK2 kinase in the DNA damage response and beyond: J Mol Cell Biol, v. 6, p. 442-57.
Zgheib, O., K. Pataky, J. Brugger, and T. Halazonetis, 2009, An oligomerized 53BP1 tudor domain suffices for recognition of DNA double-strand breaks: Molecular and cellular biology, v. 29.
Zhang, F., Q. Fan, K. Ren, and P. Andreassen, 2009, PALB2 functionally connects the breast cancer susceptibility proteins BRCA1 and BRCA2: Molecular cancer research : MCR, v. 7.
Zhang, H., X. Cao, M. Tang, G. Zhong, Y. Si, H. Li, F. Zhu, Q. Liao, L. Li, J. Zhao, J. Feng, S. Li, C. Wang, M. Kaulich, F. Wang, L. Chen, Z. Xia, T. Liang, H. Lu, X. H. Feng, and B. Zhao, 2021, A subcellular map of the human kinome: Elife, v. 10.

Zhang, X., J. Cai, Z. Zheng, L. Polin, Z. Lin, A. Dandekar, L. Li, F. Sun, R. Finley, D. Fang, Z. Yang, and K. Zhang, 2015, A novel ER-microtubule-binding protein, ERLIN2, stabilizes Cyclin B1 and regulates cell cycle progression: Cell discovery, v. 1.

Zhao, F., W. Kim, J. Kloeber, and Z. Lou, 2020, DNA end resection and its role in DNA replication and DSB repair choice in mammalian cells: Experimental & molecular medicine, v. 52.

Zheng, N., and N. Shabek, 2017, Ubiquitin Ligases: Structure, Function, and Regulation: Annu Rev Biochem, v. 86, p. 129-157.

Zhou, H., S. Di Palma, C. Preisinger, M. Peng, A. N. Polat, A. J. Heck, and S. Mohammed, 2013, Toward a comprehensive characterization of a human cancer cell phosphoproteome: J Proteome Res, v. 12, p. 260-71.

Zhou, X., W. Liao, J. Liao, P. Liao, and H. Lu, 2015, Ribosomal proteins: functions beyond the ribosome: Journal of molecular cell biology, v. 7.

Zhu, G., C. Pan, J. Bei, B. Li, C. Liang, Y. Xu, and X. Fu, 2020, Mutant p53 in Cancer Progression and Targeted Therapies: Frontiers in oncology, v. 10.

Zuin, A., M. Isasa, and B. Crosas, 2014, Ubiquitin signaling: extreme conservation as a source of diversity: Cells, v. 3, p. 690-701.